Delft University of Technology

MSc Thesis

A Circuit Lagrangian Formulation of Opto-mechanical Coupling between two Electrical Resonators mediated by a SQUID

Alexander P. A. Cronheim

10 December 2018

Supervisors:
Daniel Bothner
Ines Corveira Rodrigues
Gary A. Steele

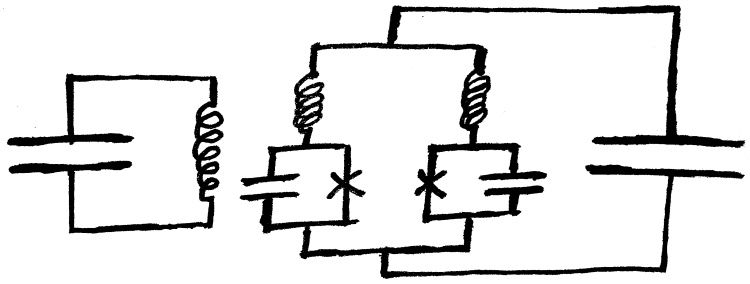

Assessment committee:
Gary A. Steele, Yaroslav M. Blanter, Ad H. Verbruggen

Steele Lab
Department of Quantum Nanoscience

Abstract

This thesis analyses a lumped element circuit proposed for an analogue quantum simulation of opto-mechanics. The circuit consists of two resonators, a simple LC-resonator, and a similar resonator in which the inductor is replaced by a SQUID as a flux tuneable inductance. The interaction between the two resonators is established by mutual inductance between the inductor in the LC-resonator and the SQUID loop part of the other resonator. This makes the resonance frequency of the SQUID-resonator a function of the flux in the LC-resonator. It is shown that mutual and self inductances in the SQUID loop give rise to two transcendental constraints, for the magnetic flux in the SQUID loop, and the generalised flux across the SQUID. By an approximate solution for the constraints and under the assumption that the loop inductance is small compared to the SQUID inductance, we derive an approximate description for the circuit dynamics. We demonstrate that the circuit Hamiltonian contains the asymmetric opto-mechanical interaction, but in addition also a self-Kerr non-linearity in the analogue optical cavity, as well as a weak cross-Kerr interaction between the two resonators.

Acknowledgement

It has been a journey, one that is now finally reaching its destination. Since it has taken longer than anticipated, many thanks for your patience. I have learned much along the way, many insights, and not only about science.

Starting from what may be described as a stubbornly idealistic mindset, I learned to embrace a bit of pragmatism; for if in a given challenge one does does not see an acceptable solution on its *surface*, one must try things that may not be *correct*. The thing is, in practice nothing really is ever perfect—there's always more behind it than fits the human mind. No answer to any question or challenge is therefore perfect, except for, perhaps, a small part in the idealised world of mathematics, but certainly not physics dealing with reality. One should also ask the question *how precise an answer is needed* for it to be useful. On the other hand, science is about really understanding reality, or at least parts of it. Thus, in a way, there is a conflict between idealism and pragmatism in research, but that is life…

What my time as a student in the Steele lab has taught me is to form a perspective in dealing with the impossible questions of research. For that I am grateful. While I do not find it necessary to broadcast the names into the world, I must say it was a pleasure to meet the members and fellow students in the group, and share and discuss thoughts and ideas of any kind.

Contents

1 Introduction **4**
- 1.1 Cavity opto-mechanics . . . 4
- 1.2 Quantum opto-mechanics . . . 5
- 1.3 Enhanced coupling through the Josephson effect . . . 6
- 1.4 Analogue quantum simulation of cavity opto-mechanics . . . 6
- 1.5 Scope of this work . . . 6

2 Resonators **8**
- 2.1 Lumped element resonators . . . 9
  - 2.1.1 Series RLC-circuit . . . 9
  - 2.1.2 Parallel RLC-circuit . . . 10
  - 2.1.3 Q-factor and decay rate . . . 10
  - 2.1.4 Adding loss through complex resonant frequency . . . 11
- 2.2 Transmission line resonators . . . 12
  - 2.2.1 Transmission line theory . . . 12
  - 2.2.2 Loaded transmission lines . . . 16
  - 2.2.3 Coplanar wave-guides . . . 18
  - 2.2.4 Transmission line resonators . . . 19
- 2.3 Capacitively coupled resonators . . . 23
  - 2.3.1 One port coupled parallel RLC-circuit . . . 23
  - 2.3.2 Side-coupled to transmission line . . . 27

3 Flux tuneable resonators **30**
- 3.1 Superconducting quantum interference device . . . 30
  - 3.1.1 Superconductivity . . . 30
  - 3.1.2 Flux quantisation . . . 31
  - 3.1.3 Josephson effect . . . 32
  - 3.1.4 Two Josephson junctions in parallel . . . 36
  - 3.1.5 A more practical SQUID considered as a lumped element . . . 39
- 3.2 Tuneable resonators . . . 40
  - 3.2.1 Flux tuneable lumped element resonator . . . 40
  - 3.2.2 Flux tuneable transmission line resonator . . . 43

4 Going from a circuit Lagrangian to a quantised Hamiltonian **51**
- 4.1 Lagrangian formulation of circuit theory . . . 52
  - 4.1.1 Generalised branch flux and branch charge . . . 52
  - 4.1.2 Constitutive relations en stored energy . . . 52
  - 4.1.3 Degrees of freedom - constraints . . . 54

4.1.4 Equations of motion and Lagrangian for an electrical circuit . . . 54
4.1.5 Limitations in circuit theory and Lagrangian mechanics . . . 56
4.2 Various linear and non-linear circuit elements . . . 57
4.2.1 A linear capacitor . . . 57
4.2.2 A linear inductor . . . 57
4.2.3 Dealing with a linear mutual inductance . . . 58
4.2.4 The Josephson non-linear inductor . . . 60
4.3 Quantum electromagnetic circuit theory . . . 60
4.3.1 Transforming to the Hamiltonian formalism . . . 60
4.3.2 Describing the Hamiltonian in terms of a complex scalar field . . . 61
4.3.3 Going from a classical to a quantum mechanical circuit description . . . 62

5 Deriving the opto-mechanical coupling from the circuit Lagrangian 63
5.1 Lumped element SQUID opto-mechanics curcuit . . . 64
5.2 Classical equations of motion . . . 64
5.2.1 Inductance matrix . . . 65
5.2.2 SQUID inductances and constraints . . . 65
5.2.3 Capacitive relations . . . 66
5.2.4 Two extra constraints in the limit of zero junction capacitances . . . 66
5.2.5 Exact equations of motion in the limit of zero junction capacitances . . . 66
5.2.6 Equilibrium positions . . . 67
5.2.7 A first attempt at an approximate solution . . . 68
5.2.8 A complication in Lagrangian mechanics . . . 69
5.2.9 Small loop inductance approximation . . . 70
5.2.10 First order recursive approximation . . . 70
5.2.11 Approximate equations of motion . . . 72
5.2.12 Equilibrium position inductor flux . . . 72
5.3 Circuit Lagrangian . . . 73
5.3.1 Approximate Lagrangian . . . 73
5.4 Quantum mechanical description . . . 74
5.4.1 Legendre transform the Lagrangian to a Hamiltonian . . . 74
5.4.2 Simplifying the Hamiltonian . . . 74
5.4.3 Canonical quantisation . . . 75
5.4.4 A further approximation . . . 77
5.4.5 Characterisation . . . 78

6 Conclusion and Outlook 79
6.1 SQUID opto-mechanics with loop inductances . . . 79
6.1.1 Complications in Lagrangian mechanics . . . 79
6.1.2 A way out? . . . 80
6.1.3 Speculations on consequences and possible applications . . . 80
6.2 SQUID opto-mechanics in first order recursive approximation with small loop inductances 81
6.3 Final remarks . . . 82

Bibliography 83

Appendix - full Hamiltonian for the SQUID opto-mechanics circuit 87

Chapter 1

Introduction

The title of this work may be considered a strange one; it encompasses an interaction between an optical and a mechanical system, yet it is about an electrical circuit formulation that involves neither optical nor mechanical parts. The essence is that we will analyse an electrically implemented "analogue quantum simulation" of an opto-mechanical system. This basically means that we analyse an electrical circuit that presumedly behaves in analogue ways as an opto-mechanical system. It is not that simple however and therefore I have much to explain. Let us start with a general but short description of what opto-mechanics entails, and then step by step explain where the idea of an analogue simulation fits in one of the possibly realisable paths leading to the goal of achieving full control over the quantum state of a mechanical object—especially for the generation of macroscopic superposition states, i.e. states described by a non-Gaussian wave-function. Afterwards we give an answer to the question "*why have we have embarked on this strange endeavour*" and explain our motivation, possible applications and further implications the results of this work may bring forth.

1.1 Cavity opto-mechanics

In a sense, starting with an observation by Kepler [1] in the year 1619 that the tail of a comet always points away from the sun, the field of cavity opto-mechanics, see Ref. [2] for a review, focusses on the interaction between optical and mechanical degrees of freedom, all based on a Hamiltonian description of optical radiation reflecting on a mechanically moveable mirror as first derived by Law [3]. Conceptually, as drawn Fig. 1.1, an opto-mechanical system is constructed from two opposing mirrors set some distance apart—forming an optical cavity in which light can bounce back and forth and may form standing wave resonances if the wavelength coincides with a resonance—and one of the mirrors mounted on a spring such that it can move back and forth, under the influence of the radiation pressure, thereby changing the separation distance between the mirrors and thus the optical resonance frequency.

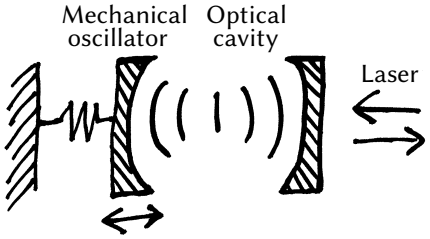

Figure 1.1: Schematic drawing of a typical cavity opto-mechanics setup.

Because the energy involved in a single quantum of light in an optical frequency is much higher than the average thermal energy in a degree of freedom at room temperature: $\hbar\omega_{\text{optics}} \gg \kappa_b T$, the field of quantum optics [4] provides a well established toolbox for manipulating the states of optical systems due to an absence of thermal de-coherence. The same cannot be said of mechanical systems due to their much lower resonant frequencies even for nano-scale mechanical resonators. However as we shall see, interacting optical systems with mechanical systems through a radiation pressure interaction yields interesting opportunities for exerting control on mechanical degrees of freedom through optical channels.

The radiation pressure force on the mechanics, being quadratic in radiation and having a back-action linear in position on the optical cavity by changing the frequency (energy) of the radiation field, constitutes a non-linear and asymmetric interaction between the optical and mechanical part of the system. This has many interesting consequences and applications, some of which have been demonstrated experimentally while others are only anticipated theoretically. Some of the already demonstrated consequences are cooling of the mechanical resonator to its quantum ground state [5, 6], opto-mechanically induced transparency (OMIT) [7, 8] and absorption/amplification [9, 10], mechanical position measurements with a precision approaching the standard quantum limit [11]—which states that, as a trade of between shot-noise in the measurement signal (photon number uncertainty, decreasing with intensity) and the measurement back-action (increasing with intensity), the total measurement imprecision in continuous measurements cannot be lower than the zero-point fluctuations of the oscillator, see Ref. [12] for a thorough discussion—generation of squeezed states of the the optical cavity field [13, 14] and the mechanical oscillator [15, 16, 17] and coherent state transfer of quantum information from one system to the mechanics [18, 19]. Note that this paragraph constitutes by no means an up to date nor complete literature survey.

1.2 Quantum opto-mechanics

With most of these phenomena, except for the transfer of a single photon of quantum information, the expectation values of the measurement outcomes behave according to what classical mechanics would predict, it is only in the statistics where one might observe quantum noise or limits such as the quantum ground state (both actually correspond with Heisenberg's uncertainty relation) that quantum effects are observable. The reason for this is that the optical and mechanical parts of the system constitute harmonic degrees of freedom and that all so far mentioned phenomena follow from a weak opto-mechanical coupling that is well described by a linearised variant of the interaction. In this regime, the interaction always turns Gaussian states (states with a Gaussian wave-function, a subclass of states whose observable's average behave according to classical mechanics) into Gaussian states. This means that it is impossible to generate non-Gaussian states that can not be described in classical mechanics—an illustrative example of such a state is a cat state which can be described as a superposition of two Gaussian states akin to Schrödinger's cat [20] being both dead and alive.

In order to generate such non-Gaussian states from Gaussian states, a significant non-linearity is needed in the system. In opto-mechanical systems this may be achieved by increasing the opto-mechanical coupling strength until the interaction generates an effective Kerr non-linearity [21] in the optical cavity that upon the addition or escape of a single photon shifts the cavity frequency by more than its resonance line-width; this marks what is called the single photon strong coupling regime.

Another options is to combine opto-mechanics with a single photon sources and detectors [22]. An example is the (non-)emission of a photon to the opto-mechanical cavity that is entangled with the quantum state of a two level system (a qubit) as a single photon source, this has been demonstrated in Ref. [19], and has potential applications as a quantum memory and carrier frequency converter for quantum information. Yet another option is to add intrinsic non-linearity to the cavity or the mechanics,

but that would conceptually be close to circuit quantum electrodynamics and would therefore not bring much news to the table; only a mechanical qubit would be a remarkable novelty as well as a low frequency qubit in a thermal state—on this work is done by other people in the group. Both these alternative options are outside the scope of this work, but are merely mentioned as alternative approaches for obtaining quantum state control over mechanical objects.

1.3 Enhanced coupling through the Josephson effect

Experimentally speaking, the single photon strong coupling regime has proven to be rather elusive; so far as at the time of writing it has not been achieved. All current approaches to opto-mechanics have been widely studied and seem to have reached a plateau in the optimisation of the coupling rate. A new idea, that has been proposed in a couple of different forms in Refs. [23, 24, 25], is to mediate the movement of a mechanical element by coupling its movement to the magnetic flux tuning a superconducting quantum interference device (SQUID), which as a flux-tuneable inductance can be seen as to frequency tune the microwave LC-circuit equivalent of an optical cavity (in contrast to traditional microwave opto-mechanics where mechanical movement of a capacitor plate tunes the capacitance). Incidentally, the second reference also proposes to incorporate the dynamical Casimir effect into the system by parametrically driving the SQUID inductance.

The crux of the idea is that the non-linearity in the Josephson inductance as a function of flux boosts the coupling. More important is that all of above references conclude that with this kind of approach it is feasible to reach the single photon strong coupling regime. Another approach using Josephson junctions in opto-mechanics based on charge tuning the inductance of a single Cooper-pair transistor is proposed in Refs. [26, 27] and first experimental results are reported in Ref. [28] but were far from strong coupling; a more recent experiment incorporating a piëzo electric mechanical oscillator in the same architecture achieved near ground state cooling [29].

1.4 Analogue quantum simulation of cavity opto-mechanics

However, such a combination of a SQUID with embedded mechanical resonator is challenging to fabricate, and recently it has been proposed in Ref. [30] that the mechanical element embedded in the SQUID be replaced by low frequency electrical resonator whose magnetic field tunes the SQUID inductance. We call this an analogue quantum simulation of an opto-mechanical system since there is no mechanics involved, but the high level dynamics should be similar enough to call such a system an electrical equivalent of an opto-mechanical system. The main point is that—even though it is not useful for e.g. observing quantum-gravitational effects (unless the mass of the electrical charge carriers is significant however unlikely)—such a system may give the opportunity to explore the physics of the single photon strong coupling regime in an intermediate all electrical circuit before making the step incorporating a mechanical element.

A first experiment with such a circuit is described in Ref. [31] demonstrated opto-mechanical effects, i.e. OMIT, but did not achieve single photon strong coupling.

1.5 Scope of this work

In this thesis we study and derive theoretical models for circuits, see e.g. Fig. 1.2, whose dynamics are analogue to opto-mechanical systems. Starting from the classical circuit equations of motion we derive the quantised Hamiltonian and predict from the result its opto-mechanical properties. We do this based on a careful analysis of a SQUID with its loop inductance sharing a mutual inductance with another

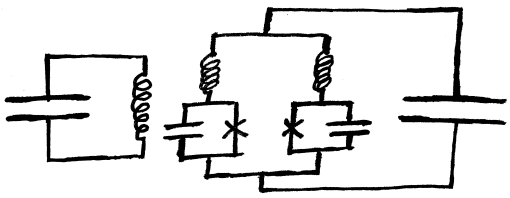

Figure 1.2: The circuit for the analogue quantum simulation of opto-mechanics. It is a lumped element version of the transmission line circuit proposed in Ref. [30]. There is a mutual inductance between the inductor on the left and the SQUID loop on the right.

disjoint inductor. From the result we predict the strength of the opto-mechanical parameters in the circuit. We also discuss the effect of the intrinsic oscillator anharmonicity due to the Josephson junctions.

The report is structured as follows. In

Chapter 2 we introduce the concept of resonators, the transmission line equations and the most common way microwave resonators are implemented.

Chapter 3 explains what a SQUID is, discusses its characteristics and how a SQUID as a flux tuneable inductance can be used to create frequency tuneable resonators.

Chapter 4 describes the procedure of circuit quantisation and how in flux variable representation mutual inductances can be taken into account in the circuit description.

Chapter 5 Applies this to the circuit simulating quantum opto-mechanics. In

Chapter 6 we conclude and provide an outlook for future research directions. In the

Appendix we derive the full Hamiltonian for the simulation circuit in the absence of approximations.

Chapter 2

Resonators

An intuitive example of a resonator is that of a swing as drawn in Fig. 2.1a. If one gives the swing a push it starts oscillating back and forth (with decaying amplitude due to friction). Now when one gives pushes periodically with a time period between each push that coincides with the time the swing takes to oscillate back and forth once, then the amplitude of the oscillatory movements increases on each consecutive push (until a balance is reached due to friction). On the other hand when the timing of the pushes is different, the growth in the amplitude of the oscillations does not occur. This is called resonant behaviour, and a device that exhibits such behaviour is called a resonator.

More formally spoken, a resonator is a device that exhibits higher oscillatory behaviour when periodically driven at one of its resonance frequencies than when driven at other non-resonant frequencies.

(a) **(b)**

Figure 2.1: An intuitive example of a resonator is that of **(a)** a swing or equivalently **(b)** a two-dimensional pendulum that consists of a mass m hanging on a (massless) rod of length ℓ attached with a hinge to the ceiling such that the mass can oscillate back and forth over part of a circular trajectory centred around the attachment point and in a vertical plane determined by the hinge.

We start with a discussion of lumped element circuit resonators because it turns out that different kinds of resonators behave similarly when driven near resonance. As such they can be described in terms of what is called an equivalent lumped element circuit. After reviewing the standard lumped element resonators, the transmission line resonator is introduced[1]. The chapter concludes with a discussion on capacitively coupling resonators to a feed-line.

[1]The sections on lumped element resonators and transmission line resonators are inspired by the explanations given in the book by Pozar [32]. A more in depth description of circuit theory can be found in e.g. the book by Peikari [33].

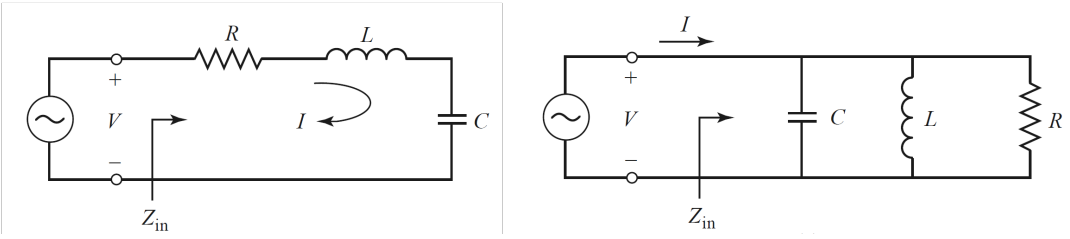

(a) **(b)**

Figure 2.2: Lumped element resonant circuits. **(a)** Series RLC-circuit. **(b)** Parallel RLC-circuit. Figures from Ref. [32].

2.1 Lumped element resonators

In circuit theory, two standard textbook examples of linear oscillators are the series and the parallel RLC-circuit. Both are depicted in Fig. 2.2.

2.1.1 Series RLC-circuit

The series RLC-circuit, depicted in Fig. 2.2a, is considered first. From the circuit topology it is evident that the current $\mathcal{I}$ is the same across all elements.

Applying Kirchhoff's voltage law (the sum of voltages across electric components connected in a loop is zero: $\Sigma_{n\in\text{loop}}\mathcal{V}_n = 0$) and substituting the voltage current relations for the resistor $\mathcal{V}_R = \mathcal{I}R$, capacitor $\mathcal{V}_C = \frac{1}{C}\int_{-\infty}^{t}\mathcal{I}\,\mathrm{d}t'$ and inductor $\mathcal{V}_L = L\frac{\mathrm{d}\mathcal{I}}{\mathrm{d}t}$ yields after taking a time derivative

$$L\frac{\mathrm{d}^2\mathcal{I}}{\mathrm{d}t^2} + R\frac{\mathrm{d}\mathcal{I}}{\mathrm{d}t} + \frac{1}{C}\mathcal{I} = \frac{\mathrm{d}\mathcal{V}}{\mathrm{d}t}\,. \tag{2.1}$$

This is the equation of motion for a damped harmonic oscillator with as mechanical analogue mass L, spring constant $\frac{1}{C}$ and damping R, driven with a force $\frac{\mathrm{d}\mathcal{V}}{\mathrm{d}t}$ generated by the source.

Equation (2.1) is most easily solved in the frequency domain. Introducing the Fourier transform $X(\omega) = \int_{-\infty}^{\infty}\mathcal{X}(t)\mathrm{e}^{-\mathrm{i}\omega t}\,\mathrm{d}t$, it is transformed to

$$I = \frac{V}{\frac{1}{\mathrm{i}\omega C} + \mathrm{i}\omega L + R} = \frac{V}{Z_{\text{in}}}\,, \tag{2.2}$$

which directly provides an algebraic solution. In the last step the input impedance at the circuit connection with the voltage source is defined as

$$Z_{\text{in}} \equiv \frac{V_{\text{in}}}{I_{\text{in}}} = \frac{1}{\mathrm{i}\omega C} + \mathrm{i}\omega L + R\,. \tag{2.3}$$

As can be seen in Eq. (2.2) resonance occurs at the frequency where $\mathrm{Im}\{Z_{\text{in}}\} = 0$ (the damping constant R prevents the oscillations from becoming unbounded). This is the condition that determines the resonant frequency. In the present case it corresponds to: $\omega_0 L - \frac{1}{\omega_0 C} = 0$, which is easily solved giving the resonance frequency

$$\omega_0 = \frac{1}{\sqrt{LC}}\,. \tag{2.4}$$

In this work the interest is in the behaviour of a resonator near resonance. To simplify in that regime, the input impedance is usually written in terms of ω_0 and is then often approximated by a Taylor expansion around the resonant frequency

$$Z_{\text{in}} = R + \mathrm{i}L\left(\omega - \frac{{\omega_0}^2}{\omega}\right) \approx R + \mathrm{i}2L(\omega - \omega_0)\,. \tag{2.5}$$

2.1.2 Parallel RLC-circuit

Next we consider the parallel RLC-circuit as depicted[2] in Fig. 2.2b. In contrast to the series RLC-circuit, it is the voltage $\mathcal{V}$ across each constitutive component that is the same as can be seen from the circuit topology.

Invoking Kirchhoff's node law (the sum of currents going through the connections of a circuit node is zero: $\Sigma_{n\in\text{node}}\mathcal{I}_n = 0$) together with the current voltage relations (now in the form emphasising current: $\mathcal{I}_R = \frac{\mathcal{V}}{R}$ for the resistor, $\mathcal{I}_C = C\frac{\mathrm{d}V}{\mathrm{d}t}$ for the capacitor and $\mathcal{I}_L = \frac{1}{L}\int_{-\infty}^{t}\mathcal{V}\,\mathrm{d}t$ for the inductor) gives

$$C\frac{\mathrm{d}^2\mathcal{V}}{\mathrm{d}t^2} + \frac{1}{R}\frac{\mathrm{d}\mathcal{V}}{\mathrm{d}t} + \frac{1}{L}\mathcal{V} = \frac{\mathrm{d}\mathcal{I}}{\mathrm{d}t}\,. \tag{2.6}$$

Similar to the series RLC-circuit, this is an equation equivalent to a driven damped harmonic oscillator, but in this case described in terms of voltage $\mathcal{V}$ and with mass C, damping $\frac{1}{R}$, spring constant $\frac{1}{L}$ and driving force $\frac{\mathrm{d}\mathcal{I}}{\mathrm{d}t}$ generated by the source.

Taking the Fourier transform of Eq. (2.6) gives

$$V = \frac{I}{\mathrm{i}\omega C + \frac{1}{\mathrm{i}\omega L} + \frac{1}{R}} = \frac{I}{Y_{\text{in}}} \tag{2.7}$$

and subsequently provides a solution in terms of the circuit input admittance

$$Y_{\text{in}} \equiv \frac{I_{\text{in}}}{V_{\text{in}}} = \frac{1}{Z_{\text{in}}} = \mathrm{i}\omega C + \frac{1}{\mathrm{i}\omega L} + \frac{1}{R}\,. \tag{2.8}$$

For this circuit the resonance condition is $\mathrm{Im}\{Y_{\text{in}}\} = 0$ which gives for the resonant frequency $\omega_0 = \frac{1}{\sqrt{LC}}$, the same as for the series RLC-circuit. A Taylor expansion of the input admittance written in terms of ω_0 gives an approximate expression

$$Y_{\text{in}} = \frac{1}{R} + \mathrm{i}C\left(\omega - \frac{{\omega_0}^2}{\omega}\right) \approx \frac{1}{R} + \mathrm{i}2C(\omega - \omega_0)\,, \tag{2.9}$$

which is valid in the region around the resonant frequency.

2.1.3 *Q*-factor and decay rate

The Q-factor (also called the quality-factor) of a resonator is defined as

$$Q \equiv \omega_0 \frac{\text{average energy stored}}{\text{energy dissipated per second}} \tag{2.10}$$

and is proportional to the fraction of stored energy that is dissipated from the resonator per oscillation. External circuits connected to the resonator decrease the Q-factor as they open additional dissipation

[2] There is a subtle error in this figure. The ideal voltage source should be an ideal current source. The reason is that an infinite internal resistance is needed in the source to avoid altering the parallel circuit characteristics.

channels. The Q-factor of the resonator itself in the absence of loading effects Q_0 is denoted the unloaded Q-factor. The Q-factor with loading effects Q_L is called the loaded Q-factor.

We now work out the unloaded Q-factor for the series RLC-resonator. Substituting the average magnetic energy $\frac{1}{4}L|I|^2$ plus electric energy $\frac{1}{4}C|V_C|^2 = \frac{1}{4}\frac{1}{C\omega_0{}^2}|I|^2$, both of which have equal contribution at resonance[3], and average energy dissipation $\frac{1}{2}R|I|^2$ into the definition (2.10) gives[4]

$$Q_0 = \frac{\omega_0 L}{R} = \frac{1}{\omega_0 RC} \quad \text{for the series RLC-circuit}\,. \tag{2.11a}$$

Next we work out the unloaded Q-factor for the parallel RLC circuit. Substitution of the electric energy $\frac{1}{4}C|V|^2$ plus magnetic energy $\frac{1}{4}L|I_L|^2 = \frac{1}{4}\frac{1}{L\omega_0{}^2}|V|^2$, which both as with the series RLC-circuit equally contribute at resonance, and the dissipation rate $\frac{1}{2}\frac{1}{R}|V|^2$ yields

$$Q_0 = \frac{R}{\omega_0 L} = \omega_0 RC \quad \text{for the parallel RLC-circuit}\,. \tag{2.11b}$$

The loading effects from external circuits connected to the resonator can be taken into account as a load resistor R_L which in case of the series RLC-circuit adds in series to the internal resistance: $R + R_\mathrm{L}$ and combines in parallel in case of the parallel RLC-circuit: $\frac{RR_\mathrm{L}}{R+R_\mathrm{L}}$. Then, the external Q-factor is defined as

$$Q_\mathrm{e} = \begin{cases} \frac{\omega_0 L}{R_\mathrm{L}} & \text{for the series RLC-circuit}\,, \\ \frac{R_\mathrm{L}}{\omega_0 L} & \text{for the parallel RLC-circuit}\,, \end{cases} \tag{2.12}$$

such that the unloaded and external Q-factor add up reciprocally to the loaded Q-factor: $\frac{1}{Q_\mathrm{L}} = \frac{1}{Q_0} + \frac{1}{Q_\mathrm{e}}$.

An analogue parameter is the decay rate which is defined as

$$\kappa \equiv \frac{\text{energy dissipated per second}}{\text{average energy stored}} = \frac{\omega_0}{Q}\,. \tag{2.13}$$

The decay rate can also be separated in an internal $\kappa_\mathrm{i} = \frac{\omega_0}{Q_0}$ and external contribution $\kappa_\mathrm{e} = \frac{\omega_0}{Q_\mathrm{e}}$, both of which however add up directly to the total decay rate: $\kappa = \kappa_\mathrm{i} + \kappa_\mathrm{e}$.

2.1.4 Adding loss through complex resonant frequency

In the book by Pozar [32], a trick is described for adding loss to a system that is initially modelled as lossless and whose input impedance or admittance is approximated as a first order Taylor expansion around a resonance frequency.

Because loss in an electrical circuit is described by the real part of its input impedance or admittance, the idea is to replace the resonant frequency in the $\omega - \omega_0$ term with a complex resonant frequency defined as

$$\omega_0 \leftarrow \omega_0 \left(1 + \frac{\mathrm{i}}{2Q_0}\right) \tag{2.14}$$

[3] That for an RLC resonator the electrical and magnetic energy are equal when driven at resonance is easily checked by substituting the resonance frequency into the respective expressions.

[4] The expressions for energy can be derived from the definition in circuit theory of instantaneous power

$$\mathcal{P}(t) = \mathcal{I}(t)\mathcal{V}(t)$$

and energy

$$\mathcal{E}(T) = \int_{-\infty}^{t} \mathcal{P}(t')\,\mathrm{d}t'$$

together with the elements constitutive relations. Using the fact that in linear circuits under time harmonic drive all state variables oscillate with the drive frequency, applying a few trigonometric identities and taking the average by leaving out the time oscillating terms, gives the used results which are easily expressed in phasor notation. For the energy integral one further assumes that the currents and voltages are switched on adiabatically between $t = -\infty$ and $t = 0$.

such that upon substitution the imaginary part of the complex resonance frequency appears as a real valued dissipative term in the input impedance. This can be shown to work for both the parallel and series resonant circuits:

$$Z_{\text{in}} \approx \mathrm{i}2L(\omega-\omega_0) \rightarrow \frac{\omega_0 L}{Q_0} + \mathrm{i}2L(\omega-\omega_0) = R + \mathrm{i}2L(\omega-\omega_0) \qquad \text{for the series RLC-circuit}, \tag{2.15a}$$

$$Y_{\text{in}} \approx \mathrm{i}2C(\omega-\omega_0) \rightarrow \frac{\omega_0 C}{Q_0} + \mathrm{i}2C(\omega-\omega_0) = \frac{1}{R} + \mathrm{i}2C(\omega-\omega_0) \qquad \text{for the parallel RLC-circuit}, \tag{2.15b}$$

where for both circuits in the last step the respective unloaded Q-factor as derived in Eqs. (2.11a) and (2.11b) is substituted.

This method yields exact results for the dissipation of the series and parallel RLC-circuits where the losses are independent of frequency. For resonators whose dissipative terms do depend on frequency this method is an approximation that

- assigns the losses at the resonant frequency to all frequencies,
- requires the resonance frequency to be independent of losses or the losses to be weak such that any subsequent shift in resonance frequency is negligible, and
- assumes that the losses can be modelled as a linear dissipative element.

This however is reasonable for high Q-factor resonators where the terms relating to dissipation are small, especially when only the region near the resonant frequency is considered.

2.2 Transmission line resonators

An introduction to transmission line resonators is provided in this chapter where we mainly follow the book on microwave engineering by Pozar [32]. A derivation for the dynamics of a transmission line based on circuit theory is given, but first the differences between a transmission line and the underlying assumptions of circuit theory are discussed. In the process a solution in the form of time harmonic propagating waves is found. Then the effects of a load by which a transmission line may be terminated are discussed. As will be explained, it gives rise to reflection of the input signal and results in the emergence of standing waves. This will finally lead us towards the theory of transmission line resonators and a description of their dynamics in terms of equivalent lumped element circuits.

2.2.1 Transmission line theory

A transmission line consists of two parallel elongated conductors, and is usually depicted as a two-wire line as in Fig. 2.3a. The conductors can have any geometry as long as they are parallel and elongated. Examples of geometries are the coaxial cable, but also the coplanar wave-guide that will be discussed later.

Distributed elements model

The main difference between circuit and transmission line theory lies in the size of the corresponding electrical circuits. Where circuit theory assumes the circuit size to be much smaller than the wavelength λ of the signals propagating through the circuit, a transmission line has a length that is at least a considerable fraction of a wavelength. This means that the voltages $\mathcal{V}(z,t)$ and currents $\mathcal{I}(z,t)$ will vary over its length. Therefore the lumped element approach of circuit theory can not be applied directly to a

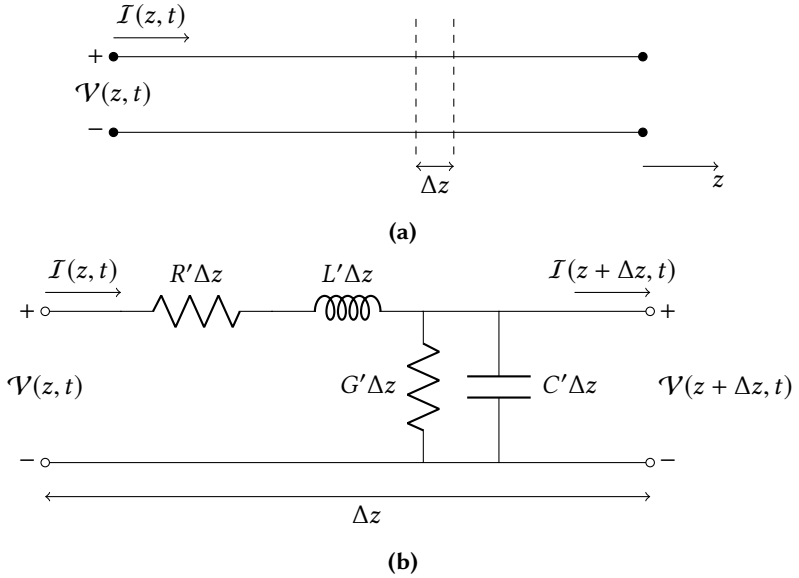

Figure 2.3: Schematics illustrating the distributed element model of a transmission line: **(a)** a two wire transmission line and **(b)** a lumped element circuit describing the dynamics of a short transmission line segment. The length Δz is much shorter than the wavelength over which the voltage or current vary spatially such that the lumped element description of the segment is valid.

transmission line, only to infinitely short line segments. As such a transmission line can be considered a distributed parameter network.

Now, if one considers only a short segment of length $\Delta z \ll \lambda$ much smaller then the wavelength (and the same applies to the separation distance between the two conductors), such a segment can be modelled as a lumped element circuit as presented in Fig. 2.3b where R' and L' respectively denote the series resistance and inductance and G' and C' respectively the shunt conductance and capacitance, all per unit length. A transmission line can be seen as a large sequence of such segments connected in series.

Applying Kirchhoff's voltage- and current law to such a segment gives

$$\mathcal{V}(z,t) - R'\Delta z\mathcal{I}(z,t) - L'\Delta z\frac{\partial \mathcal{I}(z,t)}{\partial t} - \mathcal{V}(z+\Delta z,t) = 0\,, \tag{2.16a}$$

$$\mathcal{I}(z,t) - G'\Delta z\mathcal{V}(z+\Delta z,t) - C'\Delta z\frac{\partial \mathcal{V}(z+\Delta z,t)}{\partial t} - \mathcal{I}(z+\Delta z,t) = 0\,. \tag{2.16b}$$

Dividing both equations by Δz and taking the limit $\Delta z \to 0$, letting the segments be infinitesimally short, then yields the equations

$$\frac{\partial \mathcal{V}(z,t)}{\partial z} = -R'\mathcal{I}(z,t) - L'\frac{\partial \mathcal{I}(z,t)}{\partial t}\,, \tag{2.17a}$$

$$\frac{\partial \mathcal{I}(z,t)}{\partial z} = -G'\mathcal{V}(z,t) - C'\frac{\partial \mathcal{V}(z,t)}{\partial t}\,, \tag{2.17b}$$

which are known as the "*telegrapher equations*".

Phasor notation for time harmonic signals

When dealing with time harmonic signals[5], it is convenient to work in so called phasor representation. It is a short hand notation for time harmonic signals in terms of complex exponentials which are much easier to work with than the corresponding real valued trigonometric terms.

Let $\mathcal{X}$ be a signal of time harmonic form

$$\mathcal{X}(z,t) = \mathcal{X}_0(z)\cos(\omega t + \phi_{\mathcal{X}})\,, \tag{2.18}$$

where $\mathcal{X}(z,t)$ denotes voltage or current, $\mathcal{X}_0(z)$ the real amplitudes, ω the radian frequency and $\phi_{\mathcal{X}}$ the phase shift of the signal at time $t = 0$. Its phasor representation is obtained by carrying out the following substitution

$$\mathcal{X}(z,t) \leftarrow \mathcal{X}_0(z)\mathrm{e}^{\mathrm{i}(\omega t+\phi_{\mathcal{X}})} = X(z)\mathrm{e}^{\mathrm{i}\omega t}\,, \tag{2.19}$$

where $X(z)$ as the signals complex amplitude now incorporates the phase information $\mathrm{e}^{i\phi_{\mathcal{X}}}$. Through Euler's formula $\mathrm{e}^{\mathrm{i}x} = \cos(x) + \mathrm{i}\sin(x)$, the real signals can be (re)obtained as the real part of the complex phasors

$$\mathcal{X}(z,t) = \mathrm{Re}\left\{X(z)\mathrm{e}^{\mathrm{i}\omega t}\right\}\,. \tag{2.20}$$

Phasor representation is however only valid when the mathematical operations involved are linear[6]. Here non-script letters denote the complex equivalent of the real valued signals denoted by script letters.

Wave propagation

In phasor notation the telegrapher Eqs. (2.17) simplify from two partial differential equations to two coupled ordinary differential equations

$$\frac{\mathrm{d}V(z)}{\mathrm{d}z} = -(R' + \mathrm{i}\omega L')I(z)\,, \tag{2.21a}$$

$$\frac{\mathrm{d}I(z)}{\mathrm{d}z} = -(G' + \mathrm{i}\omega C')V(z)\,. \tag{2.21b}$$

Note how the time dependence carried by the factor $\mathrm{e}^{\mathrm{i}\omega t}$ shared by all terms drops out of the equation. These equations can be decoupled by differentiating them and substituting the expression from one into the other, which yields two uncoupled second order differential equations

$$\frac{\mathrm{d}^2V(z)}{\mathrm{d}z^2} - \gamma^2 V(z) = 0\,, \tag{2.22a}$$

$$\frac{\mathrm{d}^2I(z)}{\mathrm{d}z^2} - \gamma^2 I(z) = 0\,, \tag{2.22b}$$

where $\gamma = \sqrt{(R' + \mathrm{i}\omega L')(G' + \mathrm{i}\omega C')}$ is the complex propagation constant. The general solution to the ordinary second order differential equations is

$$V(z) = V_0^+\mathrm{e}^{-\gamma z} + V_0^-\mathrm{e}^{\gamma z}\,, \tag{2.23a}$$

$$I(z) = I_0^+\mathrm{e}^{-\gamma z} + I_0^-\mathrm{e}^{\gamma z}\,. \tag{2.23b}$$

[5]Note there is no loss of generality in assuming a signal time harmonic as any signal can be denoted as a linear combination of time harmonic signals with different frequencies by its Fourier transform.

[6]That is any operator $\mathcal{L}$ that satisfies $\mathcal{L}\{aX(z) + bY(z)\} = a\mathcal{L}\{X(z)\} + b\mathcal{L}\{Y(z)\}$. If that is not the case, one should work with the full Fourier representation of the involved signals.

Writing the propagation constant as the sum of its imaginary and real part $\gamma = \alpha + \mathrm{i}\beta$ and tagging on the implied time dependence (converting back to the time domain),

$$\mathcal{V}(z,t) = \mathrm{Re}\left\{V_0^+ \mathrm{e}^{-\alpha z}\mathrm{e}^{\mathrm{i}(\omega t-\beta z)} + V_0^- \mathrm{e}^{\alpha z}\mathrm{e}^{\mathrm{i}(\omega t+\beta z)}\right\}, \tag{2.24}$$

it is seen that the general solution consists of a linear combination of waves, with wavelength (the spatial distance between two identical points on two successive waveforms at the same instance of time—neglecting dissipation)

$$\lambda = \frac{2\pi}{\beta} \tag{2.25}$$

and propagating forward and backward with speed given by the phase velocity

$$v = \frac{\mathrm{d}z}{\mathrm{d}t} = \frac{\mathrm{d}}{\mathrm{d}t}\left(\frac{\omega t - \text{constant}}{\beta}\right) = \frac{\omega}{\beta}. \tag{2.26}$$

In essence, the imaginary part β of the propagation constant, the phase-constant, fulfils the role of wave-number. Furthermore, it is seen that the real part α of the propagation constant, the attenuation constant, quantifies the decay of the signal with propagation distance z.

Characteristic impedance

Substitution of the voltage solution (2.23a) into the first telegrapher Eq. (2.17b) gives a relation between current and voltage

$$I(z) = \frac{\gamma}{R' + \mathrm{i}\omega L'}\left(V_0^+ \mathrm{e}^{-\gamma z} - V_0^- \mathrm{e}^{\gamma z}\right). \tag{2.27}$$

Comparing this result with the current solution (2.23b) we can define a "characteristic impedance"

$$Z_0 = \frac{R' + \mathrm{i}\omega L'}{\gamma} = \sqrt{\frac{R' + \mathrm{i}\omega L'}{G' + \mathrm{i}\omega C'}} \tag{2.28}$$

to relate the voltage and current amplitudes of the forward and backward propagating waves such that

$$Z_0 = \frac{V_0^+}{I_0^+} = -\frac{V_0^-}{I_0^-}, \tag{2.29}$$

in essence an impedance for running waves.

The lossless line

In this work we will be dealing with superconducting circuits that will be approximately lossless. As such we can set the terms R' and G' to zero. In that case $\gamma = \mathrm{i}\omega\sqrt{L'C'}$ which implies that the attenuation constant $\alpha = 0$ and that the wave-number $\beta = \omega\sqrt{L'C'}$. From Eq. (2.28), the characteristic impedance of the line then becomes a real number

$$Z_0 = \sqrt{\frac{L'}{C'}}. \tag{2.30}$$

With zero attenuation, the general solution for the voltage along the line becomes

$$V(z) = V_0^+ \mathrm{e}^{-\mathrm{i}\beta z} + V_0^- \mathrm{e}^{\mathrm{i}\beta z} \tag{2.31}$$

and through the definition for the characteristic impedance the general solution for the current along the line can then be written as

$$I(z) = \frac{V_0^+}{Z_0}\mathrm{e}^{-\mathrm{i}\beta z} - \frac{V_0^-}{Z_0}\mathrm{e}^{\mathrm{i}\beta z}, \tag{2.32}$$

where the wavelength is

$$\lambda = \frac{2\pi}{\beta} = \frac{2\pi}{\omega\sqrt{L'C'}} \tag{2.33}$$

and the phase velocity is given by

$$v = \frac{\omega}{\beta} = \frac{1}{\sqrt{L'C'}}\,. \tag{2.34}$$

2.2.2 Loaded transmission lines

Here we consider the properties of a lossless transmission line when one end is connected to a load impedance Z_L as drawn in figure 2.4.

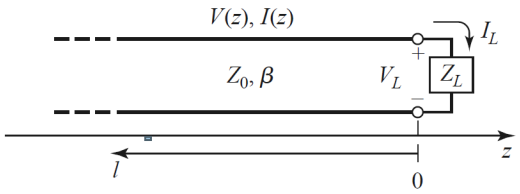

Figure 2.4: A transmission line terminated with a load impedance Z_L. Figure from Ref. [32].

The reflection parameter

It is assumed that there is an incident wave $V_0^+ \mathrm{e}^{-\gamma z}$ (generated by a source at $z \ll 0$) propagating in the positive z direction along the transmission line. The ratio between the voltage and current of the incident wave is the characteristic impedance Z_0. However, at the interface at $z = 0$, the ratio of the *net* voltage and *net* current is set by the circuit impedance Z_L of the load. Whenever $Z_0 \neq Z_\mathrm{L}$, this causes a reflected wave to be excited such that the summed voltage and current of the incident and the reflected wave satisfy the interface boundary condition set by the load impedance. Thus for $z < 0$

$$V(z) = V_0^+ \mathrm{e}^{-\gamma z} + V_0^- \mathrm{e}^{\gamma z}\,, \tag{2.35a}$$

$$I(z) = \frac{1}{Z_0}\left(V_0^+ \mathrm{e}^{-\gamma z} - V_0^- \mathrm{e}^{\gamma z}\right)\,, \tag{2.35b}$$

while at $z = 0$ we have the constraint

$$Z_\mathrm{L} = \frac{V(0)}{I(0)} = Z_0 \frac{V_0^+ + V_0^-}{V_0^+ - V_0^-}\,. \tag{2.36}$$

This equation can be solved for V_0^- which gives

$$V_0^- = \frac{Z_\mathrm{L} - Z_0}{Z_\mathrm{L} + Z_0} V_0^+ = \Gamma V_0^+\,, \tag{2.37}$$

where we have defined the voltage reflection coefficient as

$$\Gamma = \frac{Z_\mathrm{L} - Z_0}{Z_\mathrm{L} + Z_0}\,. \tag{2.38}$$

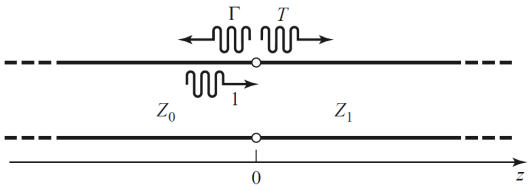

Figure 2.5: A transmission line feeding into another transmission line. Figure from Ref. [32].

With this result the voltage and current along a transmission line with a mismatched load can be written as

$$V(z) = V_0^+ \left(\mathrm{e}^{-\gamma z} + \Gamma \mathrm{e}^{\gamma z}\right) , \tag{2.39a}$$

$$I(z) = \frac{V_0^+}{Z_0} \left(\mathrm{e}^{-\gamma z} - \Gamma \mathrm{e}^{\gamma z}\right) . \tag{2.39b}$$

Input impedance

Because in case of a mismatched load, the voltage amplitudes on the line oscillate with its length, we see that the line's (input) impedance also varies with position. This can be seen from Eqs. (2.39) as follows

$$Z_{\mathrm{in}}(-l) = \frac{V(-l)}{I(-l)} = Z_0 \frac{V_0^+ \left(\mathrm{e}^{-\gamma z} + \Gamma \mathrm{e}^{\gamma z}\right)}{V_0^+ \left(\mathrm{e}^{-\gamma z} - \Gamma \mathrm{e}^{\gamma z}\right)} = Z_0 \frac{1 + \Gamma \mathrm{e}^{-2\gamma \ell}}{1 - \Gamma \mathrm{e}^{-2\gamma l}} . \tag{2.40}$$

Substituting Eq. (2.38) for Γ then gives

$$Z_{\mathrm{in}}(-l) = Z_0 \frac{Z_{\mathrm{L}} + Z_0 \tanh(\gamma l)}{Z_0 + Z_{\mathrm{L}} \tanh(\gamma l)} , \tag{2.41}$$

and for a lossless line

$$Z_{\mathrm{in}}(-l) = Z_0 \frac{Z_{\mathrm{L}} + \mathrm{i} Z_0 \tan(\beta \ell)}{Z_0 + \mathrm{i} Z_{\mathrm{L}} \tan(\beta \ell)} . \tag{2.42}$$

The transmission parameter

We also consider a line with characteristic impedance Z_0 that is loaded with another transmission line of characteristic impedance Z_1 as in Fig. 2.5.

A wave moving in the positive z direction is assumed incident on the feed line, which sees a load of impedance Z_1 from the other load line. As explained in section 2.2.2, when the impedances are not matched, when $Z_0 \neq Z_1$, then a reflected wave is excited whose amplitude is related to the amplitude of the incident wave with the reflection coefficient Γ. Thus we have

$$V(z) = V_0^+ \left(\mathrm{e}^{-\gamma z} - \Gamma \mathrm{e}^{\gamma z}\right) \quad \text{for} \quad z < 0 , \tag{2.43}$$

where just as in the previous sections V_0^+ is the amplitude of the incident wave.

At the interface, located at $z = 0$, the voltage must be the same for both the load line and the feed line. This leads to a transmitted wave which assuming no further reflections in the load line can be written as

$$V(z) = V_0^+ T \mathrm{e}^{-\gamma z} \quad \text{for} \quad z > 0 . \tag{2.44}$$

The boundary condition at the interface, equating the voltage of both lines at $z = 0$, then gives an expression for the transmission coefficient

$$T = 1 + \Gamma = 1 + \frac{Z_1 - Z_0}{Z_1 + Z_0} = \frac{2Z_1}{Z_1 + Z_0}\,, \tag{2.45}$$

where we have used Eq. (2.38) with $Z_\mathrm{L} = Z_1$.

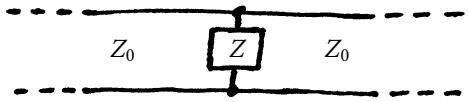

Figure 2.6: Transmission line with equal characteristic impedance on both sides and a circuit side-coupled in the middle of the line at $z = 0$.

Transmission line with side-coupled circuit As an extension to above formalisme, we also consider the case where in the middle of a transmission line some circuit with impedance Z is connected to the two leads as drawn in Fig. 2.6. The characteristic impedance Z_0 of the transmission line on both sides are taken equal. With an incident wave coming from the left, this system is very similar to the case of two coupled transmission lines with different characteristic impedances. The difference is that interface impedance as seen from the feedline at $z = 0$ is a parallel combination of the load lines characteristic impedance and the circuit impedance of the side-coupled circuit

$$Z_\mathrm{if} = \left(\frac{1}{Z_0} + \frac{1}{Z}\right)^{-1}\,. \tag{2.46}$$

Other than that, the boundary conditions for the transmitted and reflected waves remain identical to the case of two connected transmission lines. Thus for the reflection and transmission parameters we have

$$\Gamma = \frac{Z_\mathrm{if} - Z_0}{Z_\mathrm{if} + Z_0}\,, \tag{2.47a}$$

$$T = 1 + \Gamma\,. \tag{2.47b}$$

2.2.3 Coplanar wave-guides

A type of transmission line of particular importance is the coplanar wave-guide. It consists of a center-line conductor separated by a narrow gap from conducting ground planes on each side. The conductors and ground planes are created in a single layer on top of a dielectric substrate as drawn in Fig. 2.7. The ground plane together with the centerline constitute the two conductors of the transmission line.

Following an explanation in the book by Simons [34], the geometric capacitance per unit length C' is determined from a conformal mapping technique in Ref. [35] as

$$C' = 4\varepsilon_0\varepsilon_\mathrm{eff}\frac{K(k_0)}{K(k_0')}\,. \tag{2.48}$$

The effective dielectric constant ε_eff for an infinitely thick substrate is given as

$$\varepsilon_\mathrm{eff} = \frac{1 + \varepsilon_\mathrm{r}}{2}\,, \tag{2.49}$$

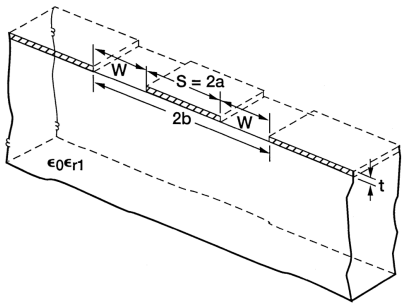

Figure 2.7: Cross section of a coplanar wave-guide on a dielectric substrate. Figure from Ref. [34].

though this is said to be an approximation [34]. The elliptic integrals are defined as

$$K(k_x) = \int_0^{\frac{\pi}{2}} \frac{\mathrm{d}\theta}{1 - {k_x}^2 \sin^2(\theta)} \tag{2.50}$$

together with the moduli

$$k_0 = \frac{S}{S + 2W}\,, \tag{2.51a}$$

$$k_0' = \sqrt{1 - {k_0}^2}\,. \tag{2.51b}$$

The geometric inductance per unit length L_g following Ref. [36] is given as

$$L_\mathrm{g} = \frac{\mu_0}{4} \frac{K(k_0')}{K(k_0)}\,. \tag{2.52}$$

In practice there is often also another contribution to the inductance per unit length of the transmission line. This arises from the inertia of the charge carriers and gives rise to a kinetic inductance L_k (where the respective energy is stored as kinetic energy in the momentum of the charge carriers). The total inductance per unit length is then given as $L' = L_\mathrm{g} + L_\mathrm{k}$.

Expressions for the kinetic inductance for the case of superconducting thin films in coplanar wave-guide geometry are presented in Refs. [36] and [37] (the latter reference points to a typo in the former) as a function of the London penetration depth for the magnetic field in the employed superconducting substrate.

2.2.4 Transmission line resonators

As we have already seen, incident waves propagating over a transmission line are (partially) reflected at a mismatched load at the end. We have also seen that this, due to interference between the reflected and incident waves, gives rise to standing waves.

In this section we consider transmission lines of specific length, loaded with a short-circuit at one end and an open-circuit at the other end as drawn in Fig. 2.8a for a quarter-wave resonator, and a line terminated with an open circuit at both ends as drawn in Fig. 2.8b for a half wave resonator. The motivation for calling the configurations as such will be explained.

How to actually couple externally to such devices will be discussed in a later section (usually the boundary condition is imposed approximately by employing a capacitor or inductor to connect the input end to an external circuit).

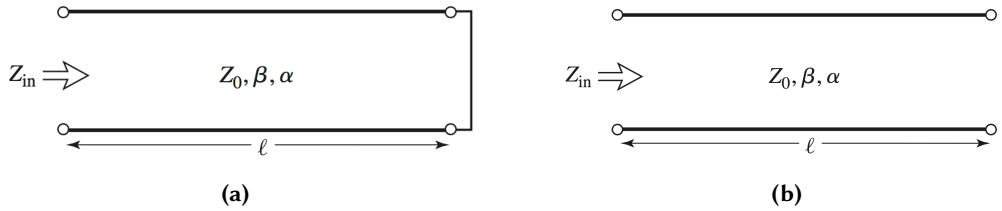

Figure 2.8: Transmission lines of length ℓ **(a)** loaded with a short-circuit and with an open-circuit imposed on the input end, and **(b)** an open termination on both sides. Figures from Ref. [32].

As can be seen from Eq. (2.38), a boundary with an open-circuit leads to a reflection parameter $\Gamma = -1$, which corresponds to complete reflection of incoming waves, but with a phase shift of π radians in the voltage of reflecting waves. The case where the boundary is terminated with a short-circuit also leads to complete reflection of incident waves, but with zero phase shift, i.e. $\Gamma = 1$. This shows that the short-circuited boundary acts as a voltage node and that the open-circuited boundary acts as a voltage anti-node (with $\frac{\mathrm{d}V}{\mathrm{d}z} = 0$ at the boundary) as follows from Eq. (2.39a). The roles of the two different boundary conditions are reversed when considering the current along the line as can be seen in Eq. (2.39b).

Quarter-wave resonator

First we consider the quarter-wave resonator from Fig. 2.8a. The boundary condition imposed by the open circuit in tandem with the one imposed by the load, allow only a specific set of standing waves, called normal modes, to emerge. The normal modes then consist of interfering forward and backward propagating waves (bouncing back and forth between the two ends of the transmission line) with such phase velocity and wavelength that the boundary conditions are satisfied.

This can be made concrete by considering the input impedance of a short-circuit terminated transmission line as a function of length ℓ, which referring to Eq. (2.41), can be written as

$$\begin{aligned} Z_{\text{in}} &= Z_0 \tanh\left((\alpha + \mathrm{i}\beta)\ell\right) \\ &= Z_0 \frac{\tanh(\alpha\ell) + \mathrm{i}\tan(\beta\ell)}{1 + \mathrm{i}\tan(\beta\ell)\tanh(\alpha\ell)} \\ &= Z_0 \frac{\tanh(\alpha\ell)\left(1 + \tan^2(\beta\ell)\right) + \mathrm{i}\tan(\beta\ell)\left(1 - \tanh^2(\alpha\ell)\right)}{1 + \tan^2(\beta\ell)\tanh^2(\alpha\ell)}, \end{aligned} \tag{2.53}$$

where the second equality follows from an identity for the hyperbolic tangent [32]. In the limit of small attenuation, the input impedance is $Z_{\text{in}} \approx \mathrm{i}Z_0 \tan(\beta\ell)$ as for a lossless line[7]. It can be seen to be periodic in length, or equivalently in wave-number β.

Thus, by imposing an open circuit at the lines input end, the input impedance at that point must be that of an open-circuit: $Z_{\text{in}} = \infty$, which gives the constraint $\tan(\beta\ell) = \infty$ that determines the normal modes. If on the other hand one would place a short-circuit on the input of the line, the constraint would be $\frac{Z_{\text{in}}}{\mathrm{i}Z_0} = \tan(\beta\ell) = 0$.

Taking into account the π periodicity in $\beta\ell$ of the resonance conditions, two sets of resonance

[7]Note that transmission line losses do not influence the resonance conditions, but rather cause the input impedance not to reach to the extremes zero or infinity as in the lossless case, see the last line in Eq. (2.53).

conditions are found one for a diverging input impedance and one for a vanishing input impedance

$$\beta_n \ell = \frac{\omega_n}{v}\ell = 2\pi\frac{\ell}{\lambda_n} = \begin{cases} \pi(n+1)\,, & Z_{\text{in}} \approx 0 \\ \pi(n+\frac{1}{2})\,, & Z_{\text{in}} \approx \infty \end{cases} \quad , \quad n \in \{0, 1, 2, \ldots\}\,. \tag{2.54}$$

Each conditions corresponds with a different normal mode. Here, the length is regarded as given, and the λ_n correspond to the different normal modes. We restrict our attention to the case with $Z_{\text{in}} = \infty$ and the $n = 0$ fundamental mode, which corresponds with $\ell = \frac{\lambda_0}{4}$ and is as such called the quarter-wave resonance. Its resonant frequency as determined by Eq. (2.54) is

$$\omega_0 = \frac{\pi v}{2\ell}\,. \tag{2.55}$$

The voltage and current distribution corresponding to the normal modes follow from Eqs. (2.39a) and (2.39b) with $\Gamma = 1$ as corresponds to the short circuit loading. Then, for the lossless case we have,

$$V_n(z) = V_n(\ell)\sin\left(\frac{\omega_n}{v}z\right)\,, \tag{2.56a}$$

$$I_n(z) = \mathrm{i}\frac{V_n(\ell)}{Z_0}\cos\left(\frac{\omega_n}{v}z\right)\,, \tag{2.56b}$$

where ω_n follows from Eq. (2.54). Note that V_n and I_n respectively represent the complex voltage and current amplitude along the line. for the nth mode. In the time domain, this constitutes a waveform of which every point oscillates around zero at the same frequency and in phase[8]. The voltage and current distributions corresponding to the first few modes are plotted in Fig. 2.9a.

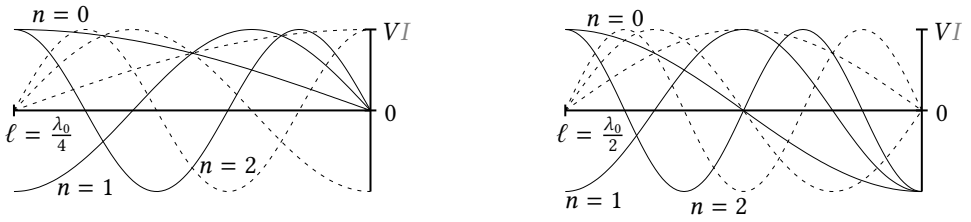

(a) Quarter-wave resonator **(b)** Half-wave resonator

Figure 2.9: Voltage standing wave modes for **(a)** the quarter-wave resonator and **(b)** the half wave resonator. The fundamental mode is drawn together with the next two higher modes. The mode shapes for the corresponding current amplitude distributions are depicted in thin dashed lines.

In order to derive the equivalent lumped element circuit that represents the quarter-wave resonance, the input admittance, the reciprocal of Eq. (2.53), is Taylor expanded around the quarter-wave resonant frequency ω_0, but first the input impedance is simplified somewhat. In the envisioned application to superconducting circuits, the attenuation constant is assumed to be in the limit $\alpha\ell \ll 1$ such that

[8] When adding losses, deviations from the given mode-shapes occur due to the running waves, which give rise to the standing waveforms as a result of interference, now exponentially decaying with propagation distance. The waveform is no longer real as in Eqs. (2.56), but carries a position dependent phase, causing the different parts of the waveform to no longer oscillate in phase, though still at the same frequency.

$\tanh(\alpha\ell) \approx \alpha\ell$. Then the input admittance is written as

$$\begin{aligned} Y_{\text{in}} &\approx \frac{1}{Z_0}\frac{1+\mathrm{i}\alpha\ell\tan(\beta\ell)}{\alpha\ell+\mathrm{i}\tan(\beta\ell)} = \frac{1}{Z_0}\frac{\alpha\ell-\mathrm{i}\cot(\beta\ell)}{1-\mathrm{i}\alpha\ell\cot(\beta\ell)} \\ &\approx \frac{\alpha\ell}{Z_0}+\mathrm{i}\frac{\ell\left(1-\alpha^2\ell^2\right)}{vZ_0}(\omega-\omega_0) \\ &\approx \frac{\alpha\ell}{Z_0}+\mathrm{i}\frac{\pi}{2\omega_0 Z_0}(\omega-\omega_0)\,, \end{aligned} \tag{2.57}$$

where the second step follows from a first order Taylor expansion. The last step follows from the approximation $1-\alpha^2\ell^2 \approx 1$ and substitution of the mode frequency back into the equation.

Referring to section 2.1.2, the last expression is equivalent to the input impedance of a parallel RLC-circuit (2.9) with

$$\begin{aligned} R &= \frac{Z_0}{\alpha\ell}\,, \\ C &= \frac{\pi}{4Z_0\omega_0}\,, \end{aligned} \tag{2.58}$$

and invoking the resonance condition of an RLC-resonator

$$L = \frac{1}{C{\omega_0}^2} = \frac{4Z_0}{\pi\omega_0}\,. \tag{2.59}$$

A parallel combination of above three components constitutes the equivalent lumped element circuit.

Half-wave resonator

Now we discuss the half wavelength resonator as drawn in Fig. 2.8b. In contrast to the quarter-wave resonator, the transmission line is terminated with an open circuit on both ends. As discussed, this requires that the allowed modes have a voltage anti-node at both ends, which results in normal mode voltage distributions such as drawn in Fig. 2.9b.

To make this concrete we note that the input impedance of a transmission line loaded with an open circuit referring to Eq. (2.41) after letting $Z_{\text{L}} \to \infty$ is

$$\begin{aligned} Z_{\text{in}} &= Z_0\coth\left((\alpha+\mathrm{i}\beta)\ell\right) \\ &= Z_0\frac{1+\mathrm{i}\tan(\beta\ell)\tanh(\alpha\ell)}{\tanh(\alpha\ell)+\mathrm{i}\tan(\beta\ell)}\,. \end{aligned} \tag{2.60}$$

In the limit of no loss, when $\alpha \approx 0$, the input impedance can be approximated as $Z_{\text{in}} \approx -\mathrm{i}Z_0\cot(\beta\ell)$, just as with the quarter-wave resonator a π-periodic function in $\beta\ell$.

This shows that also in this case two kinds of resonances are possible depending on the input impedance imposed on the lines input, one for which Z_{in} vanishes and one for which Z_{in} diverges. Not going into too much detail, we note that an open circuit is imposed on the input, for which the corresponding resonance condition is $\cot(\beta\ell) = \infty$. This implies that

$$\beta_n\ell = \frac{\omega_n}{v}\ell = 2\pi\frac{\ell}{\lambda_n} = \pi(n+1)\,, \quad n \in \{0,1,2,\ldots\}\,. \tag{2.61}$$

The fundamental ($n = 0$) mode corresponds with $\ell = \frac{\lambda_0}{2}$, hence the name half wave resonator. The fundamental resonance frequency is

$$\omega_0 = \frac{\pi v}{\ell}\,. \tag{2.62}$$

Following Eqs. (2.39a) and (2.39b), for this case with the reflection parameter set as $\Gamma = -1$ corresponding to the open circuit boundary condition, and neglecting loss gives for the voltage and current distribution corresponding to the normal modes

$$V_n(z) = V_n(\ell)\cos\left(\frac{\omega_n}{v}z\right), \tag{2.63a}$$

$$I_n(z) = -\mathrm{i}\frac{V_n(\ell)}{Z_0}\sin\left(\frac{\omega_n}{v}z\right), \tag{2.63b}$$

where the ω_n follow from Eq. (2.61).

Next deriving an equivalent lumped element circuit, we take the input impedance Eq. (2.60). Assuming the loss to be low $\alpha\ell \ll 1$ we make a Taylor expansion of the input admittance around the fundamental resonance frequency $\omega_0 = \pi\frac{v}{\ell}$ with the result

$$\begin{aligned} Y_{\text{in}} &\approx \frac{1}{Z_0}\frac{\alpha\ell + \mathrm{i}\tan(\beta\ell)}{1 + \mathrm{i}\alpha\ell\tan(\beta\ell)} \\ &\approx \frac{1}{\alpha\ell} + (\omega - \omega_0)\frac{\mathrm{i}}{Z_0}\left(1 + \alpha^2\ell^2\right)\frac{\ell}{v} \\ &\approx \frac{1}{\alpha\ell} + \mathrm{i}\frac{\pi}{\omega_0 Z_0}(\omega - \omega_0), \end{aligned} \tag{2.64}$$

where we have set $1 + \alpha^2\ell^2 \approx 1$ and substituted $\frac{\ell}{v} = \frac{\pi}{\omega_0}$. This expression is equivalent to the input admittance of a parallel lumped element circuit resonator as described by Eq.(2.9) with

$$\begin{aligned} R &= \frac{Z_0}{\alpha\ell}, \\ C &= \frac{\pi}{2\omega_0 Z_0}, \\ L &= \frac{1}{{\omega_0}^2 C} = \frac{2Z_0}{\pi\omega_0}. \end{aligned} \tag{2.65}$$

2.3 Capacitively coupled resonators

This section discusses how to couple to a resonator such that it can be excited from an external circuit. Two kinds of capacitive coupling to a transmission line (feed-line) will be introduced: one-port coupling and side coupling, both of which are shown in figures 2.10 for the case of a parallel RLC resonator. The role of the external Q-factor will be discussed together with the response functions describing the scattering parameters for input signal reflection and also transmission in the case of side-coupling.

2.3.1 One port coupled parallel RLC-circuit

Input impedance

The circuit of a parallel RLC-resonator capacitively coupled to a feed-line is drawn in Fig. 2.10a. The input impedance of the resonator as seen from the feed-line through the coupling capacitor

$$Z_{\text{in}} = \frac{1}{\frac{1}{R} + \frac{1}{\mathrm{i}\omega L} + \mathrm{i}\omega C} + \frac{1}{\mathrm{i}\omega C_{\text{c}}} \tag{2.66}$$

is difficult to work out when including the resistance. Instead the lossless case with an infinite resistance, $R \to \infty$ is worked out after which loss is included by the complex frequency trick described in section 2.1.4.

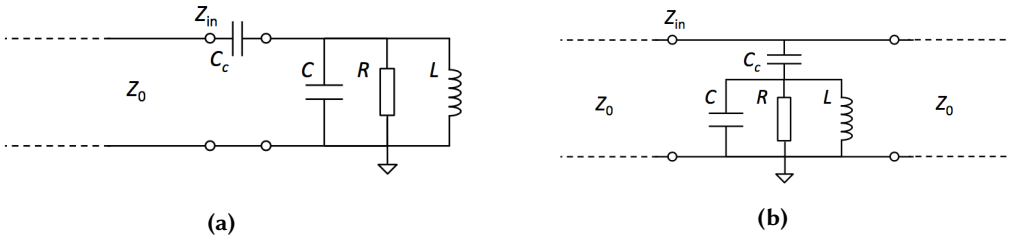

Figure 2.10: RLC-circuits capacitively coupled to transmission line. **(a)** One port coupled parallel RLC-circuit. **(b)** side-coupled parallel RLC-circuit. Figures courtesy of Daniel Bothner.

A bit of algebraic manipulation in this limit on the input impedance of the corresponding coupled lossless resonator yields

$$Z_{\text{in}} = \mathrm{i}\frac{\omega^2 L\left(C + C_{\text{c}}\right) - 1}{\omega C_{\text{c}}\left(1 - \omega^2 LC\right)}\,, \tag{2.67}$$

which vanishes at the resonant frequency $\omega_0 = \frac{1}{\sqrt{L(C+C_{\text{c}})}}$, where a series type of RLC-circuit resonance is found[9], slightly shifted from the resonator's uncoupled resonant frequency[10]. Rewriting the input impedance in terms of the resonant frequency and making a Taylor expansion around that point gives

$$Z_{\text{in}} = \frac{\mathrm{i}\left(\frac{\omega^2}{{\omega_0}^2} - 1\right)}{\omega C_{\text{c}}(1 - \omega^2 LC)} \approx \frac{2\mathrm{i}}{C_{\text{c}}{\omega_0}^2\left(1 - {\omega_0}^2 LC\right)}\left(\omega - \omega_0\right) = \frac{2\mathrm{i}L\left(C + C_{\text{c}}\right)^2}{{C_{\text{c}}}^2}\left(\omega - \omega_0\right) \tag{2.68}$$

after which losses are added by substitution of the complex resonant frequency $\omega_0 \leftarrow \omega_0\left(1 + \frac{\mathrm{i}}{2Q_0}\right)$ in the $(\omega - \omega_0)$ term with the result

$$Z_{\text{in}} \approx \frac{L\left(C - C_{\text{c}}\right)^2}{{C_{\text{c}}}^2}\left(\frac{\omega_0}{Q_0} + 2\mathrm{i}\left(\omega - \omega_0\right)\right)\,. \tag{2.69}$$

[9] Incidentally this shows that the coupling capacitor acts as an impedance inverter.

[10] Actually, there are two resonances as in the lossless case the input impedance diverges for $\omega = \frac{1}{\sqrt{LC}}$, the resonators uncoupled resonance frequency. Separating the input impedance in its full form including losses by setting $0 < R < \infty$ into its real and imaginary part

$$Z_{\text{in}} = \frac{\frac{\omega C_{\text{c}}}{R} + \mathrm{i}\left(\left(\omega C - \frac{1}{\omega L}\right)\left(\frac{1}{\omega L} - \omega\left(C + C_{\text{c}}\right)\right) - \frac{1}{R^2}\right)}{\frac{\omega C_{\text{c}}}{R^2} + \omega C_{\text{c}}\left(\omega C - \frac{1}{\omega L}\right)^2}$$

incidentally shows that the resonance condition $\mathrm{Im}\{Z_{\text{in}}\} = 0$ does depend on R and thus losses. However for high but finite Q-factor resonators, i.e. those with $0 \ll R < \infty$, the resonance condition becomes approximately

$$0 \approx \left(\omega C - \frac{1}{\omega L}\right)\left(\frac{1}{\omega L} - \omega\left(C + C_{\text{c}}\right)\right)$$

which shows that the from the lossless case derived resonance frequencies are reasonably accurate. From this we see that

$$Z_{\text{in}}\left(\omega = \frac{1}{\sqrt{L\left(C + C_{\text{c}}\right)}}\right) \approx \frac{1}{R\left(\omega C - \frac{1}{\omega L}\right)^2} \quad \text{and that} \quad Z_{\text{in}}\left(\omega = \frac{1}{\sqrt{LC}}\right) \approx R\,,$$

which shows that the difference between the two resonances is expressed by

$$Z_{\text{in}}\left(\omega = \frac{1}{\sqrt{LC}}\right) \gg Z_{\text{in}}\left(\omega = \frac{1}{\sqrt{L\left(C + C_{\text{c}}\right)}}\right)\,.$$

This difference is important because in order to transfer energy from the feed-line to the resonator, the feed-line and resonator should be impedance matched, i.e. setting $Z_{\text{in}} \approx Z_0$, which effectively allows no more than one of the two resonators to be accessible at the same time.

The approximate input impedance for the coupled resonator is of the form $Z_{\text{in}} = R_{\text{s}} + 2\text{i}L_{\text{s}}(\omega - \omega_0)$ as for a series RLC circuit (discussed in Sec. 2.1.1) with

$$R_{\text{s}} = \frac{\omega_0 L (C - C_{\text{c}})^2}{Q_0 {C_{\text{c}}}^2}, \quad L_{\text{s}} = \frac{L(C - C_{\text{c}})^2}{{C_{\text{c}}}^2} = \frac{1}{C_{\text{c}} {\omega_0}^2 (1 - {\omega_0}^2 LC)} \quad \text{and} \quad C_{\text{s}} = \frac{1}{{\omega_0}^2 L_{\text{s}}}. \tag{2.70}$$

Internal and external Q-factor

This analysis does not provide the necessary information for relating the Q-factor to the lumped elements of the coupled parallel RLC circuit. In order to do this and to understand the loading effects of the coupling capacitor together with the transmission line, we consider the *external* circuit impedance connecting to the resonator as seen from the resonator.

Noting that a semi-infinite transmission line at its interface can be considered a resistance to ground equal to the line's characteristic impedance Z_0, we can write the external impedance as

$$Z_{\text{e}} = Z_0 + \frac{1}{\text{i}\omega C_{\text{c}}}. \tag{2.71}$$

This impedance can be written in terms of an equivalent parallel combination of a resistor R_{L} and a capacitor C_{L} as follows

$$\frac{1}{Z_{\text{e}}} = \frac{1}{Z_0 + \frac{1}{\text{i}\omega C_{\text{c}}}} = \frac{\text{i}\omega C_{\text{c}}}{1 + \text{i}\omega C_{\text{c}} Z_0} = \frac{\omega^2 {C_{\text{c}}}^2 Z_0 + \text{i}\omega C_{\text{c}}}{1 + \omega^2 {C_{\text{c}}}^2 {Z_0}^2} = \frac{1}{R_{\text{L}}} + \text{i}\omega C_{\text{L}} \tag{2.72}$$

with for the lumped elements in the equivalent parallel combination

$$R_{\text{L}} = \frac{1 + \omega^2 {C_{\text{c}}}^2 {Z_0}^2}{\omega^2 {C_{\text{c}}}^2 Z_0} \approx \frac{1}{\omega^2 {C_{\text{c}}}^2 Z_0}, \tag{2.73a}$$

$$C_{\text{L}} = \frac{C_{\text{c}}}{1 + \omega^2 {C_{\text{c}}}^2 {Z_0}^2} \approx C_{\text{c}}. \tag{2.73b}$$

The approximations are valid for $\omega^2 {C_{\text{c}}}^2 {Z_0}^2 \ll 1$ which is usually the case in practice where the coupling capacitors are often chosen small.

Taking the external impedance together with the internal impedance shows that the coupled resonator can be considered a loaded parallel RLC circuit with a modified capacitance

$$C_{\text{t}} \approx C + C_{\text{c}} \tag{2.74a}$$

and effective resistance

$$R_{\text{t}} = \frac{R R_{\text{L}}}{R + R_{\text{L}}} \approx \frac{R}{1 + \omega^2 {C_{\text{c}}}^2 Z_0 R}, \tag{2.74b}$$

and unmodified inductance L. Thus the resonance frequency of this circuit is the same as the approximate shifted resonance condition found from the input impedance.

The Q-factor can then be found by applying the definitions from Sec. 2.1.3. The loaded Q-factor for the loaded resonator is

$$Q_{\text{L}} = R_{\text{t}} \omega_0 C_{\text{t}} = \frac{R R_{\text{L}}}{R + R_{\text{L}}} \omega_0 (C + C_{\text{c}}) \approx \frac{R \omega_0 (C + C_{\text{c}})}{1 + {\omega_0}^2 {C_{\text{c}}}^2 Z_0 R}. \tag{2.75}$$

Considering $R_\mathrm{L} \approx \frac{1}{\omega^2 {C_\mathrm{c}}^2 Z_0}$ the external load and R the internal load we find for the unloaded and external Q-factor[11] respectively

$$Q_0 = \omega_0 R\,(C + C_\mathrm{c})\ , \tag{2.76a}$$

$$Q_\mathrm{e} \approx \frac{\omega_0\,(C + \mathrm{Cc})}{{\omega_0}^2 {C_\mathrm{c}}^2 Z_0} = \frac{\omega_0 L\,(C + \mathrm{Cc})^2}{{C_\mathrm{c}}^2 Z_0}\ . \tag{2.76b}$$

We can easily check that these add up reciprocally to the loaded Q-factor. The latter form of the external Q-factor will be useful for finding a convenient expression for the reflection parameter.

Scattering parameter

The reflection parameter or equivalently the S_{11} scattering parameter can be determined using Eq. (2.38) in Sec. 2.2.2 from transmission line theory:

$$\begin{aligned}
\Gamma = \frac{Z_\mathrm{in} - Z_0}{Z_\mathrm{in} + Z_0} &= \frac{\frac{L(C-C_\mathrm{c})^2}{{C_\mathrm{c}}^2}\left(\frac{\omega_0}{Q_0} + 2\mathrm{i}\,(\omega - \omega_0)\right) - Z_0}{\frac{L(C-C_\mathrm{c})^2}{{C_\mathrm{c}}^2}\left(\frac{\omega_0}{Q_0} + 2\mathrm{i}\,(\omega - \omega_0)\right) + Z_0} \\
&= \frac{\frac{\omega_0}{Q_0} - \frac{Z_0 {C_\mathrm{c}}^2}{L(C-C_\mathrm{c})^2} + 2\mathrm{i}\,(\omega - \omega_0)}{\frac{\omega_0}{Q_0} + \frac{Z_0 {C_\mathrm{c}}^2}{L(C-C_\mathrm{c})^2} + 2\mathrm{i}\,(\omega - \omega_0)} \\
&= \frac{\frac{\omega_0}{Q_0} - \frac{\omega_0}{Q_\mathrm{e}} + 2\mathrm{i}\,(\omega - \omega_0)}{\frac{\omega_0}{Q_0} + \frac{\omega_0}{Q_\mathrm{e}} + 2\mathrm{i}\,(\omega - \omega_0)}\ .
\end{aligned} \tag{2.77}$$

Note that substituting in the external Q-factor results in a reasonably compact expression. There are a few things to observe:

- at resonance, the reflection parameter $\Gamma \longrightarrow 0$ when the difference $Q_\mathrm{e} - Q_0 \longrightarrow 0$;
- far from resonance, the reflection parameter $\Gamma \longrightarrow 1$, regardless of the Q-factors;
- the sign of above difference determines whether the real part of the reflection parameter is positive or negative at the resonance.

These observations can be derived straightforwardly from Eq. (2.77) and its modulus. They however also point to another aspect that is a relation between the matching of the input impedance Z_in to the transmission line characteristic impedance Z_0 and the ratio between the internal and the external Q-factor.

[11] Note that we assume the internal Q-factor of this parallel equivalent circuit to be identical to the internal Q-factor imposed by the complex frequency trick on the input impedance of the resonator as seen from the feed-line. To show that this is true, we refer to footnote 10 where the full input impedance is worked out in the approximation of a high but finite Q-factor resonator. Note that the imaginary part of the input impedance in this regime is approximately equal to the input impedance in the limit of an infinite Q-factor. Thus, considering only the shifted resonance with $\omega_0 \approx \frac{1}{\sqrt{L(C+C_\mathrm{c})}}$, the series equivalent inductance $L_\mathrm{s} = \frac{1}{C_\mathrm{c}{\omega_0}^2(1-{\omega_0}^2 LC)}$ of this resonator should be the same as the one in Eqs. (2.70). Further, we can relate the approximate input impedance from footnote 10 at the resonance frequency to the series equivalent resistance $\frac{1}{R_\mathrm{s}} = R\left(\omega_0 C - \frac{1}{\omega_0 L}\right)^2$. Substituting this into the definition for the internal Q-factor for a series RLC resonator gives after some algebra

$$Q_0 = \frac{\omega_0 L_\mathrm{s}}{R_\mathrm{s}} = \frac{R\left(\frac{1}{{\omega_0}^2 L} - C\right)}{\omega_0 L C_\mathrm{c}} = \omega_0 R\,(C + C_\mathrm{c})$$

which shows that indeed the internal Q-factor for the two representations are pretty much equivalent in the given approximations.

Coupling coefficient

Defining the coupling coefficient as

$$g = \frac{Q_0}{Q_e} = \frac{\kappa_e}{\kappa_i} \tag{2.78}$$

we can distinguish three conditions, all of which can be verified from the response function Eq. (2.77):

$g < 1$: The external decay rate is smaller than the internal decay rate (or $Q_e > Q_0$); The real part of the reflection parameter remains positive and the resonator is said to be under-coupled.

$g = 1$: The external decay rate is equal to the internal decay ($Q_e = Q_0$) and at resonance the incident wave is totally absorbed by the resonator; This shows that the condition is equivalent to the impedance matching condition $Z_{in} = Z_0$; In this case the resonator is said to be critically coupled.

$g > 1$: The external decay rate is greater than the internal decay rate (or $Q_e < Q_0$); The real part of the reflection parameter becomes negative in the region around the resonant frequency and the resonator is said to be over-coupled.

2.3.2 Side-coupled to transmission line

The case of a side-coupled parallel RLC-circuit as drawn in Fig. 2.10b is from a circuit perspective similar to the one port coupled resonator as described in the previous subsection. The difference is a transmission line identical to the feed-line is also connected to the resonator interface. This allows incident waves to not only be reflected or absorbed at the interface, but also to for them to be transmitted over the new line. The extra load this imposes will be seen to affect the input impedance as seen from the feed-line as wel as the external circuit seen by the resonator.

Q-factors

The only difference in the external circuit as seen from the parallel RLC resonator's perspective for the case of side-coupling compared with one-port coupling is that the resistive external load is now a parallel combination of two identical resistors to ground with impedance Z_0. This leads to an effective resistance of $\frac{Z_0}{2}$ in a circuit that is otherwise indistinguishable from the corresponding circuit for the one-port coupled resonator. Thus if one substitutes

$$Z_0 \leftarrow \frac{Z_0}{2} \tag{2.79}$$

into the relations derived from the circuit corresponding to the one-port coupled resonator derived, the result should be the corresponding relations for the side-coupled resonator.

Carrying out this substitution, load resistance in the parallel equivalent for the external circuit is found to be

$$R_L \approx \frac{2}{\omega_0{}^2 C_c{}^2 Z_0} \,. \tag{2.80}$$

There is a slight influence on the parallel equivalent load capacitance

$$C_L = \frac{C_c}{1 + \frac{\omega^2 C_c{}^2 Z_0{}^2}{4}} \approx C_c \,, \tag{2.81}$$

which is however negligible. The extending transmission line has no further effect on the approximate expressions for the resonant frequency and internal Q-factor. The external Q-factor (and thus also

the loaded Q-factor) is modified however. Using the corresponding equation for the one-port coupled resonator and the substitution we directly write

$$Q_\mathrm{e} = \omega_0 R_\mathrm{L} \left(C + C_\mathrm{c}\right) \approx \frac{2\omega_0 L \left(C + C_\mathrm{c}\right)^2}{{C_\mathrm{c}}^2 Z_0} \,. \tag{2.82}$$

Input impedance

The input impedance as seen from the feed-line at the interface is a parallel combination of the resonator input impedance for the case of single port coupling—which we already derived in Eq. (2.69)—and the other transmission line which behaves as a resistance to ground equal to its characteristic impedance Z_0. Working this out gives the input impedance for the side-coupled resonator

$$\begin{aligned}
\frac{1}{Z_\mathrm{in}} &= \frac{{C_\mathrm{c}}^2}{L\left(C - C_\mathrm{c}\right)^2 \left(\frac{\omega_0}{Q_0} + 2\mathrm{i}\left(\omega - \omega_0\right)\right)} + \frac{1}{Z_0} \,, \\
Z_\mathrm{in} &= \frac{Z_0 L \left(C + C_\mathrm{c}\right)^2 \left(\frac{\omega_0}{Q_0} + 2\mathrm{i}\left(\omega - \omega_0\right)\right)}{Z_0 {C_\mathrm{c}}^2 + L\left(C + C_\mathrm{c}\right)^2 \left(\frac{\omega_0}{Q_0} + 2\mathrm{i}\left(\omega - \omega_0\right)\right)} \\
&= Z_0 \frac{\frac{\omega_0}{Q_0} + 2\mathrm{i}\left(\omega - \omega_0\right)}{\frac{Z_0 {C_\mathrm{c}}^2}{L\left(C + C_\mathrm{c}\right)^2} + \frac{\omega_0}{Q_0} + 2\mathrm{i}\left(\omega - \omega_0\right)} \\
&= Z_0 \frac{\frac{\omega_0}{Q_0} + 2\mathrm{i}\left(\omega - \omega_0\right)}{2\frac{\omega_0}{Q_\mathrm{e}} + \frac{\omega_0}{Q_0} + 2\mathrm{i}\left(\omega - \omega_0\right)} \,.
\end{aligned} \tag{2.83}$$

The equation with the Q-factors substituted in is already brought to a form that is convenient for obtaining the scattering parameters.

We can already see that for large $\omega - \omega_0$ the ratio $\frac{Z_\mathrm{in}}{Z_0} \to 1$. From this we can conclude that for highly off-resonant incident waves the feed-line and the net load impedance are matched such that for this case virtually no reflection occurs.

Scattering parameters for reflection and transmission

With the input impedance, the reflection parameter

$$\begin{aligned}
\Gamma &= \frac{Z_0 \frac{\frac{\omega_0}{Q_0} + 2\mathrm{i}\left(\omega - \omega_0\right)}{2\frac{\omega_0}{Q_\mathrm{e}} + \frac{\omega_0}{Q_0} + 2\mathrm{i}\left(\omega - \omega_0\right)} - Z_0}{Z_0 \frac{\frac{\omega_0}{Q_0} + 2\mathrm{i}\left(\omega - \omega_0\right)}{2\frac{\omega_0}{Q_\mathrm{e}} + \frac{\omega_0}{Q_0} + 2\mathrm{i}\left(\omega - \omega_0\right)} + Z_0} \\
&= \frac{\frac{\omega_0}{Q_0} + 2\mathrm{i}\left(\omega - \omega_0\right) - 2\frac{\omega_0}{Q_\mathrm{e}} - \frac{\omega_0}{Q_0} - 2\mathrm{i}\left(\omega - \omega_0\right)}{\frac{\omega_0}{Q_0} + 2\mathrm{i}\left(\omega - \omega_0\right) + 2\frac{\omega_0}{Q_\mathrm{e}} + \frac{\omega_0}{Q_0} + 2\mathrm{i}\left(\omega - \omega_0\right)} \\
&= \frac{-\frac{\omega_0}{Q_\mathrm{e}}}{\frac{\omega_0}{Q_0} + \frac{\omega_0}{Q_\mathrm{e}} + 2\mathrm{i}\left(\omega - \omega_0\right)}
\end{aligned} \tag{2.84}$$

is determined from its defining equation from transmission line theory Eq. (2.38).

The transmission parameter is derived from the reflection parameter by invoking Eq. (2.45), which in Sec. 2.2.2 we have seen to be valid for this case of an interface incorporating an embedded circuit—the

coupled resonator—between two transmission lines,

$$T = 1 + \Gamma = \frac{\frac{\omega_0}{Q_0} + 2\mathrm{i}\,(\omega - \omega_0)}{\frac{\omega_0}{Q_0} + \frac{\omega_0}{Q_\mathrm{e}} + 2\mathrm{i}\,(\omega - \omega_0)}\,. \tag{2.85}$$

Note that where the reflection coefficient is almost zero for highly off-resonant waves, the transmission coefficient is very close to unity. Thus when plotting the modules of the scattering parameters, the reflection parameter forms a peak while the transmission parameter forms a dip. Their respective maximum and minimum occurs at the resonant frequency with the values determined by the internal and external Q-factors:

$$|\Gamma(\omega_0)| = \frac{Q_0}{Q_\mathrm{e} + Q_0} = \frac{\kappa_\mathrm{e}}{\kappa_\mathrm{e} + \kappa_0}\,, \tag{2.86a}$$

$$|T(\omega_0)| = \frac{Q_\mathrm{e}}{Q_\mathrm{e} + Q_0} = \frac{\kappa_0}{\kappa_\mathrm{e} + \kappa_0}\,. \tag{2.86b}$$

There are a couple of further observation to be made here that are interesting to put in contrast with the response function for the one-port coupled resonator:

- A large internal Q-factor $Q_0 \gg Q_\mathrm{e}$ favors reflection and reduces transmission;
- Vice versa, a large external Q-factor $Q_\mathrm{e} \gg Q_0$ favors transmission and reduces reflection;
- Whenever the internal and external Q-factors are equal, i.e. $Q_\mathrm{e} = Q_0$, then modulus of the reflection and the transmission parameter obtain their respective maximum and minimum, both with the same value:

$$|\Gamma(\omega_0)|_{Q_\mathrm{e}=Q_0} = |T(\omega_0)|_{Q_\mathrm{e}=Q_0} = \frac{1}{2}\,. \tag{2.87}$$

Above three points indicate that the coupling coefficients $g = \frac{Q_0}{Q_\mathrm{e}}$ fulfills an analogue role for the case of a side coupled resonator.

Chapter 3

Flux tuneable resonators

The theory of opto-mechanics is defined in terms at least two resonators where the position of one resonator (the mechanical resonator) sets the resonance frequency of the other (the optical cavity). This constitutes a *parametric* interaction since the resonance frequency is changed by changing one of the resonator parameters. In case of an optical cavity these are the length between its mirrors, but modifying the propagation velocity of light in the optical medium is also possible. For an electrical resonator, its resonant frequency can be tuned by varying the inductance or capacitance parameters of its constituent components. For our purpose we analyse the embedding of a SQUID as variable inductance in electrical resonators, since in the analogue simulation circuit this essentially constitutes the electrical analogue of the distance between the mirrors in an optical cavity.

The chapter is divided in two parts; first an introduction is given to superconductivity, quantum mechanical phenomena such as flux quantisation and the Josephson effect and how the last two can be used to create a tuneable inductance in a device called a SQUID; then its embedding in electrical resonators for creating flux tuneable resonators is analysed.

3.1 Superconducting quantum interference device

Before introducing flux tuneable resonators, we first consider what is a crucial element. This section provides a short introduction to what a SQUID (Superconducting QUantum Interference Device) is. It starts with a discussion of a Josephson junction (a tunnel barrier in a superconducting circuits). Then, putting two junctions in parallel connected in a loop, thereby creating two pathways, the interference that will result as a consequence is discussed. The section will conclude with a discussion of the lumped element description of a SQUID. Some attention to the non-linearity in the inductance will also be given as it will be relevant later on. For the parts of superconductivity and flux quantisation inspiration is drawn from Refs. [38, 39] while the discussion on Josephson junctions and the SQUID is mainly based on the latter reference but considerably extended.

3.1.1 Superconductivity

While by no means meant as a formal introduction, some aspects of superconductivity are relevant in this work. Superconductivity as described by BCS theory [40] in essence occurs because at low temperatures in some substrates, the electrons, fermions with spin-½ following the Pauli exclusion principle, form pairs which behave as bosonic particles with spin-1 or spin-0. The main point is that, in the quantum statistics of identical particles, at low temperature, as described by the Bose-Einstein distribution, most bosons tend to condense into the ground-state, the wave-function of which is spread over the whole superconductor,

forming a super-fluid. This all follows from the symmetry postulate for identical and indistinguishable particles that under particle permutation, the Hamiltonian is invariant, which for bosons means that the many particle wave-function is even symmetric under every two-particle permutation[1].

At low temperature below the critical temperature upon which the phase transition occurs that marks the point where the so called Cooper-pairs start to form and condense into a super-fluid, the amplitude of the ground-state component of the many particle Cooper-pair wave-function ψ becomes a macroscopically large complex number. Because of that, the probability density of finding a Cooper-pair at a certain point

$$P(\vec{r},t) = \psi^*(\vec{r},t)\psi(\vec{r},t) \tag{3.1}$$

can be interpreted as as a particle density. With this, it is intuitive to write the wave function as

$$\psi(r) = \sqrt{\rho(r)}\mathrm{e}^{\mathrm{i}\theta(r)}\,, \tag{3.2}$$

where the particle density ρ can be considered a classical variable. The phase θ, which drops out upon observation of the density, will be seen to play a role upon observation of particle current.

The local variation in particle density can be expressed through a continuity equation

$$\frac{\partial P}{\partial t} = -\nabla\cdot\vec{J} \tag{3.3}$$

in terms of the probability current which for the case of a super-fluid may be interpreted as a particle current density. For charged particles in a magnetic field the latter is equivalent to[2]

$$\vec{J} = \frac{1}{2}\left(\psi^*\frac{\frac{\hbar}{\mathrm{i}}\nabla - q\vec{A}}{m}\psi + \psi\frac{-\frac{\hbar}{\mathrm{i}}\nabla - q\vec{A}}{m}\psi^*\right). \tag{3.4}$$

In this expression, $\vec{A}$ is the magnetic vector potential, q the charge of a Cooper-pair and m the pairs effective mass. The meaning of the phase θ can then be made concrete by substituting the macroscopic wave-function (3.2) into expression for the current (3.4) which gives

$$\vec{J} = \frac{\hbar}{m}\left(\nabla\theta - \frac{q}{\hbar}\vec{A}\right)\rho\,. \tag{3.5}$$

Considering $\vec{J}$ as a current density ρv of a fluid, then the momentum of a particle can be expressed as $mv = \hbar\nabla\theta - q\vec{A}$. This shows that the gradient of the phase corresponds to a particle's observable kinetic momentum in the absence of a magnetic vector potential.

3.1.2 Flux quantisation

The fact that in the superconducting state all Cooper-pairs condense into the same macroscopic wave-function has profound consequences. One such consequence is flux quantisation which emerges whenever a superconductor has a hole, as is the case with a superconducting ring. Flux quantisation stems from

[1] Why this is the right symmetry as for the bosons, and why pairs of electrons behave as bosons is beyond the scope of this work, for that consult a textbook on quantum mechanics.

[2] The expression for the current, as explained in e.g. Ref. [39] can be derived by differentiating Eq. (3.1), and substituting the result into the Schrödinger equation for charged particles in an electromagnetic field,

$$\mathrm{i}\hbar\frac{\partial\psi}{\partial t} = \frac{1}{2m}\left(\frac{\hbar}{\mathrm{i}}\nabla - q\vec{A}\right)^2\psi + q\phi\psi$$

with ϕ the electric potential, and then rewriting the result in the form of Eq. (3.3).

the requirement that the wave-function (3.2) for a superconducting condensate spanning a ring must be a single-valued function for quantum mechanics to be consistent.

Noting that according to the London theory of superconductivity [41] the current well inside a superconductor (deeper than the London penetration depth) can be considered zero, the phase difference between two points of the Cooper-pair wave-function is found by integrating the current for a superconducting fluid (3.5) over a path ℓ connecting the two points

$$\Delta\theta = \frac{q}{\hbar}\int_{\ell}\vec{A}\cdot\mathrm{d}\vec{s}\,, \tag{3.6}$$

where the path is to be taken well within the boundaries of the superconductor. This gives a direct relation between the relative phase of the wave-function and the magnetic field.

So far so good, however integration of Eq. (3.5) over a closed path C inside a superconductor must satisfy further constraints such that the wave-function (3.2) is single-valued. For instance, if the path encloses a hole[3], the phase difference accumulated over one roundtrip should be equal to an integer multiple n of 2π

$$\frac{q}{\hbar}\oint_{\mathrm{C}}\vec{A}\cdot\,\mathrm{d}\vec{s} = 2\pi n\,,\quad n\in\mathbb{Z}\,. \tag{3.7}$$

Recognising that as follows from stokes theorem $\oint_{\mathrm{C}}\vec{A}\cdot\,\mathrm{d}\vec{s} = \Phi$ is equal to the magnetic flux Φ enclosed by the closed path C, we have

$$\Phi = n\frac{2\pi\hbar}{q} = n\phi_0\,,\quad n\in\mathbb{Z}\,, \tag{3.8}$$

that the flux threading a hole in a superconductor is quantised in units of the flux quantum

$$\phi_0 = \frac{2\pi\hbar}{q}\,. \tag{3.9}$$

3.1.3 Josephson effect

Now, we apply this macroscopic quantum mechanics to a concrete system that consists of two superconductors separated by a non-conducting barrier called a Josephson junction. The crucial point is that if the barrier is made thin enough, electrons or Cooper-pairs can tunnel through. The system is depicted schematically in Fig. 3.1.

The Josephson relations

Following the lectures of Feynman [39], written in the basis where the ground state for a particle on one side is ψ_1 and on the other side ψ_2, and considering that there is a tunnelling amplitude for a particle to cross the barrier, the Schrödinger equation (with magnetic field left out) for this system is

$$\mathrm{i}\hbar\frac{\partial}{\partial t}\begin{pmatrix}\psi_1\\ \psi_2\end{pmatrix} = \begin{pmatrix}U_1 & K\\ K & U_2\end{pmatrix}\begin{pmatrix}\psi_1\\ \psi_2\end{pmatrix}\,, \tag{3.10}$$

where the U describe the energies of the states corresponding to the two respective sides, and K denotes the tunnelling amplitude as a characteristic of the junction.

Now, It is important to note that in the superconducting phase, the states ψ_1 and ψ_2 are the respective ground-states occupied by approximately all Cooper-pairs on each side of the barrier (if K where zero).

[3] In case the path does not contain a hole, the integral in Eq. (3.7) should be equal to zero to avoid a singularity inside the domain of definition—in essence the space spanned by the superconductor—for the wave-function (3.2).

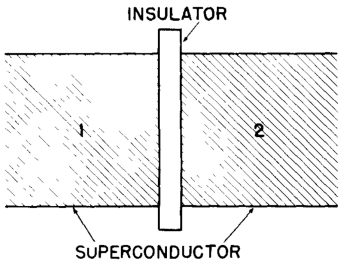

Figure 3.1: A Josephson junction: two superconductors connected by a thin non-conducting barrier. Figure from Ref. [39].

Connecting the two superconductors to a battery with voltage V leads to an energy difference $U_1 - U_2 = qV$ between the two states separated by the barrier. Redefining the zero of energy to be halfway between the two states and substituting in the potential difference gives

$$i\hbar \frac{\partial}{\partial t} \begin{pmatrix} \psi_1 \\ \psi_2 \end{pmatrix} = \begin{pmatrix} \frac{qV}{2} & K \\ K & -\frac{qV}{2} \end{pmatrix} \begin{pmatrix} \psi_1 \\ \psi_2 \end{pmatrix}, \tag{3.11}$$

the Schrödinger equation for a two level system with inter level coupling.

Because we are dealing with a superconducting system, we make the substitutions

$$\begin{aligned} \psi_1 &= \sqrt{\rho_1} e^{i\theta_1}, \\ \psi_2 &= \sqrt{\rho_2} e^{i\theta_2}, \end{aligned} \tag{3.12}$$

where the respective θ and ρ denote respectively the phase and density of the Cooper-pairs on each side. Equating the real and imaginary part, the result, with $\delta = \theta_2 - \theta_1$, is a set of four equations

$$\begin{aligned} \frac{\partial \rho_1}{\partial t} &= +\frac{2}{\hbar} K \sqrt{\rho_1 \rho_2} \sin(\delta), \\ \frac{\partial \rho_2}{\partial t} &= -\frac{2}{\hbar} K \sqrt{\rho_1 \rho_2} \sin(\delta), \end{aligned} \tag{3.13a}$$

$$\begin{aligned} \frac{\partial \theta_1}{\partial t} &= +\frac{K}{\hbar} \sqrt{\frac{\rho_2}{\rho_1}} \cos(\delta) - \frac{qV}{2\hbar}, \\ \frac{\partial \theta_2}{\partial t} &= +\frac{K}{\hbar} \sqrt{\frac{\rho_1}{\rho_2}} \cos(\delta) + \frac{qV}{2\hbar}. \end{aligned} \tag{3.13b}$$

The first two say that the rate of change in the Cooper-pair densities is equal but opposite on each side, but because the two superconductors are connected to a battery, an approximately infinite supply of in this case Cooper-pairs, the densities will remain constant. Therefore these equations actually describe the current that traverses the barrier, which is seen to depend on the phase difference δ across the barrier

$$\mathcal{I}_J = \frac{2K}{\hbar} \sin(\delta) = I_c \sin(\delta), \tag{3.14}$$

where we have defined the critical current of the junction as $I_c = \frac{2K\rho_0}{\hbar}$ with ρ_0 the Cooper-pair density taken equal on both sides.

Subtracting the time evolution Eqs. (3.13b) for the phases on each side gives an equation for the phase difference in relation to the voltage across the junction

$$\frac{\partial \delta}{\partial t} = \frac{q\mathcal{V}_\mathrm{J}}{\hbar} = \frac{2\pi}{\phi_0}\mathcal{V}_\mathrm{J} \tag{3.15}$$

or differently written

$$\mathcal{V}_\mathrm{J} = \frac{\hbar}{q}\frac{\partial \delta}{\partial t} = \frac{\phi_0}{2\pi}\frac{\partial \delta}{\partial t}\,, \tag{3.16}$$

where in the last step, the flux quantum is defined as $\phi_0 = \frac{h}{2e}$ with the charge $q = 2e$ of a Cooper-pair substituted[4].

Equations (3.16) and (3.14) are called the Josephson relations and together describe the dynamics of the Josephson junction as first described by Josephson [42]. Integrating the last equation, it is seen that at zero voltage, there can be a super-current across the junction between $-I_\mathrm{c}$ and I_c. It is also easy to see that when applying a DC voltage, the current becomes oscillatory with an average of zero.

Josephson non-linear inductance

Following lecture notes of Martinis and Osborn [43], the dynamics of the junction can be mapped to a lumped element circuit by differentiating the current relation Eq. (3.14) and substituting the voltage relation Eq. (3.16) for $\frac{\partial \delta}{\partial t}$ which gives

$$\mathcal{V}_\mathrm{J} = \frac{\phi_0}{2\pi I_\mathrm{c}\cos(\delta)}\frac{\partial \mathcal{I}_\mathrm{J}}{\partial t} = L_\mathrm{J}\frac{\partial \mathcal{I}_\mathrm{J}}{\partial t}\,. \tag{3.17}$$

In the last step we have defined the Josephson inductance as

$$L_\mathrm{J} = \frac{\phi_0}{2\pi I_\mathrm{c}\cos(\delta)} = \pm\frac{\phi_0}{2\pi I_\mathrm{c}\sqrt{1-\left(\frac{\mathcal{I}_\mathrm{J}}{I_\mathrm{c}}\right)^2}} \tag{3.18}$$

with the sign being *negative* only when $|\delta \bmod \pi| > \frac{\pi}{2}$. Since the phase difference δ depends on current through Eq. (3.14), the inductance is non-linear. Note that this shows that the Josephson inductance can be positive or negative depending on the phase difference.

[4]Note that the Josephson relations can be used to derive a kind of generalised flux that can be stored in a Josephson junction. If we define the generalised flux for a circuit element x as

$$\phi_x \equiv \int_{-\infty}^{t} \mathcal{V}_x \,\mathrm{d}t\,,$$

then upon substitution of the voltage Josephson relation, we see that

$$\phi_\mathrm{J} = \frac{\phi_0}{2\pi}\left(\delta(t) - \delta(-\infty)\right), \quad \text{or similarly} \quad \delta(t) = 2\pi\frac{\phi_\mathrm{J}}{\phi_0} + \delta(-\infty)\,.$$

Putting this last result into the current Josephson relation gives the constitutive relation for the Josephson element

$$\mathcal{I}_\mathrm{J} = I_\mathrm{c}\sin\left(2\pi\frac{\phi_\mathrm{J}}{\phi_0} + \delta(-\infty)\right),$$

which evidently can be considered a non-linear inductor. This will prove to be very useful later on. Also observe how the definition of generalised flux coincides with magnetic flux when applied to a magnetic inductor with self-inductance L:

$$\phi_L = \int_{-\infty}^{t} L\frac{\mathrm{d}\mathcal{I}_L}{\mathrm{d}t}\,\mathrm{d}t = L\left(\mathcal{I}_L(t) + \mathcal{I}_L(-\infty)\right),$$

up to an offset. Note that the offset in the magnetic and generalised flux do not need to come from a loop current or phase difference at $t = -\infty$ if the systems in question are not isolated from the rest of the universe as then other processes may also contribute to an offset.

To make the last equality explicit, we note that inversion of the current Josephson relations Eq. (3.14) to find an expression for the phase difference in terms of current, gives two infinite sets of solutions

$$\delta = \begin{cases} \arcsin\left(\frac{\mathcal{I}_\mathrm{J}}{I_\mathrm{c}}\right) + 2n\pi\,, & \text{if } |\delta \bmod \pi| \leq \frac{\pi}{2} \\ \pi - \arcsin\left(\frac{\mathcal{I}_\mathrm{J}}{I_\mathrm{c}}\right) + 2n\pi\,, & \text{if } |\delta \bmod \pi| > \frac{\pi}{2} \end{cases} \quad \text{with} \quad n \in \mathbb{Z} \tag{3.19}$$

and where we have defined the principle branch for the multivalued arcsine function as having the codomain $-\frac{\pi}{2} \leq \arcsin(.) < \frac{\pi}{2}$, i.e. as returning a value in that range. Within each set, the solutions are separated from each other by integer multiples of 2π. Thus putting this result in the argument of the cosine function, which is 2π-periodic, merges al the solutions within a set together, leaving us with two valid solutions

$$\cos(\delta) = \pm\cos\left(\arcsin\left(\frac{\mathcal{I}_\mathrm{J}}{I_\mathrm{c}}\right)\right) = \pm\sqrt{1 - \sin^2\left(\arcsin\left(\frac{\mathcal{I}_\mathrm{J}}{I_\mathrm{c}}\right)\right)} = \pm\sqrt{1 - \left(\frac{\mathcal{I}_\mathrm{J}}{I_\mathrm{c}}\right)^2}\,, \tag{3.20}$$

with the sign being *negative* only when $|\delta \bmod \pi| > \frac{\pi}{2}$.

Josephson energy

The energy stored in a Josephson junction can be derived straightforwardly through the usual path in circuit theory together with the Josephson relations

$$\begin{aligned} U_\mathrm{J} &= \int_{-\infty}^{t} \mathcal{I}_\mathrm{J}\mathcal{V}_\mathrm{J}\,\mathrm{d}t \\ &= \frac{I_\mathrm{c}\phi_0}{2\pi}\int_{-\infty}^{t} \sin(\delta)\frac{\partial\delta}{\partial t}\,\mathrm{d}t \\ &= \frac{I_\mathrm{c}\phi_0}{2\pi}\int_{\delta(-\infty)}^{\delta(t)} \sin(\delta)\,\mathrm{d}t \\ &= \frac{I_\mathrm{c}\phi_0}{2\pi}\big(\cos(\delta(-\infty)) - \cos(\delta(t))\big) \end{aligned}\,, \tag{3.21}$$

Usually $\delta(-\infty)$ is assumed such that the system is completely at rest in the beginning of time, meaning that at $t = -\infty$ the current and voltage are both zero, which corresponds to setting $\delta(-\infty) = 0$ (or $\delta(-\infty) = \pi$ which would let the system start with a negative inductance, but also in an unstable equilibrium, thus not fully at rest). This still leaves a constant offset in the energy, which however can be neglected—i.e. set to zero without further assumptions on $\delta(-\infty)$—since this is a potential energy. As such the Josephson energy is usually defined as

$$\mathcal{E}_\mathrm{J}(\delta) = -\frac{I_\mathrm{c}\phi_0}{2\pi}\cos(\delta) = \mp\frac{I_\mathrm{c}\phi_0}{2\pi}\sqrt{1 - \left(\frac{\mathcal{I}_\mathrm{J}}{I_\mathrm{c}}\right)^2} \tag{3.22}$$

with the sign being *positive* only when $|\delta \bmod \pi| > \frac{\pi}{2}$.

Incidentally this shows—when considered from a thermodynamics perspective assuming a low temperature environment—that a Josephson junction will usually prefer to be in the state with $|\delta \bmod \pi| < \frac{\pi}{2}$ which corresponds with a positive inductance, as this corresponds with an energy minimum. The negative inductance state on the other hand corresponds with an energy maximum and is as such unstable, and will if not constrained evolve into a positive inductance state. As such the negative inductance state usually does not occur in practice allowing us to replace $\cos(\delta)$ with its absolute value, thus selecting the positive branch of its representation in terms of current.

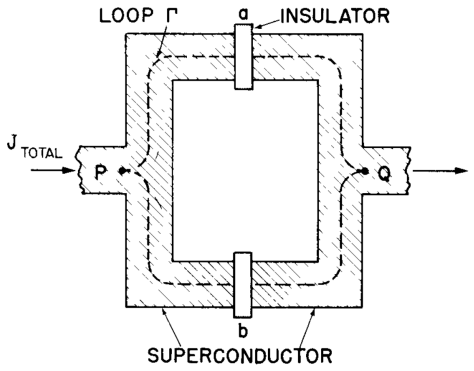

Figure 3.2: Drawing of a SQUID, two Josephson junctions in parallel, with respective phase jumps δ_a and δ_b. Figure from Ref. [39].

3.1.4 Two Josephson junctions in parallel

At this point we have enough information to introduce what is called a SQUID, in essence it consists of two Josephson junctions connected in parallel as drawn in Fig. 3.2. Now there are two paths, an upper and a lower, connecting the two superconducting leads, and this time (due to similarity with the discussion in Sec. 3.1.2) it is important to include the magnetic field in the discussion.

Considering the superconducting circuit and following one of Feynman's lectures [39], the wavefunction (3.2) must be single-valued across the whole circuit, which means that the phase difference across the two paths from one side to the other, should be the same plus-minus an integer factor n of 2π. This is the same argument as with flux quantisation in a superconducting ring, the only difference being that there is a phase jump δ_a and also δ_b across each tunnel junction.

Working out the phase differences θ across the upper and lower path, using Eq. (3.6), but including the phase jumps, we have

$$\begin{aligned} \Delta\theta_{\text{lower}} &= \delta_b + \frac{2e}{\hbar}\int_{\text{lower}} \vec{A}\cdot \mathrm{d}\vec{s}\,, \\ \Delta\theta_{\text{upper}} &= \delta_a + \frac{2e}{\hbar}\int_{\text{upper}} \vec{A}\cdot \mathrm{d}\vec{s}\,. \end{aligned} \tag{3.23}$$

Then working out the constraint $\Delta\theta_{\text{upper}} = \Delta\theta_{\text{lower}} + 2\pi n$ and subtracting the two equations from each other gives

$$\delta_b - \delta_a = \frac{2e}{\hbar}\oint_\Gamma \vec{A}\cdot \mathrm{d}\vec{s} + 2n\pi = \frac{2e}{\hbar}\Phi + 2\pi n = 2\pi\left(\frac{\Phi}{\phi_0} + n\right) \tag{3.24}$$

with Φ the flux threading the loop connecting the two junctions

SQUID with negligible loop inductance

Defining $\delta_0 \equiv \frac{\delta_a+\delta_b}{2}$, the average of the phase differences across the two junctions, we express the individual junction phase differences as

$$\delta_a = \delta_0 - \pi\left(\frac{\Phi}{\phi_0} + n\right) \quad \text{and} \quad \delta_b = \delta_0 + \pi\left(\frac{\Phi}{\phi_0} + n\right). \tag{3.25}$$

Then the total current across the circuit can, invoking Eq. (3.14) twice and then a trigonometric identity, be expressed as

$$I_{\text{total}} = I_{c_1} \sin\left(\delta_0 + \pi\left(\frac{\Phi}{\phi_0} + n\right)\right) + I_{c_1} \sin\left(\delta_0 - \pi\left(\frac{\Phi}{\phi_0} + n\right)\right) = 2I_{c_1} \cos\left(\pi\frac{\Phi}{\phi_0} + \pi n\right) \sin(\delta_0) \tag{3.26}$$

where we have taken the critical current—now denoted with a subscript 1 to emphasize its means as a *single* junction property—of both junctions identical.

Now this equation is of the same form as the current Jophson relation Eq. (3.14) if we regard the pre-factor of the sine as a critical current

$$I_{c_\Sigma}(\Phi) = 2I_{c_1} \cos\left(\pi\frac{\Phi}{\phi_0} + \pi n\right) . \tag{3.27}$$

This suggests that a SQUID may effectively be considered as a single Josephson junction whose critical current is modulated by the flux threading the SQUID loop[5].

In order to show that a SQUID can indeed be considered as such, a relation between the voltage $\mathcal{V}$ over the SQUID and average phase δ_0 of the same form as the voltage Josephson relation (3.16) must hold. This is easy to show through Kirchhoff's loop law, but first note that we must take into account an emf equal to $\frac{\mathrm{d}\Phi}{\mathrm{d}t}$ in the loop due to Faraday's law[6]. This leads to

$$\mathcal{V} = \mathcal{V}_a + \frac{1}{2}\frac{\mathrm{d}\Phi}{\mathrm{d}t} = \mathcal{V}_b - \frac{1}{2}\frac{\mathrm{d}\Phi}{\mathrm{d}t} \tag{3.28}$$

where we take the loop inductance as being distributed equally over the two arms of the loop.

Substituting into Eq. (3.28) the voltage Josephson relation Eq. (3.16) for each junction, and express the phase differences δ_a and δ_b in terms of the average phase difference δ_0 and the magnetic flux Φ as in Eqs. (3.25), the flux dependent terms are seen to drop out wich leaves us with

$$\mathcal{V} = \frac{2\pi}{\phi_0}\frac{\mathrm{d}\delta_0}{\mathrm{d}t} , \tag{3.29}$$

thus showing that it is indeed the case that a SQUID can be considered effectively as a single Josephson junction.

SQUID with significant loop inductance

There is however one fact we stepped over in the description above: If the loop inductance L_ℓ is not negligibly small (see Fig. 3.3), the currents circulating in the SQUID loop also contribute to the magnetic flux; Moreover, because a net current through the SQUID breaks the symmetry in the current through the two branches of the SQUID loop, Eq. (3.28) is not exactly valid.

The correct version of this equation is

$$\mathcal{V} = \mathcal{V}_a + \frac{\dot{\Phi}_e}{2} + \frac{L_\ell}{2}\dot{I}_a = \mathcal{V}_b - \frac{\dot{\Phi}_e}{2} + \frac{L_\ell}{2}\dot{I}_b , \tag{3.30}$$

[5]Note that it is possible that the effective critical current is negative; the effect is a reversal of the currents but also a negative inductance as demonstrated in Eq. (3.18). on the other hand, if a πshift occurs in both the average phase and phase difference of the junctions, then the sign of the inductance is preserved and only the net magnetic flux has made a jump to another solution of the transcendental relation in Eq. (3.33).

[6]As a side-note focussing on the latter equality in Eq. (3.28). Substituting in the voltage Josephson relation (3.16) for the two junctions and rearranging a bit

$$\frac{\mathrm{d}\delta_b}{\mathrm{d}t} - \frac{\mathrm{d}\delta_a}{\mathrm{d}t} = \frac{2\pi}{\phi_0}\frac{\mathrm{d}\Phi}{\mathrm{d}t}$$

shows that Faraday's law must be included in order to allow for a time varying flux.

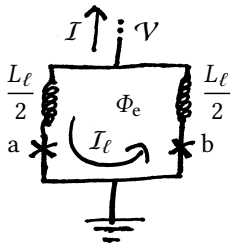

Figure 3.3: SQUID in lumped element representation with Loop inductance incorporated. It is assumed that the loop inductance L_ℓ is distributed uniformly over the loop. Also the orientation of the inductance in the two arms is opposite such that they both contribute constructively to the flux Φ in loop. Junction capacitances and sub-gap resistances are left out of the consideration for now.

where an over-dot denotes a time derivative and the variable Φ_e is introduced as an externally applied flux. This shows that the we can write the magnetic flux as

$$\Phi = \Phi_e - \frac{L_\ell}{2}\left(\mathcal{I}_b - \mathcal{I}_a\right) = \Phi_e - L_\ell \mathcal{I}_\ell \tag{3.31}$$

where we have defined $\mathcal{I}_\ell \equiv \frac{\mathcal{I}_b - \mathcal{I}_a}{2}$ as the current circulating in the loop. The latter can be worked out using the Josephson relations, a trigonometric relation and Eqs. (3.25):

$$\mathcal{I}_\ell = \frac{I_c}{2}\sin\left(\delta_0 + \pi\frac{\Phi}{\phi_0} + \pi n\right) - \frac{I_c}{2}\sin\left(\delta_0 - \pi\frac{\Phi}{\phi_0} - \pi n\right) = I_c\cos(\delta_0)\sin\left(\pi\frac{\Phi}{\phi_0} + \pi n\right). \tag{3.32}$$

This in turn allows us to find a non-invertible transcendental equation for the total flux threading the loop

$$\Phi = \Phi_e - L_\ell I_c\cos(\delta_0)\sin\left(\pi\frac{\Phi}{\phi_0} + \pi n\right). \tag{3.33}$$

Observe that the circulating loop current screens the magnetic loop flux away from half-integer flux quanta towards an integer number of flux quanta. Finally, we derive a modified expression for the voltage across the SQUID from Eq. (3.30)

$$\begin{aligned}\mathcal{V} &= \mathcal{V}_a + \tfrac{1}{2}\dot{\Phi}_e + \tfrac{1}{2}L_\ell\dot{\mathcal{I}}_a \\ &= \tfrac{1}{2\pi}\phi_0\dot{\delta}_0 - \tfrac{1}{2}\dot{\Phi} + \tfrac{1}{2}\dot{\Phi}_e + \tfrac{1}{2}L_\ell\dot{\mathcal{I}}_a \\ &= \tfrac{1}{2\pi}\phi_0\dot{\delta}_0 + \tfrac{1}{4}L_\ell\left(\dot{\mathcal{I}}_a + \dot{\mathcal{I}}_b\right) \\ &= \tfrac{1}{2\pi}\phi_0\dot{\delta}_0 + \tfrac{1}{2}L_\ell I_c\tfrac{\mathrm{d}}{\mathrm{d}t}\left(\cos\left(\pi\tfrac{\Phi}{\phi_0} + n\pi\right)\sin(\delta_0)\right)\end{aligned} \tag{3.34}$$

where we have taken the a-branch of the loop. First we substitute the voltage Josephson relation with the phase difference written in terms of the average phase δ_0 and the flux Φ, and then Eq. (3.31), which causes a lot of terms to drop out, and finally allows us to substitute Eq. (3.26) to get a closed form expression in terms of flux and the average phase. Note that this shows that from a voltage perspective a SQUID with a loop self-inductance can be regarded effectively as a single (tuneable) Josephson junction in series with an inductor.

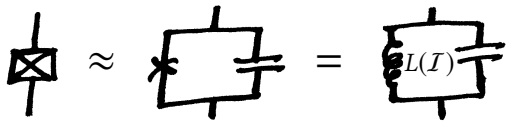

Figure 3.4: Equivalent circuit for a more realistic Josephson junction. We do leave out the less then infinite electrical resistance of the substrate forming the tunnel barrier.

In summary, a SQUID with non-zero loop inductance is described by the three equations

$$\mathcal{I} = 2I_{c_1} \cos\left(\pi \tfrac{\Phi}{\phi_0} + n\pi\right) \sin(\delta_0)\,; \tag{3.35a}$$

$$\mathcal{V} = \tfrac{1}{2\pi}\phi_0\dot{\delta}_0 + \tfrac{1}{2}L_\ell I_c \tfrac{\mathrm{d}}{\mathrm{d}t}\left(\cos\left(\pi \tfrac{\Phi}{\phi_0} + n\pi\right)\sin(\delta_0)\right); \tag{3.35b}$$

$$\Phi = \Phi_e - L_\ell I_c \cos(\delta_0) \sin\left(\pi \tfrac{\Phi}{\phi_0} + n\pi\right)\,. \tag{3.35c}$$

It is however unfortunate that the net magnetic flux Φ is not a simple function of the applied magnetic flux Φ_e, but is the solution to a transcendental equation that also depends on the average phase difference δ_0. This not only makes it perhaps impossible to find closed form solutions for the set of equations by analytical means, but also makes the net flux a variable that cannot be controlled precisely in experiments[7]. A practical way out is to make the loop inductance negligibly small such that $\Phi \approx \Phi_e$ and the SQUID can be considered a single effective Josephson junction with a tuneable critical current described as by Eq. (3.27) and behaviour as described in Sec 3.1.3.

3.1.5 A more practical SQUID considered as a lumped element

So far we have discussed ideal Josephson junctions and SQUIDs consisting of ideal Josephson junctions. In practice however, a Josephson junction has associated with it a capacitance as well as a less than infinite resistance called the "sub-gap resistance". The latter opens a dissipation channel as it allows normal conduction of unpaired electrons through the barrier whenever a voltage across it appears. These two practical additions as well as effects of thermal (and quantum?) noise are described in the RCSJ-model of a Josephson junction; see Ref. [44] for a more in depth discussion regarding its application in SQUIDs. For the scope of this work, we will ignore most of these practical additions, but we will consider the effect of junction capacitances in this section. Losses due to the sub-gap resistance can be lumped into an overall Q-factor for the resonator in which the SQUID is incorporated.

Then a practical junction should be considered a parallel combination of an ideal Josephson junction and a capacitor C_J as depicted in Fig. 3.4. This introduces a so called plasma mode with (depending on the connecting circuit) a resonance frequency

$$\omega_J = \frac{1}{\sqrt{L_J C_J}} \tag{3.36}$$

where the effective inductance is given by Eq. (3.18) at zero current or zero phase difference. Because we are dealing with a non-linear inductance, above frequency is strictly speaking only valid for oscillations who's current amplitude satisfies

$$1 - \left(\frac{\mathcal{I}_J}{I_c}\right)^2 \approx 1\,. \tag{3.37}$$

[7] Actually, Eq. (3.33) has the form of a constraint, effectively reducing the amount of degrees of freedom in the SQUID by one. Moreover, while we cannot solve this equation for Φ, it can be used to express $\cos(\delta_0)$ as a function of flux. Something to try and work out later…

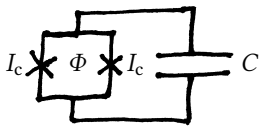

Figure 3.5: The electrical circuit for an ideal lumped element SQUID-cavity. In essence it is an LC-resonator with the inductor replaced by a SQUID. Because the SQUID forms a non-linear inductance, the resonator becomes anharmonic.

The plasma frequency decreases for higher currents as those effectively increase the Josephson inductance.

The presence of plasma modes influences the other modes in the circuit incorporating Josephson junctions. The effect, however, is in almost all cases negligible, because in practice the junction capacitances can to good approximation be considered zero. This causes the plasma mode frequencies to be much higher than any of the other mode frequencies occurring in the circuit. The plasma modes are thus highly off resonance and therefore have little effect on the other dynamics occurring in the circuit.

Another aspect that needs further consideration is that the Josephson elements may be driven into a non-linear regime. For instance, when increasing the current amplitude, at some point, the Josephson inductance can no longer be considered constant. From that point on, one must include the non-linearity into the circuit description. This, however, complicates circuit theory as the phasor network description breaks down in the presence of non-linearities.

3.2 Tuneable resonators

Here we introduce two kinds of flux tuneable resonators:

1. a lumped element implementation which is essentially a SQUID shunted with a large capacitance;
2. a transmission line resonator that is terminated at one end with a SQUID as an analogue to a moveable mirror.

For each we start with a time domain analysis in order to investigate non-linear circuits, and then move on to an effective lumped element description.

3.2.1 Flux tuneable lumped element resonator

As the simplest example of a flux tuneable resonator, we disregard dissipation and start from a simple LC-resonator and replace the inductor with a SQUID. This way we have essentially a SQUID that is shunted with a large capacitance, as drawn in Fig. 3.5. The self-inductance of the SQUID loop we neglect for now. For completeness we begin our discussion with the time domain equations of motion as derived from Kirchhoff's laws. Lumping together the junction capacitances and the large shunt capacitance, and expressing the voltage and current in terms of the average phase and loop flux through the effective Josephson relations for a SQUID, Eqs. (3.26) and (3.29), we obtain

$$C\frac{\phi_0}{2\pi}\frac{\mathrm{d}^2\delta_0}{\mathrm{d}t^2} + 2I_c\cos\left(\pi\frac{\Phi}{\phi_0}\right)\sin\left(\delta_0\right) = 0\,, \tag{3.38}$$

a non-linear second order differential equation. Dividing by $C\frac{\phi_0}{2\pi}$ and making a third order taylor expansion: $\sin(\delta_0) \approx \delta_0 - \frac{{\delta_0}^3}{6}$, gives the equation for a Duffing oscillator

$$\frac{\mathrm{d}^2\delta_0}{\mathrm{d}t^2} + {\omega_0}^2(\Phi)\delta_0 - K(\Phi){\delta_0}^3 = 0 \tag{3.39}$$

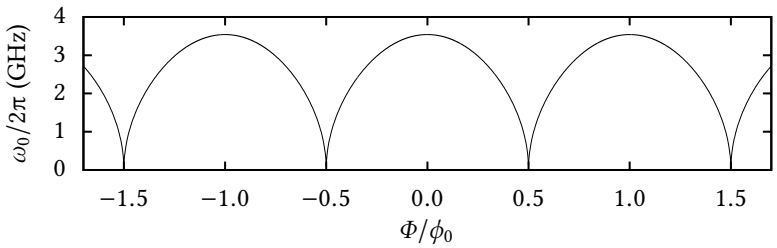

Figure 3.6: Resonance frequency of an ideal lumped element SQUID resonator as a function of flux tuning in the small amplitude limit. The critical current of the Josephson junctions is taken as 0.75 μA; the capacitor is set to 9.21 pF.

where

$$\omega_0(\Phi) = \sqrt{\frac{4\pi I_c}{C\phi_0}\cos\left(\pi\frac{\Phi}{\phi_0}\right)} \tag{3.40}$$

is the resonant frequency in the small amplitude limit where the cubic term vanishes; note that we would have obtained the same resonant frequency had we substituted the linear approximation of the Josephson inductance for the SQUID. A plot of the small amplitude resonance frequency is given in Fig. 3.6.

The strength of the Duffing non-linearity is given by

$$K(\Phi) = \frac{2\pi I_c}{3C\phi_0}\cos\left(\pi\frac{\Phi}{\phi_0}\right). \tag{3.41}$$

Harmonic approximation

In any case, Eq. (3.39) shows that when the amplitude of the average phase δ_0 is not too large depending on $K(\Phi)$, we can essentially assume $|{\omega_0}^2\delta_0| \gg |K{\delta_0}^3|$ and neglect the Duffing term. This effectively renders the system a harmonic oscillator. This is important because it allows us to express it as a linear lumped element LC-resonator with capacitance C and for the inductance the expression for the linearised SQUID inductance $L = \frac{\phi_0}{4\pi I_c \cos\left(\pi\frac{\Phi}{\phi_0}\right)}$.

Effect of the Duffing non-linearity

Here we discuss qualitatively some of the effects the cubic non-linearity may have. The arguments presented are by no means exact, but are given merely to provide an intuitive description of two important characteristics of driven weakly damped Duffing oscillators. Thus the results should be regarded as nothing more than a very crude approximation. There is much more to be said about Duffing oscillators (including e.g. chaotic dynamics) but for the scope of this work we leave it at an amplitude dependent resonance frequency and bifurcation of the resonance curve for the driven weakly damped version. For a more in depth discussion see Ref. [45] or the original publication by Duffing Ref. [46].

Let us first rewrite Eq. (3.39) as

$$\frac{\mathrm{d}^2\delta_0}{\mathrm{d}t^2} + \left({\omega_0}^2(\Phi) - K(\Phi){\delta_0}^2\right)\delta_0 = 0\,. \tag{3.42}$$

Now, if we replace, in the term enclosed by parenthesis, the average phase squared with its average: $\overline{{\delta_0}^2} \to {\delta_0}^2$, we see that we there is an amplitude dependent shift in resonance frequency. Since this is a

hand-waving argument, we will make it a bit more concrete by substituting a harmonic trial solution $A\cos(\omega t)$ in the equation of motion even though the the system is anharmonic

$$\left({\omega_0}^2 - \omega^2\right) A\cos(\omega t) - KA^3\cos^3(\omega t) = 0\,. \tag{3.43}$$

Upon substitution of a trigonometric power reduction formula: $\cos^3(\omega t) = \frac{1}{4}\left(3\cos(\omega t) + \cos(3\omega t)\right)$, we obtain

$$\left({\omega_0}^2 - \frac{3}{4}KA^2 - \omega^2\right)\cos(\omega t) - \frac{1}{4}KA^2\cos(3\omega t) = 0 \tag{3.44}$$

where we see that the non-linearity introduces a third harmonic in the equation (and should introduce more harmonics as shown by recursively substituting the higher order terms into the equation). For long time scales we may disregard the higher harmonic(s) by which we consider the motion effectively harmonic. Then we find an approximate expression for the amplitude dependent resonance frequency

$$\omega_0' \approx \sqrt{{\omega_0}^2 - \frac{3}{4}KA^2} \approx \omega_0 - \frac{3}{8}KA^2\,. \tag{3.45}$$

This is still hand-waving since the effects of damping and driving are not taken into account, but the result is close enough for our discussion.

When we add harmonic driving $F\cos(\omega t)$ and weak linear damping $\gamma\frac{\mathrm{d}\delta_0}{\mathrm{d}t}$ to the equation

$$\frac{\mathrm{d}^2\delta_0}{\mathrm{d}t^2} + \gamma\frac{\mathrm{d}\delta_0}{\mathrm{d}t} + {\omega_0}^2\delta_0 - K(\Phi){\delta_0}^3 = F\cos(\omega t)\,, \tag{3.46}$$

another phenomenon may be observable for sufficiently strong driving: a bifurcation of the resonance curve. This can be understood as follows. The oscillatory amplitude depends on a balance between driving and damping, while the effectiveness of the driving depends on how much the driving frequency falls within the resonance line-width around the resonance frequency. Since the latter depends on the actual amplitude of oscillation, one can imagine that for some oscillatory amplitudes, the frequency is shifted by more than a line-width. This indicates a bifurcation where there are two stable solutions: one where the in this case highly excited resonator is driven on its strongly shifted resonance; and one where the resonator is driven at the same frequency but is only weakly excited causing the drive to miss the now negligibly shifted resonance.

The average of the non-linear SQUID inductance we derive from the approximate resonance frequency

$$L_{\mathrm{eff}} = \frac{1}{{\omega_0'}^2 C} \approx \frac{1}{\left({\omega_0}^2 - \frac{3}{4}KA^2\right)C} = \frac{\phi_0}{4\pi I_{\mathrm{c}}\cos\left(\pi\frac{\Phi}{\phi_0}\right)\left(1 - \frac{1}{8}A^2\right)}\,. \tag{3.47}$$

Note that this may be different from the non-linear SQUID inductance averaged assuming harmonic motion. If we are to write the input impedance—a formalism defined in the framework of *linear electrical networks*—for this non-linear system, it is the former effective inductance we should use; the amplitude A must however be known beforehand.

Input impedance

The input impedance in the harmonic approximation is easily written in terms of the effective SQUID inductance and the shunt capacitance as if it were a parallel LC-resonator

$$Z_{\mathrm{in}} = \frac{\mathrm{i}\omega L}{1 - \omega^2 LC} = \frac{\mathrm{i}\omega\phi_0}{4\pi I_{\mathrm{c}}\cos\left(\pi\frac{\Phi}{\phi_0}\right) - \omega^2\phi_0 C}\,. \tag{3.48}$$

A crude generalisation to the weakly non-linear version is given by instead substituting Eq. (3.47) for the effective SQUID inductance

$$Z_{\text{in}} = \frac{\mathrm{i}\omega\phi_0}{4\pi I_{\text{c}} \cos\left(\pi\frac{\Phi}{\phi_0}\right)\left(1-\frac{1}{8}A^2\right) - \omega^2\phi_0 C}\,. \tag{3.49}$$

For the electrical characteristics one may observe when coupling this system to a feed-line, see Sec. 2.3.

3.2.2 Flux tuneable transmission line resonator

This subsection introduces a SQUID loaded transmission line resonator, which consists of a transmission line terminated with a SQUID at one end and with an open circuit at the other end. Changing the SQUID inductance modifies the boundary conditions for the current and voltage distribution over the transmission line, and therefore influences the standing wave resonances. As such, this results in a tuneable resonator whose resonant frequency depends on the bias flux through the SQUID loop. This setup is discussed and analysed in Refs. [47, 48]; especially the former reference contains a thorough analysis that also discusses the effects of the non-linear SQUID inductance. On a side note, hysteresis effects arising when the SQUID loop-inductance is significant are analysed on a phenomenological level in Ref. [49]. In order to understand the dynamics of the system, we first discuss a transmission line loaded with an inductor in a time domain analysis. Then we consider the effect of making the inductor non-linear by replacing it with the flux tuneable inductance of a SQUID, before deriving an approximate lumped element description.

Transmission line loaded with inductor

We start with a discussion of the dynamics of a transmission line open ended on one side and terminated with an inductor on the other side, as drawn in Fig. 3.7. Since a transmission line is a one dimensional medium that supports linear wave propagation, the current or voltage dynamics in its bulk satisfy a wave equation; where in Sec. 2.2.1 we discussed the frequency domain characteristics we will here instead start in the time domain.

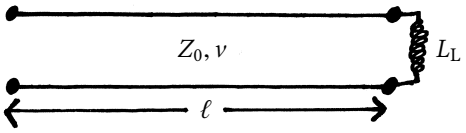

Figure 3.7: Transmission line loaded with an inductor

Time domain characteristics The bulk equation of motion for the current leaving out dissipation is given as

$$\frac{\partial^2 \mathcal{V}}{\partial t^2} - v^2\frac{\partial^2 \mathcal{V}}{\partial x^2} = 0\,; \tag{3.50}$$

the current distribution $\mathcal{I}(x,t)$ satisfies the same equation. Boundary conditions are derived from the principle of current conservation. At the open end, charge cannot jump into the vacuum, and therefore

$$\mathcal{I}(0) = 0 \quad \text{and similarly} \quad \frac{\partial \mathcal{V}(0)}{\partial x} = 0 \tag{3.51}$$

as can easily be seen from the telegrapher equations (2.17). The other boundary condition is less trivial to work out as, at the other end where the inductor is connected, it relates the current to the voltage

through a time derivative

$$\mathcal{V}(\ell) = L\frac{\partial \mathcal{I}(\ell)}{\partial t}\,; \tag{3.52}$$

assuming charge conservation at the interface, we can by the telegrapher relation $\frac{\partial \mathcal{V}}{\partial z} = -L'\frac{\partial \mathcal{I}}{\partial t}$ transform it to a Robin type boundary condition

$$\mathcal{V}(\ell) = -\frac{L}{L'}\frac{\partial \mathcal{V}(\ell)}{\partial x}\,. \tag{3.53}$$

Harmonic resonances Since the electrical network is linear and the wave equation supports plane wave propagation we try a harmonic solution of the form

$$\mathcal{V} = A\sin(\omega t)\cos(kx) \tag{3.54}$$

that automatically satisfies the insulating boundary condition at $x = 0$. Given a solution of this form, the dispersion relation is obtained from the bulk equation of motion

$$\omega = kv\,. \tag{3.55}$$

Substitution the trial solution into the other boundary condition gives

$$\cos\left(\frac{\omega}{v}\ell\right) = \frac{\omega}{v}\frac{L}{L'}\sin\left(\frac{\omega}{v}\ell\right) \quad \text{or} \quad \cot\left(\frac{\omega}{v}\ell\right) = \frac{\omega}{v}\frac{L}{L'} = \frac{\omega L}{Z_0}\,. \tag{3.56}$$

Solving this transcendental boundary condition determines the harmonic resonance frequencies and corresponding normal modes.

Non-linear correction

If we replace the linear load inductor with a SQUID with negligible loop inductance and junction capacitances, we obtain the circuit drawn in Fig. 3.8. Because the load inductance has now become non-linear, the replacement modifies the boundary condition at the interface between the load and the transmission line. While in principle we can substitute into the boundary condition the the non-linear SQUID inductance, it would not bring the boundary conditions to a useful form. The reason is that the inductance is a non-linear function of current and the latter is not easily expressed in terms of voltage without including a time derivative; That complicates the boundary condition.

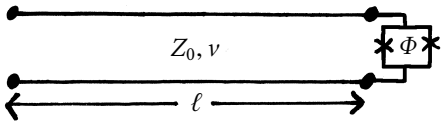

Figure 3.8: A SQUID loaded transmission line of specific length.

Transformation to node flux variables The way out is to integrate the equation of motion and boundary conditions over time and transform the equations to a new variables defined as

$$\phi(x,t) \equiv \int_{-\infty}^{t} \mathcal{V}(x,t)\,\mathrm{d}t\,. \tag{3.57}$$

Such variables are called node fluxes; more about those will be discussed later, but see e.g. the book by Peikari [33] for a thorough and general treatment of circuit theory in this representation. Note that in this representation the current and voltage along the transmission line are easily expressed in terms of respectively a spatial- and time derivative of the node variables (as can be checked easily with the telegrapher equations).

Anharmonic boundary condition In terms of node flux variables, the equations of motion and boundary conditions read

$$\frac{\partial^2\phi}{\partial t^2} - v^2\frac{\partial^2\phi}{\partial x^2} = 0 \tag{3.58a}$$

$$\frac{\partial\phi(0)}{\partial x} = 0 \tag{3.58b}$$

$$\phi(\ell) = \frac{\phi_0}{2\pi}\delta_0 \tag{3.58c}$$

$$\frac{-1}{L'}\frac{\partial\phi(\ell)}{\partial x} = 2Ic\cos\left(\pi\frac{\Phi}{\phi_0}\right)\sin(\delta_0) \tag{3.58d}$$

The last two equations form the equivalent of the boundary condition at the interface between the transmission line and the SQUID. The first of the two follows from equality of voltage at both sides of the interface and the voltage Josephson relation; the second follows from charge conservation and the current Josephson relation. Combining the last two equations into a single boundary condition gives

$$\frac{-1}{L'}\frac{\partial\phi(\ell)}{\partial x} = 2Ic\cos\left(\pi\frac{\Phi}{\phi_0}\right)\sin\left(2\pi\frac{\phi(\ell)}{\phi_0}\right). \tag{3.59}$$

Since the boundary condition at the open end has remained invariant in the transformation, we try the same harmonic trial solution, even though the other boundary condition is now non-linear. First making a Taylor expansion to third order in $\phi(\ell)$ of Eq. 3.59

$$\frac{-\phi_0}{4\pi Ic\cos\left(\pi\frac{\Phi}{\phi_0}\right)}\frac{1}{L'}\frac{\partial\phi(\ell)}{\partial x} = \phi(\ell) - \frac{2}{3}\left(\frac{\pi}{\phi_0}\right)^2\phi^3(\ell). \tag{3.60}$$

Then upon substution of $\phi = A\cos(\omega t)\cos(\frac{\omega}{v}x)$ we obtain

$$\frac{\phi_0}{4\pi I_c\cos\left(\pi\frac{\Phi}{\phi_0}\right)}\frac{\omega}{L'v}\cos(\omega t)\sin\left(\frac{\omega}{v}\ell\right) = \cos(\omega t)\cos\left(\frac{\omega}{v}\ell\right) - \frac{2}{3}\left(\frac{\pi}{\phi_0}\right)^2 A^2\cos^3(\omega t)\cos^3\left(\frac{\omega}{v}\ell\right). \tag{3.61}$$

Rewriting using the trigonometric power reduction formula $\cos^3(\omega t) = \frac{1}{4}(3\cos(\omega t) + \cos(3\omega t))$ we see that a third harmonic is generated by the non-linear boundary condition[8]. Since the effect of the third harmonic should average out on long time scales if the dynamics remain approximately harmonic at the original resonance, we may (as we did with the lumped element variant) disregard the contributions to the boundary condition oscillating at three times the resonance frequency. This yields

$$\frac{\phi_0}{4\pi I_c\cos\left(\pi\frac{\Phi}{\phi_0}\right)}\frac{\omega}{L'v}\sin\left(\frac{\omega}{v}\ell\right) = \cos\left(\frac{\omega}{v}\ell\right) - \frac{1}{2}A^2\left(\frac{\pi}{\phi_0}\right)^2\cos^3\left(\frac{\omega}{v}\ell\right) \tag{3.62}$$

Dividing by $\cos\left(\frac{\omega}{v}\ell\right)$ or $\sin\left(\frac{\omega}{v}\ell\right)$ gives the amplitude dependent resonance condition in more practical form

$$\frac{\phi_0}{4\pi I_c\cos\left(\pi\frac{\Phi}{\phi_0}\right)}\frac{\omega}{L'v}\tan\left(\frac{\omega}{v}\ell\right) = 1 - \frac{1}{2}A^2\left(\frac{\pi}{\phi_0}\right)^2\cos^2\left(\frac{\omega}{v}\ell\right) \tag{3.63a}$$

[8]The third harmonic in the boundary condition may excite higher harmonics in the transmission line and thereby may effectively create a coupling between neighbouring resonant modes that are otherwise independent.

or

$$\frac{\phi_0}{4\pi I_c \cos\left(\pi\frac{\Phi}{\phi_0}\right)}\frac{\omega}{L'v} = \cot\left(\frac{\omega}{v}\ell\right) - \frac{1}{2}A^2\left(\frac{\pi}{\phi_0}\right)^2\frac{\cos^3\left(\frac{\omega}{v}\ell\right)}{\sin\left(\frac{\omega}{v}\ell\right)} \tag{3.63b}$$

which has the same form as the expression derived in Ref. [47] (though the constants may be different, I have not checked precisely; in that paper they have a slightly different approach also incorporating the SQUID's plasma frequency).

In contrast to the lumped element resonator, here it is not so easy to obtain a closed form expression for the resonance frequency. One thus has to resort to numerical methods for solving the transcendental boundary condition.

Effective load inductance An effective load inductance can be derived by comparing Eq. 3.62 with the same equation for the harmonic case Eq. 3.56 and lumping the non-linear correction together with the SQUID inductance inductance

$$L_{\text{eff}} = \frac{\phi_0}{4\pi I_c \cos\left(\pi\frac{\Phi}{\phi_0}\right)} + \left(\frac{\pi}{\phi_0}\right)^2\frac{A^2L'v}{2\omega}\frac{\cos^3\left(\frac{\omega}{v}\ell\right)}{\sin\left(\frac{\omega}{v}\ell\right)}\,. \tag{3.64}$$

This however requires one to know the resonance frequency beforehand and corresponds to adjusting the a linear inductance in the harmonic model until the resonance frequency corresponds to a main resonance of the anharmonic resonator.

If we are to model the primary anharmonic resonance as a linear lumped element network, this is the effective inductance we should employ; thereby not forgetting the effective inductance and resonance frequency both depend on the amplitude of oscillations. Equation (3.64) may further prove useful for determining the relative strength of the non-linearity.

Input impedance

The next thing to do is figure out the input impedance of the transmission line loaded with an inductor, as drawn in Fig. 3.7. The inductor loads the line with an impedance $Z_L = i\omega L_L$ We use Eq. (2.41) for the input impedance of a loaded transmission line from Sec. 2.2.2. With that and leaving out losses we obtain

$$\begin{aligned} Z_{\text{in}} &= Z_0\frac{i\omega L_L + iZ_0\tan(\beta\ell)}{Z_0 + i^2\omega L_L\tan(\beta\ell)} \\ &= iZ_0\frac{\frac{\omega L_L}{Z_0} + \tan\left(\frac{\omega\ell}{v}\right)}{1 - \frac{\omega L_L}{Z_0}\tan\left(\frac{\omega\ell}{v}\right)}\,. \end{aligned} \tag{3.65}$$

The input impedance can be simplified further by noting the following relations,

- that for any branch of the arctangent function

$$\frac{\omega L_L}{Z_0} = \tan\left(\arctan\left(\frac{\omega L_L}{Z_0}\right)\right)\,;$$

- and (see e.g. the handbook by Abromowitz and Stegun [50]) the tangent relation

$$\tan(z_1 + z_2) = \frac{\tan z_1 + \tan z_2}{1 - \tan z_1\tan z_2}\,.$$

These allow us to rewrite the input impedance as

$$Z_{\text{in}} = iZ_0\tan\left(\arctan\left(\frac{\omega L_L}{Z_0}\right) + \frac{\omega\ell}{v}\right)\,. \tag{3.66}$$

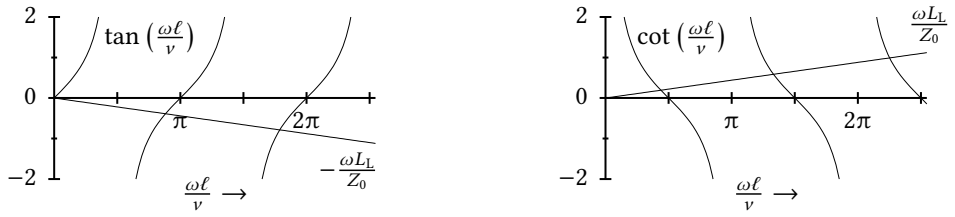

(a) Series type resonances **(b)** Parallel type resonances

Figure 3.9: Graphical solutions of the resonance conditions for an inductor loaded transmission line resonator. The resonance frequencies are at the intersections of the two plotted functions in each graph. The length of the transmission line 5 mm, its characteristic impedance 50 Ω, the phase velocity 100 km/s and the load inductance 35 nH.

Resonance conditions As we know from circuit theory (see Sec. 2.1 or 2.2.4), series type of resonances are found at the zeros of input impedance in its imaginary part while parallel kinds of resonances occur at the poles thereof. Then, from Eq. (3.65) we see that as expected for a transmission line resonator, two infinite sets of resonances exists, one containing all the series kind of resonances, the other all the parallel kind resonances. A bit of algebra gives us explicit expressions for the resonance conditions

$$\tan\left(\frac{\omega\ell}{v}\right) = -\frac{\omega L_\mathrm{L}}{Z_0} \quad \text{for} \quad Z_\mathrm{in} = 0\,, \tag{3.67a}$$

$$\cot\left(\frac{\omega\ell}{v}\right) = \frac{\omega L_\mathrm{L}}{Z_0} \quad \text{for} \quad Y_\mathrm{in} = 0\,. \tag{3.67b}$$

In contrast to the resonance conditions for the quarter- and half-wave resonators, these are transcendental equations and can as such not be solved exactly. They can however be solved numerically, or graphically. The latter method is demonstrated in the graphs in Fig. 3.9. Note that the resonance frequency with increasing mode-number n approaches $(n + \frac{1}{2})\pi$ for the series resonances and $n\pi$ for the parallel resonances, while the first few moded, depending on the load inductance, this can be the other way around.

Using the fact that $\cot(x) = \tan(-x + \frac{\pi}{2})$ we can write the resonance conditions in more explicit form

$$\frac{\omega\ell}{v} + \arctan\left(\frac{\omega L_\mathrm{L}}{Z_0}\right) = (1+n)\,\pi \quad \text{for} \quad Z_\mathrm{in} = 0 \tag{3.68a}$$

$$\frac{\omega\ell}{v} + \arctan\left(\frac{\omega L_\mathrm{L}}{Z_0}\right) = \left(\tfrac{1}{2}+n\right)\pi \quad \text{for} \quad Y_\mathrm{in} = 0 \tag{3.68b}$$

where $n \in \{0, 1, \ldots\}$ and we use the principle branch of the arctangent function $-\frac{\pi}{2} < \arctan(.) < \frac{\pi}{2}$. Note that we have restricted the range of allowed integers n to avoid negative frequency solutions. Because the arctangent function is a one-to-one map, these resonance conditions can easily be solved by any numerical root finding algorithm[9]. In figure 3.10 a numerical approximation for the resonant frequencies for the first few modes are plotted as a function of the load inductance.

We focus on the parallel kind of resonance where $n = 0$ and $Y_\mathrm{in} = 0$. This is the lowest frequency mode present in this system. This resonant frequency ω_0 then is defined as the solution of

$$\arctan\left(\frac{\omega_0 L_\mathrm{L}}{Z_0}\right) + \frac{\omega_0\ell}{v} = \frac{1}{2}\pi\,. \tag{3.69}$$

[9] As long as the argument for the arctangent is not too large, since that would cause the function's derivative to vanish.

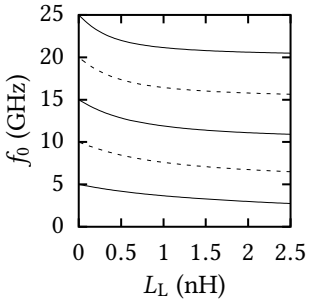

Figure 3.10: Mode frequencies for an inductor loaded transmission line resonator. The symmetric modes are drawn with dashed lines. Note how for higher mode numbers the frequency modulation is stronger in the region where the Load inductance approaches zero Henry. The transmission line has the following characteristics: v = 100 km/s, ℓ = 5 mm and Z_0 = 50 Ω.

We note that in the limit of $L_L = 0$, the resonance frequency (3.69) becomes $\omega_0 \to \frac{\pi}{2}\frac{v}{\ell}$, that of a quarter-wave resonator, which is to be expected as in this case the transmission line is effectively loaded with a short. In the other limit of a very large Load inductance, $\arctan\left(\frac{\omega_0 L_L}{Z_0}\right) \to \frac{\pi}{2}$ such that resonance frequency $\omega_0 \to \pi\frac{v}{\ell}$, equivalent to that of a half-wave resonator, this can also be explained intuitively by noting that a very large inductance can effectively be considered an open circuit.

Equivalent circuit Carrying out a first order Taylor expansion for the reciprocal of the input impedance written in compact form in Eq. (3.66) around the resonance frequency defined in Eq. (3.69) gives an expression for the input admittance that is valid for frequencies close to the resonance frequency

$$\begin{aligned} Y_{\text{in}} &\approx Y_{\text{in}}\Big|_{\omega_0} + (\omega-\omega_0)\left.\frac{\mathrm{d}Y_{\text{in}}}{\mathrm{d}\omega}\right|_{\omega_0} \\ &= \frac{-\mathrm{i}}{Z_0}\frac{\frac{\ell}{v}+\frac{L_L}{Z_0}\frac{1}{1+\left(\frac{\omega_0 L_L}{Z_0}\right)^2}}{-\sin^2\left(\arctan\left(\frac{\omega_0 L_L}{Z_0}\right)+\frac{\omega_0\ell}{v}\right)}(\omega-\omega_0) \\ &= \frac{\mathrm{i}}{Z_0}\left(\frac{\ell}{v}+\frac{1}{\frac{Z_0}{L_L}+{\omega_0}^2\frac{L_L}{Z_0}}\right)(\omega-\omega_0) \end{aligned} \tag{3.70}$$

where in the last step the sine squared is seen to be equal to unity upon substitution of the resonance condition Eq. (3.69).

The result can be mapped upon a parallel RLC-circuit (see Sec. 2.1.2). A comparison with Eq. (2.9), the input admittance of a parallel RLC-resonator in a first order Taylor expansion, gives

$$C = \frac{1}{2Z_0}\left(\frac{\ell}{v}+\frac{1}{\frac{Z_0}{L_L}+{\omega_0}^2\frac{L_L}{Z_0}}\right), \tag{3.71a}$$

$$L = \frac{1}{{\omega_0}^2 C}, \tag{3.71b}$$

and through the addition of a Q-factor (i.e. dissipation) by substitution of a complex resonance frequency $\omega_0 \leftarrow \omega_0(1 + \frac{\mathrm{i}}{2Q_0})$ as described in Sec. 2.1.4

$$R = \frac{Q_0}{\omega_0 C}\,. \tag{3.71c}$$

SQUID loaded transmission line resonator

Now, building upon the results of the previous section, we replace the load inductor used in the previous section with the effective inductance of a SQUID, which due to the SQUID's flux tuneability, makes the resonant frequency tuneable simply by changing the flux threading the SQUID loop.

For the results in this section, we consider the SQUID as a single Josephson junction whose critical current is a function of flux, for this we assume the Loop inductance to be negligibly small. We further assume that the Junction capacitances are negligibly small, thereby neglecting the internal modes in the junctions as explained in Sec. 3.1.5. We further assume that the current going through the SQUID is much smaller than its critical current. These assumptions taken together cause SQUID to be considered a (flux tuneable) linear inductance. Then Eq. (3.18) for the Josephson inductance together with Eq. (3.27) for the critical current give

$$L_\Sigma(\Phi) \approx \frac{\phi_0}{4\pi I_{c_1} \cos\left(\pi \frac{\Phi}{\phi_0}\right)\sqrt{1 - \left(\frac{I}{2I_{c_1}\cos\left(\pi \frac{\Phi}{\phi_0}\right)}\right)^2}} \approx \frac{\phi_0}{4\pi I_{c_1} \cos\left(\pi \frac{\Phi}{\phi_0}\right)}\,. \tag{3.72}$$

Because the only difference between a SQUID loaded transmission line and the previously discussed inductor loaded transmission line, is that the load inductance now is a function of flux as expressed in Eq. (3.72), we can reuse the results derived in the previous section by substitution of the SQUID inductance. Considering only the lowest frequency mode, this results within a first order Taylor approximation in an equivalent parallel RLC-circuit with input admittance

$$Y_{\text{in}} \approx \frac{1}{R(\Phi)} + \mathrm{i}2C(\Phi)\big(\omega - \omega_0(\Phi)\big) \tag{3.73}$$

and circuit elements as given by[10]

$$C(\Phi) = \frac{1}{2Z_0}\left(\frac{\ell}{v} + \frac{1}{\frac{4\pi I_{c_1} Z_0 \cos\left(\pi \frac{\Phi}{\phi_0}\right)}{\phi_0} + \frac{\phi_0 {\omega_0}^2(\Phi)}{4\pi I_{c_1} Z_0 \cos\left(\pi \frac{\Phi}{\phi_0}\right)}}\right), \tag{3.74a}$$

$$L(\Phi) = \frac{1}{{\omega_0}^2(\Phi) C(\Phi)}\,, \tag{3.74b}$$

$$R(\Phi) = \frac{Q_0(\Phi)}{\omega_0(\Phi) C(\Phi)}\,. \tag{3.74c}$$

Translating Eq. (3.69), The resonant frequency $\omega_0(\Phi)$ for the lowest frequency mode is the solution of

$$\arctan\left(\frac{\omega_0 \phi_0}{4\pi I_{c_1} Z_0 \cos\left(\pi \frac{\Phi}{\phi_0}\right)}\right) + \frac{\omega_0 \ell}{v} = \frac{\pi}{2}\,. \tag{3.75}$$

[10] Note that we assume the Q-factor to depend on flux. Such dependence may be possible because the resonance frequency may be a function of losses inside the SQUID as can be seen in Eq. (3.65) by adding a real component to the load impedance, even though this is difficult to work out due to equations becoming very cumbersome when doing this.

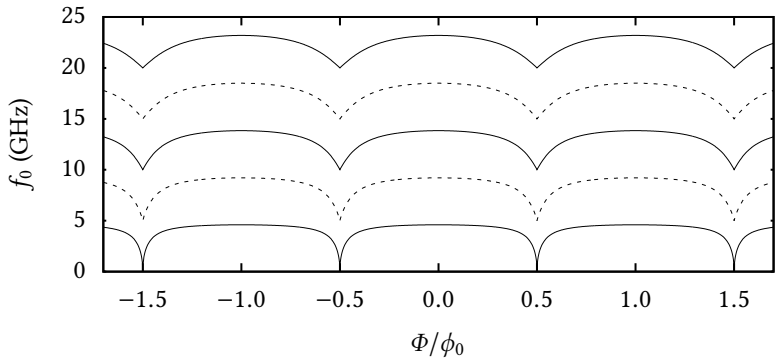

Figure 3.11: Resonant frequency of a SQUID transmission line resonator as a function of flux threading the SQUID loop. The transmission line length is 5 mm, its characteristic impedance 50 Ω and its phase velocity 100 km/s. The critical currents of both Josephson junctions are taken equal and set to 0,75 μA. Higher modes have less flattened modulation curves as for these modes the frequency sensitivity is higher in the lower load inductance region as is demonstrated in Fig. 3.10.

The resonance frequency numerically solved as a function of flux is plotted in Fig. 3.11. These results show that this system constitutes a resonator whose frequency is tuned as a function of magnetic flux through the SQUID loop.

Note that by this procedure we have essentially disregarded all anharmonic effects in the resonator. In addition to that, our time domain discussion of this system did suggest that an interaction is possible between the different resonances mediated by the non-linearity in the boundary conditions. Hower, in case one is only interested in the "harmonic" resonances in the small amplitude regime, this seems reasonable.

Chapter 4

Going from a circuit Lagrangian to a quantised Hamiltonian

In classical mechanics any system is usually described by its equations of motions; for mechanical systems Newton's second law together with the laws describing the forces acting on or between the system's elements/parts; and for electrical circuits Kirchhoff's laws together with constitutive relations between the voltages and currents across the networks constituent lumped elements (as branches). There are however other but equivalent formulations of classical mechanics such as the Lagrangian and the Hamiltonian formalism. Both use a mathematical object defined in terms of the system's kinetic and potential energy as the starting point together with Hamilton's principle for deriving/generating the equations of motion. Provided the energy related expressions are in correspondence with physical laws and written consistently in terms of generalised coordinates plus generalised velocities or conjugate momenta in case of the Hamiltonian formalism, these alternative formalisms present a different path for obtaining the equations of motion besides carefully analysing Newton's second law for the system together with the forces mediating interactions between its elements. Furthermore, most formalisms of quantum mechanics build on top of the Hamiltonian formalism of classical mechanics.

In this chapter we will rephrase the circuit theory we have employed so far into an equivalent Lagrangian formulation. In doing so we will also transform our circuit description from a representation in terms of voltages and currents to one in terms of accumulated charges and generalised fluxes in anticipation of an intuitive mapping to canonical position and momentum like coordinates in the Hamiltonian formalism as well as quantum mechanics. Using generalised flux as coordinate further will allow us to incorporate Josephson tunnel junctions into the circuit description on the same level as other circuit elements; more on that later.

Considerable attention will be given to mutual inductances and biassing fields and their mapping to the voltages and currents in the circuit. This is needed in the next chapter to explain the interaction between two disjoint circuits mediated by a mutual inductance between an inductor embedded in one circuit and the loop of a SQUID embedded in the other. In essence this chapter presents the final parts of the theoretical background required for providing a quantum circuit description of a analogue opto-mechanical circuit. In doing so we follow the path for finding a quantum mechanical description of electrical circuits as explained by Devoret [51].

4.1 Lagrangian formulation of circuit theory

In this section we discuss in general a formulation of circuit theory in terms of flux and charge variables rather than currents and voltages, the constitutive relations for a few circuit elements in terms of the new variables, and how to find the equations of motion. We particularly discuss how to systematically deal with mutual inductances. The section concludes with a Lagrangian description of the same circuit theory together with limitations arising from the underlying circuit theory as well as those arising from Lagrangian mechanics.

4.1.1 Generalised branch flux and branch charge

An electrical network can be described as a network of branches each containing a dipole element connected to nodes. Each branch b is characterised by the voltage $\mathcal{V}_\mathrm{b}$ across the dipole element it contains and the current $\mathcal{I}_\mathrm{b}$ flowing through it.

For a Hamiltonian description of an electromagnetic circuit, branch voltages or current are not convenient as generalised coordinates as they are analogues to forces and velocities in a mechanical system and as such do not map well to position and momentum like coordinate pairs. For that, the charge

$$q_\mathrm{b} = \int_{-\infty}^{t} \mathcal{I}_\mathrm{b}\,\mathrm{d}t \tag{4.1a}$$

accumulated on a capacitive element, or generalised flux, a generalisation of magnetic flux stored in an inductive element

$$\phi_\mathrm{b} = \int_{-\infty}^{t} \mathcal{V}_\mathrm{b}\,\mathrm{d}t \tag{4.1b}$$

can be chosen as coordinate. It will be seen that in the Hamiltonian description, the generalised branch fluxes and charges are canonically conjugate position and momentum (or vice versa). In these definitions we assume that at $t = -\infty$ the system is completely at rest with all currents and voltages equal to zero; any static biassing fields are assumed to be switched on adiabatically between $t = -\infty$ and $t = 0$.

Note that in the circuits we will be considering branch charge corresponds intuitively with electrical charge accumulated on capacitor plates, but as is the case with a Josephson junction it is not necessarily true that generalised flux corresponds with magnetic flux generated by current through the element; the latter is only true for an inductor coil. This will be made clear in the following section where we introduce the constitutive relations for inductors and capacitors, as well as Josephson elements (for which generalised flux will prove to be a convenient coordinate in dealing with the non-linearity inherent to elements of this kind).

4.1.2 Constitutive relations en stored energy

This section briefly rephrases in terms of flux and charge variables the general constitutive relations as well as expressions corresponding to stored energy for capacitive and inductive elements.

Inductive and capacitive elements

The circuit components are further characterised by constitutive relations that link the branch voltages to branch currents. We distinguish[1]between capacitive elements, for which the relation is of the form

$$\mathcal{V}_\mathrm{b} = f(q_\mathrm{b}) \tag{4.2}$$

[1]As a Lagrangian or Hamiltonian description in itself does not incorporate dissipation, we only consider inductive and capacitive components.

and inductive elements for which the relation is of the form

$$\mathcal{I}_\mathrm{b} = g(\phi_\mathrm{b} - \phi_\mathrm{offset})\,. \tag{4.3}$$

In the latter relation however, mutual inductance is neglected—when this is taken into account, this relation should also be a function of the branch fluxes in the other components that interact through mutual inductances—we consider both cases in the following subsections. A static external flux through an inductor switched on adiabatically has the effect of introducing an offset flux ϕ_offset in the constitutive relations.

Energy stored in capacitive and inductive elements

With the usual sign convention for the branch currents and voltages employed in circuit theory the energy absorbed by a circuit element is defined as the time integral of the branch voltage times current

$$\mathcal{E}_\mathrm{b} = \int_{-\infty}^{t} \mathcal{V}_\mathrm{b}\mathcal{I}_\mathrm{b}\,\mathrm{d}t\,. \tag{4.4}$$

Note that branch voltage can be written as the time derivative of generalised branch flux:

$$\mathcal{V}_\mathrm{b} = \frac{\mathrm{d}\phi_\mathrm{b}}{\mathrm{d}t}\,; \tag{4.5a}$$

and that similarly the branch current can be expressed as the time derivative of branch charge:

$$\mathcal{I}_\mathrm{b} = \frac{\mathrm{d}q_\mathrm{b}}{\mathrm{d}t}\,. \tag{4.5b}$$

This means that we can express the energy accumulated on a branch in terms of generalised branch flux

$$\mathcal{E}_\mathrm{b} = \int_{-\infty}^{t} \mathcal{I}_\mathrm{b}\dot{\phi}_\mathrm{b}\,\mathrm{d}t = \int_{\phi_\mathrm{b}(-\infty)}^{\phi_\mathrm{b}(t)} g(\phi_\mathrm{b})\,\mathrm{d}\phi_\mathrm{b} \tag{4.6a}$$

for an inductive element or in terms of branch charge for a capacitive element

$$\mathcal{E}_\mathrm{b} = \int_{-\infty}^{t} \mathcal{V}_\mathrm{b}\dot{q}_\mathrm{b}\,\mathrm{d}t = \int_{q_\mathrm{b}(-\infty)}^{q_\mathrm{b}(t)} f(q_\mathrm{b})\,\mathrm{d}q_\mathrm{b} \tag{4.6b}$$

where an over-dot denotes a time derivative.

The general case for two inductive elements sharing a mutual inductance

Let's consider the case of two inductor labeled 1 and 2 sharing a mutual inductance. In this case, the constitutive relations are

$$\mathcal{I}_1 = g_1(\phi_1, \phi_2) \tag{4.7a}$$
$$\mathcal{I}_2 = g_2(\phi_1, \phi_2) \tag{4.7b}$$

and the energy contained in both elements

$$\mathcal{E}_1 + \mathcal{E}_2 = \int_{-\infty}^{t} g_1(\phi_1, \phi_2)\dot{\phi}_1 + g_2(\phi_1, \phi_2)\dot{\phi}_2\,\mathrm{d}t = \int_{-\infty}^{t} \frac{\mathrm{d}}{\mathrm{d}t} G_\mathrm{M}(\phi_1, \phi_2)\,\mathrm{d}t = G_\mathrm{M}(\phi_1, \phi_2)\Big|_{-\infty}^{t} \tag{4.8}$$

which requires that a function G_M exists such the following two equations

$$g_1(\phi_1, \phi_2) = \frac{\partial G_\mathrm{M}}{\partial \phi_1} \quad \text{and} \quad g_2(\phi_1, \phi_2) = \frac{\partial G_\mathrm{M}}{\partial \phi_2} \tag{4.9}$$

are true.

4.1.3 Degrees of freedom - constraints

As we know already, the voltages and currents across the branches of a network do not constitute an independent set of degrees of freedom because they are constrained as a function of the network topology by Kirchhoff's laws introduced in Sec. 2.1. Rephrasing these in terms of generalised branch fluxes and charges by an integration over time gives[2]

$$\sum_{\text{all } b \text{ around loop } \ell} \phi_b = \widetilde{\phi}_\ell \tag{4.10}$$

$$\sum_{\text{all } b \text{ arriving at node } n} q_b = \widetilde{q}_n \tag{4.11}$$

where the magnetic flux $\widetilde{\phi}_\ell$ threading loop ℓ or the charge $\widetilde{q}_n$ accumulated on node n are usually taken constant and fulfil the role of external biassing fields. Any of the two Kirchhoff laws can be used to generate an independent set of equations describing the circuit dynamics.

For more complicated circuits it can be challenging to find a convenient set of independent degrees of freedom. A systematic procedure for constructing such a set is the method of nodes which is the most popular; this method is the one employed in the lecture notes by Devoret [51]. The other method, the method of loops, is defined in terms of loop charges and provides a circuit description that is dual to the one obtained by the method of nodes. A thorough explanation of both can be found in the book by Peikari [33]. The former method in essence works by choosing one node in the network as ground and from that node constructing a spanning tree connecting every other node to the ground node by exactly one path; then for each node a node flux is defined as the sum of all branch fluxes along the path connecting the node to ground in the spanning tree.

For the circuits we will be considering such a procedure is not needed as the number of degrees of freedom in the circuits we will be considering is small.

4.1.4 Equations of motion and Lagrangian for an electrical circuit

Taking the following together,

- that the voltage and current in a branch are related by the time derivative of respectively the branch flux and charge, see Eqs. (4.5);
- that each branch has a constitutive relation linking the voltage to charge or the current to flux; and
- Kirchhoff's two laws as constraints respectively coupling the branch charge or the branch flux degrees of freedom as a function of network topology,

we are presented with an an over-complete set of equations describing the dynamics of the circuit. This allow us to distil a smaller sets of independent equations describing the circuit's dynamics. The difference between the sets being in the choice of variables—flux or charge—and in the specific form in which one or more of Kirchhoff's laws are applied. The only caveat is that one needs to be able to invert one or

[2] It is perhaps surprising, but Eq. (4.10) is consistent with our treatment of a SQUID and flux quantisation. This can be seen most easily by considering the flux quantisation condition for a SQUID

$$\Phi + \delta_\mathrm{b} - \delta_\mathrm{a} = 2\pi n\,, \quad n \in \mathbb{Z}\,.$$

Expressing the phase jumps in terms of generalised flux using Eq. (4.36) one basically obtains Kirchhoff's law, setting $n = 0$ as is possible due to the periodicity of the Josephson relations. From a circuit perspective, the flux can be incorporated as the magnetic flux in an inductor. This does however show that, for Kirchhoff's loop law to remain consistent with flux quantisation, inductive elements must couple to the phase of the superconducting wave-function (either indirectly through the magnetic field or directly as is the case with tunnel junctions).

more of the constitutive relations when both an inductive and capacitive branch are involved in the same equation—this then gives rise to a differential equation and thus dynamics, while otherwise it is only an algebraic relation. This gives us a bit of freedom in constructing the circuit Lagrangian or equations of motion as it allows us to express any degree of freedom in terms of charge or in terms of generalised flux. The latter option will be the most natural coordinate for incorporating Josephson elements.

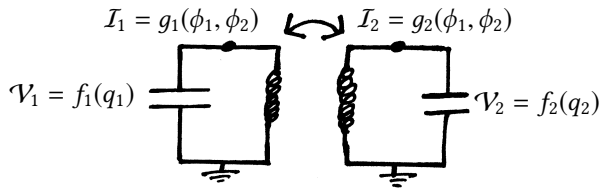

Figure 4.1: Example lumped element network consisting of two LC-resonators interacting through a mutual inductance. Note that we keep the constitutive relations completely general.

As a general example for the circuits of interest, we derive the equations of motion for the circuit in Fig. 4.1 that incorporates a mutual inductance between two LC-resonators. We intentionally keep the constitutive relations extremely general. An easy path for obtaining the equations of motion for these kinds of topologically simple networks, where each (sub)network contains no more than one inductive branche and no more than one capacitive branch, is to equate the current $\dot{q}_\mathrm{b}$ coming from a capacitive branch to the current $-g_\mathrm{b}$ going into the connecting inductive branch (or vice versa). For the circuit in Fig. 4.1 this yields

$$\frac{\mathrm{d}q_1}{\mathrm{d}t} = \frac{\mathrm{d}}{\mathrm{d}t} f_1^{-1}(\mathcal{V}_1) = \frac{\mathrm{d}}{\mathrm{d}t} f_1^{-1}(\dot{\phi}_1) = -g_1(\phi_1, \phi_2) \tag{4.12a}$$

$$\frac{\mathrm{d}}{\mathrm{d}t} f_2^{-1}(\dot{\phi}_2) = -g_2(\phi_1, \phi_2) \tag{4.12b}$$

where the superscript $^{-1}$ on top of a function f_x denotes the inverse of that function. Note that we could have equally written the equation in terms of branch charges rather than fluxes, though this would have required us to invert the inductive constitutive relations instead; also we could have obtained the equations of motion by equating branch voltages rather than currents (in essence using the other Kirchhoff law); all of these give however equivalent results, only in charge rather than flux variables. However, when only the inductances are non-linear and all capacitances are linear the representation in terms of flux variables is the most convenient.

One can verify that these are Euler-Lagrange equations

$$\frac{\mathrm{d}}{\mathrm{d}t} \frac{\partial \mathcal{L}}{\partial \dot{\phi}_b} = \frac{\partial \mathcal{L}}{\partial \phi_b}, \quad b \in \{1, 2\} \tag{4.13}$$

that can be derived from the Lagrangian[3]where the inductive constitutive relations satisfy the requirements specified in Sec. 4.1.2

$$\mathcal{L} = \int_{q_1(-\infty)}^{q_1(t)} \dot{\phi}_1 \, \mathrm{d}f_1^{-1}(\dot{\phi}_1) \; + \int_{q_2(-\infty)}^{q_2(t)} \dot{\phi}_2 \, \mathrm{d}f_2^{-1}(\dot{\phi}_2) \; - \int_{-\infty}^{t} g_1(\phi_1, \phi_2)\dot{\phi}_1 + g_2(\phi_1, \phi_2)\dot{\phi}_2 \, \mathrm{d}t \tag{4.14}$$

[3]A general explanation for Lagrangian (as well as Hamiltonian) mechanics can e.g. be found in the book by Goldstein [52] on classical mechanics. Explaining how the Euler-Lagrange equations are equivalent to Newton's laws or follow from Hamilton's principle of least action, that is the vanishing of the first order derivative in the variation of the integral over the Lagrangian (considered as a functional) from an initial to a final state, is beyond the scope of this report.

which as we will show corresponds to the difference between the capacitive energy and inductive energy in the circuit

$$\mathcal{L} = \mathcal{E}_{\text{kin}} - \mathcal{E}_{\text{pot}} \tag{4.15}$$

fulfilling respectively the role of kinetic energy and potential energy if this were a mechanical system. The last two terms can be related to Eq. (4.6a) and is thus the inductive energy stored in the combination of two inductive elements

$$\mathcal{E}_{\text{pot}} = \int_{-\infty}^{t} g_1(\phi_1, \phi_2)\dot{\phi_1} + g_2(\phi_1, \phi_2)\dot{\phi_2}\,\mathrm{d}t = G_{\text{M}}(\phi_1, \phi_2)\,. \tag{4.16}$$

The other part of the Lagrangian is slightly more difficult to relate to capacitive energy; however a bit of rewriting of Eq. (4.6b)

$$\mathcal{E}_{\text{c}} = \int_{q_{\text{b}}(-\infty)}^{q_{\text{b}}(t)} f_{\text{b}}(q)\,\mathrm{d}q = \int f_{\text{b}}\left(f_{\text{b}}^{-1}(\mathcal{V}_{\text{b}})\right)\,\mathrm{d}f_{\text{b}}^{-1}(\mathcal{V}_{\text{b}}) = \int_{q_{\text{b}}(-\infty)}^{q_{\text{b}}(t)} \dot{\phi_{\text{b}}}\,\mathrm{d}f_{\text{b}}^{-1}(\dot{\phi_{\text{b}}}) \tag{4.17}$$

shows that this is indeed the case, such that the kinetic energy of the Lagrangian

$$\mathcal{E}_{\text{kin}} = \int_{q_1(-\infty)}^{q_1(t)} \dot{\phi}_1\,\mathrm{d}f_1^{-1}(\dot{\phi}_1) \;+ \int_{q_2(-\infty)}^{q_2(t)} \dot{\phi}_2\,\mathrm{d}f_2^{-1}(\dot{\phi}_2) \tag{4.18}$$

is the capacitive energy in the circuit; note that this implicitly relies on Kirchhoff's voltage law. Had we chosen charge as coordinate, the roles for the capacitive and inductive energies would have been the other way around.

References [53, 51] further explain how to construct the Lagrangian and Hamiltonian for electrical circuits. The former introduces the main idea in terms of charge variables and the former generalises that idea by doing the same in terms of flux variables. We have mainly followed the latter approach.

4.1.5 Limitations in circuit theory and Lagrangian mechanics

There are two aspects with above's procedure that need emphasis. Observe that in order to obtain the equations of motion in differential form, we needed to invert the constitutive relation for either the capacitive or the inductive branch connecting to the same node; this constitutes a limitation in circuit theory.

There is also a limitation in Lagrangian mechanics. For the Lagrangian to generate equations of motion that are of the form one would obtain from Kirchhoff's laws in circuit theory, the analogue kinetic energy part must be a quadratic form when written in terms of the time-derivatives of the flux or charge degrees of freedom in the circuit. The latter is generally the case for mechanical systems, but in circuit theory this is not necessarily true when one or more components are non-linear.

Thus in summary there are two requirements:

- from Lagrangian mechanics that the kinetic energy is a quadratic form of the generalised velocities;
- from circuit theory that at least one of constitutive relations between the two is invertible.

Generally if in the capacitive branch and inductive branch connecting to the same node only one is non-linear, one can make a choice to describe that node's dynamics in either charge or flux variables such that the non-linearity will be part of the potential energy keeping the kinetic energy a quadratic from. If however both the capacitive and inductive branches are non-linear, than it seems not generally possible to find a Lagrangian that would generate Kirchhoff's laws through the Euler-Lagrange equations. A good description on different approaches exploiting the duality in circuit theory and the limitations is given in Ref. [54].

An extra limitation that we will encounter is that constraints imposed on the system by circuit nodes connecting only capacitive or only inductive elements can impose non-invertible coordinate transformation on the equations of motion and the Lagrangian. For the latter it is however always assumed that any transformation to generalised coordinates is invertible [52], see Sec. 5.2.8 for a more thorough discussion.

4.2 Various linear and non-linear circuit elements

In this section we describe various linear and non-linear circuit elements that will be necessary for constructing the Lagrangian for the circuit opto-mechanics analogue that is the topic of this thesis. We start with linear capacitors and inductors and then move to the non-linear inductance in Josephson tunnel junctions and SQUIDs.

4.2.1 A linear capacitor

Setting the influence of any external electric field zero, the charge on a capacitor is to good approximation linearly related to the voltage across it

$$\mathcal{V}_\mathrm{b} = f(q_\mathrm{b}) = \frac{q_\mathrm{b}}{C_\mathrm{b}} \tag{4.19}$$

where C_b is the capacitance of the branch.

Capacitive energy

Using Eqs. (4.19) and (4.6b) the energy stored in a linear capacitor is found to be

$$\mathcal{E}_\mathrm{C} = \int_{-\infty}^{t} \frac{q_\mathrm{C}}{C}\dot{q_\mathrm{C}}\,\mathrm{d}t = \int_{q_\mathrm{C}(-\infty)}^{q_\mathrm{C}(t)} \frac{q_\mathrm{C}}{C}\,\mathrm{d}q_\mathrm{C} = \frac{{q_\mathrm{C}}^2}{2C} \tag{4.20}$$

where we have set the charge at $t = -\infty$ to zero, as is consistent with a system starting completely at rest.

Because we will be choosing generalised flux as coordinate for the Lagrangian, we first express energy in terms of voltage using the constitutive relation (4.19) and then substitute Eq. (4.5a)

$$\mathcal{E}_\mathrm{C} = \frac{1}{2}C{\mathcal{V}_\mathrm{C}}^2 = \frac{1}{2}C\dot{\phi_\mathrm{C}}^2 \tag{4.21}$$

where ϕ_C is the branch flux in an inductive element connected parallel to the capacitor.

4.2.2 A linear inductor

A relation between the generalised flux and magnetic flux in an inductor coil is easily derived from Lenz's law, which relates the voltage across an inductor to the time-derivative of the magnetic flux φ in the inductor

$$\mathcal{V}_\mathrm{b} = L\frac{\mathrm{d}\mathcal{I}_\mathrm{b}}{\mathrm{d}t} + \frac{\mathrm{d}\varphi_\mathrm{b}}{\mathrm{d}t} \tag{4.22}$$

where we have separated contributions to the flux from the current $\mathcal{I}_\mathrm{b}$ and external fields φ_b. Substitution into Eq. (4.1b), the definition of generalised flux, and integration over time from $-\infty$ to the present time t gives

$$\phi_\mathrm{b} = \int_{-\infty}^{t} L\frac{\mathrm{d}\mathcal{I}_\mathrm{b}}{\mathrm{d}t} + \frac{\mathrm{d}\varphi_\mathrm{b}}{\mathrm{d}t}\,\mathrm{d}t = L\mathcal{I}_\mathrm{b} + \varphi_\mathrm{b}\,. \tag{4.23}$$

where in accordance with a system completely at rest, we have assumed all fluxes and currents zero at $t = -\infty$. We see that the generalised flux in an inductor coil is linearly proportional the magnetic flux it contains, the net sum of the contributions from the current through the inductor and external fields. If the latter is to fulfil the role of a static biassing field, it wil have to be switched on adiabatically between $t = -\infty$ and $t = 0$ to avoid inducing any excitations in the electrical network that embeds the inductor. Inversion of above relation gives the constitutive relation for a linear inductor

$$\mathcal{I}_\mathrm{b} = \frac{\phi_\mathrm{b} - \varphi_\mathrm{b}}{L} \tag{4.24}$$

in the presence of a static external magnetic field.

Energy stored in a linear inductor

Similarly we find the energy in an inductor using the consitutive relation (4.24) and Eq. (4.6a)

$$\mathcal{E}_\mathrm{L} = \int_{-\infty}^{t} \mathcal{I}_\mathrm{b}\mathcal{V}_\mathrm{b}\,\mathrm{d}t = \mathcal{E}_\mathrm{offset} + \int_0^t \frac{\phi_\mathrm{b} - \varphi_\mathrm{b}}{L}\dot{\phi}_\mathrm{b}\,\mathrm{d}t = \mathcal{E}_\mathrm{offset} + \frac{(\phi_\mathrm{b} - \varphi_\mathrm{b})^2}{2L}\,. \tag{4.25}$$

The adiabatic switching on of the bias flux introduces a constant energy offset that is difficult to evaluate but otherwise uninteresting since it does not contribute to any dynamics.

4.2.3 Dealing with a linear mutual inductance

As a small intermezzo, before moving on to the next section, we briefly introduce how to deal with a linear mutual inductance. A linear mutual inductance M between two inductors is defined such that the contribution of magnetic flux in one inductor L_1 due to the current $\mathcal{I}_2$ in the other is given by $M\mathcal{I}_2$. Because a magnetic mutual inductance is reciprocal, the same relation holds when swapping the inductors. In practice, the mutual inductance can be expressed in terms of the self-inductances of the two involved coils

$$M = k\sqrt{L_1 L_2}\,, \tag{4.26}$$

where $k \in [0, 1]$ is the coupling coefficient.

Linear inductors with mutual inductance and static external flux

We consider the case where two inductors L_1 and L_2 are interacting through a mutual inductance and are under the influence of external static fluxes φ_1 and φ_2 respectively. In this case there are three contributions to the magnetic flux inside the inductors:

- a contributions from each inductor's self inductance;
- a contribution from an externally applied static flux; and
- a contribution emerging from the flux in another inductor through the mutual inductance.

The circuit relations for the two inductors under influence of a mutual inductance are

$$\mathcal{V}_1 = L_1\frac{\mathrm{d}\mathcal{I}_1}{\mathrm{d}t} \pm M\frac{\mathrm{d}\mathcal{I}_2}{\mathrm{d}t} + \frac{\mathrm{d}\varphi_1}{\mathrm{d}t} \tag{4.27a}$$

$$\mathcal{V}_2 = L_2\frac{\mathrm{d}\mathcal{I}_2}{\mathrm{d}t} \pm M\frac{\mathrm{d}\mathcal{I}_1}{\mathrm{d}t} + \frac{\mathrm{d}\varphi_2}{\mathrm{d}t} \tag{4.27b}$$

where the sign of the mutual inductance terms depends on whether the inductors are aiding- or working against each other (it depends on the sign convention for the currents and the orientation of the inductors with respect to each other). Substituting these into the definition of generalised flux (4.1b), we obtain

$$\phi_1 = \int_{-\infty}^{t} L_1 \frac{\mathrm{d}\mathcal{I}_1}{\mathrm{d}t} \pm M \frac{\mathrm{d}\mathcal{I}_2}{\mathrm{d}t} + \frac{\mathrm{d}\varphi_1}{\mathrm{d}t}\,\mathrm{d}t = L_1\mathcal{I}_1 \pm M\mathcal{I}_2 + \varphi_1 \tag{4.28a}$$

$$\phi_2 = \int_{-\infty}^{t} L_2 \frac{\mathrm{d}\mathcal{I}_2}{\mathrm{d}t} \pm M \frac{\mathrm{d}\mathcal{I}_1}{\mathrm{d}t} + \frac{\mathrm{d}\varphi_2}{\mathrm{d}t}\,\mathrm{d}t = L_2\mathcal{I}_2 \pm M\mathcal{I}_1 + \varphi_2 \tag{4.28b}$$

where we have set the currents at $t = -\infty$ to zero and also assume the static external fluxes φ_1 and φ_2 to be switched on adiabatically from $t = -\infty$ to $t = 0$. Above set of equations is more conveniently expressed in matrix notation

$$\begin{pmatrix} \phi_1 - \varphi_1 \\ \phi_2 - \varphi_2 \end{pmatrix} = \begin{pmatrix} L_1 & \pm M \\ \pm M & L_2 \end{pmatrix} \begin{pmatrix} \mathcal{I}_1 \\ \mathcal{I}_2 \end{pmatrix} . \tag{4.29}$$

Solving this set of equations for $\mathcal{I}_1$ and $\mathcal{I}_2$ is a matter of inverting the inductance matrix. This yields the constitutive relations for the inductors mutually interacting with each other.

$$\begin{pmatrix} \mathcal{I}_1 \\ \mathcal{I}_2 \end{pmatrix} = \frac{1}{L_1L_2 - M^2} \begin{pmatrix} L_2 & \mp M \\ \mp M & L_1 \end{pmatrix} \begin{pmatrix} \phi_1 - \varphi_1 \\ \phi_2 - \varphi_2 \end{pmatrix} . \tag{4.30}$$

It is also possible to incorporate the external bias fluxes into the circuit description by means of constraints imposed by Kirchhoff's voltage law in the spirit of Eq. (4.10). For now, since we have not defined any connecting network in this example, we keep the external flux explicitly in inductors, but do note that this approach allows one to move the description of external flux to the constitutive relations of e.g. Josephson junctions if it occurs in series with the linear inductors in the network topology. This is usefull because in contrast to linear inductors, a static flux offset does influence the dynamics in a non-linear inductor.

Energy stored in a pair of mutually coupled inductors

The energy stored in a pair of inductors coupled through a mutual inductance can be expressed as the sum of the energies in the respective branches

$$\mathcal{E}_{\mathrm{L_1L_2}} = \int_{-\infty}^{t} \mathcal{I}_1\mathcal{V}_1 + \mathcal{I}_2\mathcal{V}_2\,\mathrm{d}t \tag{4.31}$$

where the number subscripts denote to which branch the corresponding variable belongs. Using the constitutive relations (4.30) and Eq. (4.5a) gives the integral

$$\mathcal{E}_{L_1L_2} = \int_{-\infty}^{t} \frac{1}{L_1L_2 - M^2} \begin{pmatrix} \dot{\phi}_1 \\ \dot{\phi}_2 \end{pmatrix}^{\mathrm{T}} \begin{pmatrix} L_2 & \mp M \\ \mp M & L_1 \end{pmatrix} \begin{pmatrix} \phi_1 - \varphi_1 \\ \phi_2 - \varphi_2 \end{pmatrix} \mathrm{d}t \tag{4.32}$$

which when evaluated[4] gives

$$\mathcal{E}_{L_1L_2} = \frac{1}{2}\frac{1}{L_1L_2 - M^2} \begin{pmatrix} \phi_1 - \varphi_1 \\ \phi_2 - \varphi_2 \end{pmatrix}^{\mathrm{T}} \begin{pmatrix} L_2 & \mp M \\ \mp M & L_1 \end{pmatrix} \begin{pmatrix} \phi_1 - \varphi_1 \\ \phi_2 - \varphi_2 \end{pmatrix} + \mathcal{E}_{\mathrm{offset}} \tag{4.34}$$

up to an irrelevant energy offset due to the adiabatic switching on of the bias fluxes between $t = -\infty$ and $t = 0$.

[4] It is interesting to compare this with the expression for the same energy in terms of currents

$$\mathcal{E}_{\mathrm{M}} = \frac{1}{2}L_1{\mathcal{I}_1}^2 + \frac{1}{2}L_2{\mathcal{I}_2}^2 \pm M\mathcal{I}_1\mathcal{I}_2 . \tag{4.33}$$

this relation can be derived from the expression for work in electrical circuits and Kirchhoff's laws together with the definition of the mutual inductance.

4.2.4 The Josephson non-linear inductor

For a Josephson tunnel junction, the generalised branch flux is not a magnetic flux, but is rather related to the phase difference δ across the junction of the wave-function for the superconducting condensate. This is made clear by substitution of the Josephson relation for the Josephson voltage Eq. (3.16) into the definition for generalised flux Eq. (4.1b)

$$\phi_\mathrm{J} = \int_{-\infty}^{t} \frac{\phi_0}{2\pi} \frac{\mathrm{d}\delta}{\mathrm{d}t} \,\mathrm{d}t = \frac{\phi_0}{2\pi}\delta \,. \tag{4.35}$$

Thus the phase difference can be conveniently expressed in terms of generalised flux

$$\delta = 2\pi \frac{\phi_\mathrm{J}}{\phi_0} \,. \tag{4.36}$$

Substituting this result into the expression for the Josephson current Eq. (3.14) we obtain the constitutive relation for a Josephson junction

$$I_\mathrm{J} = I_\mathrm{c} \sin\left(2\pi \frac{\phi_\mathrm{J}}{\phi_0}\right) , \tag{4.37}$$

which shows that in the picture of generalised flux, a Josephson junction is a non-linear inductor, as the current traversing it can be expressed entirely as a non-linear function of generalised flux.

Energy stored in a Josephson tunnel element

The energy in a single tunnel junction is easily found through its constitutive relation (4.37)

$$\mathcal{E}_\mathrm{J} = \int_{-\infty}^{t} I_\mathrm{J} \sin\left(2\pi \frac{\phi_\mathrm{J}}{\phi_0}\right) \dot{\phi}_\mathrm{J} \,\mathrm{d}t = \frac{\phi_0 I_\mathrm{J}}{2\pi} \left(1 - \cos\left(2\pi \frac{\phi_\mathrm{J}}{\phi_0}\right)\right) \tag{4.38}$$

where again we set $\phi_\mathrm{J}(-\infty) = 0$ corresponding to current being completely at rest initially.

4.3 Quantum electromagnetic circuit theory

Following the procedure for quantising electromagnetic circuits by Devoret [51], we review a method for constructing the circuit Lagrangian, transform it to a Hamiltonian, and then quantise the system by promoting the generalised position and momentum coordinates to quantum operators while imposing the canonical commutation relations.

4.3.1 Transforming to the Hamiltonian formalism

While in the framework of classical mechanics the Lagrangian and Hamiltonian formalism can be considered equivalent, quantum mechanics usually is based on a Hamiltonian description of reality. The Hamiltonian formalism has an advantage in that it allows us to describe the classical physics and the quantum physics of the system in a more compatible language. We will make use of this by describing the amplitude of the optical resonator in terms of a complex scalar field that corresponds with the expectation value of the quantum annihilation operator from the second quantisation formalism in quantum mechanics. More on that later.

In any case, formally a system's Hamiltonian is defined as the Legendre transform of the Lagrangian

$$\mathcal{H} = \sum_x q_x \phi_x - \mathcal{L} \tag{4.39}$$

in which the generalised velocities are transformed to the conjugate momenta defined as

$$q_x = \frac{\partial \mathcal{L}}{\partial \dot{\phi}_x} \,. \tag{4.40}$$

Note that whereas the Lagrangian is a function of the generalised coordinates and velocities, the Hamiltonian is a function of the generalised coordinates and their conjugate momenta.

The equations of motion then are given by Hamilton's equations

$$\frac{\mathrm{d}q_x}{\mathrm{d}t} = -\frac{\partial \mathcal{H}}{\partial \phi_x} \tag{4.41}$$

$$\frac{\mathrm{d}\phi_x}{\mathrm{d}t} = \frac{\partial \mathcal{H}}{\partial q_x} \tag{4.42}$$

which generate a set of equations equivalent to the Euler-Lagrange equations.

4.3.2 Describing the Hamiltonian in terms of a complex scalar field

Following a book on advanced quantum mechanics [38], in the classical Hamiltonian formalism we bring the system to a form that closely resembles the second quantisation formalism of quantum mechanics. For that we first rewrite the Hamiltonian in a form that corresponds to that of a set of harmonic oscillators of mass one

$$\mathcal{H} = \sum_x \frac{1}{2}\left({P_x}^2 + {\omega_x}^2 {Q_x}^2\right) + \mathcal{H}_{\text{other}} \,. \tag{4.43}$$

We call the P_x and Q_x the system's generalised positions and momenta respectively. Note that for this to be true, the term $\mathcal{H}_{\text{other}}$, which describes the interactions and deviations from harmonic behaviour, should be a small. The next step is to express the Hamiltonian in terms of a kind of complex scalar coordinates d_x defined as

$$d_x = \frac{\omega_x Q_x + \mathrm{i} P_x}{\sqrt{2\omega_x}} \,. \tag{4.44}$$

Expressing the generalised position and momentum in terms of the complex scalar coordinates

$$Q_x = \frac{1}{\sqrt{2\omega_x}}\left(d_x + {d_x}^*\right) \tag{4.45a}$$

$$P_x = -\mathrm{i}\sqrt{\frac{\omega_x}{2}}\left(d_x - {d_x}^*\right) \,, \tag{4.45b}$$

and substituting the result into the Hamiltonian we obtain

$$\mathcal{H} = \sum_x \omega_x {d_x}^* d_x + \mathcal{H}_{\text{other}} \,. \tag{4.46}$$

This result is already very close to the quantum mechanical description, but misses the commutation relations.

Note that the d_x correspond with the normal coordinates of the harmonic oscillators in the *absence* of coupling. These are, however, not the normal coordinates corresponding with the normal modes in the system of *coupled* resonators that may hybridise in any non-trivial way.

4.3.3 Going from a classical to a quantum mechanical circuit description

The next step is to treat the system as a set of harmonic oscillators, promote the position and momentum variables to quantum operators and impose the right commutation relations, which according to Dirac [55] are related to the Poisson brackets from classical mechanics.

For the conjugate momentum and generalised coordinate pairs in the Hamiltonian, the commutation relations are

$$[Q_x, P_x] = \mathrm{i}\hbar\,. \tag{4.47}$$

Further, since the system is a set of harmonic oscillators, the Hamiltonian can be written in terms of boson creation and annihilation operators by the substitution

$$Q_x = \sqrt{\frac{\hbar}{2\omega_x}}\left(a_x + {a_x}^\dagger\right) \tag{4.48}$$

$$P_x = -\mathrm{i}\sqrt{\frac{\hbar\omega_x}{2}}\left(a_x - {a_x}^\dagger\right) \tag{4.49}$$

where the creation a_x and annihilation ${a_x}^\dagger$ operators are defined as

$$a_x = \frac{\omega_x Q_x + \mathrm{i}P_x}{\sqrt{2\hbar\omega_x}} \tag{4.50}$$

and satisfy the commutation relations

$$[a_x, {a_x}^\dagger] = 1\,. \tag{4.51}$$

Afterwards, the Hamiltonian can be brought to a from similar to

$$\mathcal{H} = \sum_x \hbar\omega_x\left({a_x}^\dagger a_x + \frac{1}{2}\right) + \mathcal{H}_{\text{other}} \tag{4.52}$$

where H_{other} describes any interaction between the oscillators, deviations from harmonic behaviour, or coupling to other systems such as a thermal environment or a forcing one one or more of the oscillators.

Chapter 5

Deriving the opto-mechanical coupling from the circuit Lagrangian

Opto-mechanics is a field that is traditionally focused on the interaction between an optical resonator and a mechanical resonator. An optical resonator can be seen as two mirrors trapping a standing electromagnetic wave. Typically the mechanical resonator constitutes a vibrating end mirror of the optical cavity. The mechanical oscillator, in its oscillating back and forth movement, changes the length of the optical cavity and thereby changes its resonance frequency. This scheme is schematically explained in figure 5.1a.

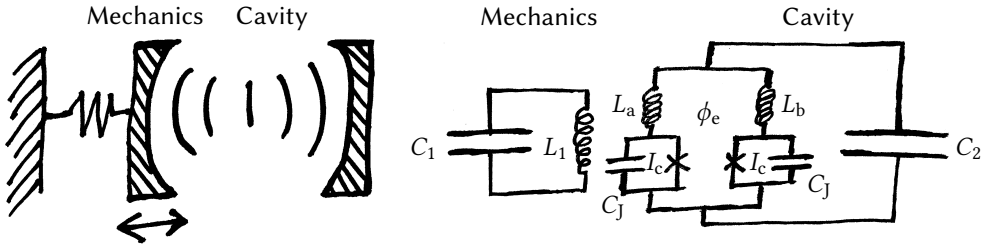

(a) Traditional opto-mechanics setup. **(b)** Lumped element analogue.

Figure 5.1: Side to side drawing of **(a)** a cavity opto-mechanics setup and **(b)** a lumped element analogue of that system with the interaction being mediated by a SQUID as variable inductance. The LC-resonator on the left whose components are labelled 1 is the analogue of the mechanical resonator, while the SQUID resonator on the right with embedded SQUID corresponds to a microwave cavity. The capacitances always present in the tunnel junctions are represented as C_a and C_b in parallel to their respective Josephson junctions incorporated as x's in the circuit. The Inductance of the SQUID loop is represented as L_a and L_b in the two branches, each equal to half the total self inductance L_ℓ of the loop. Biassing of the SQUID by an external flux is incorporated as a constant external flux ϕ_e threading the loop, which will be taken into account as residing half in each of the two inductors part of the loop, but with opposite orientation.

In a more general sense, opto-mechanics is a field that focusses on a parametric coupling between two resonators, in which a quadrature of one oscillator sets the frequency of the other resonator. The latter can also be realised in an analogue system consisting of two electrical resonators where the strength of the inductor (i.e. an embedded SQUID) in one is a function of the of the magnetic flux in the other as drawn in Fig. 5.1b. In essence, the circuit consists of two electrical resonators, an LC-resonator

and a similar resonator where the inductor is replaced by a SQUID fulfilling the role of flux tuneable inductor. An interaction is established by a mutual inductance M between the SQUID loop and inductor L_1. The magnetic flux in inductor L_1 then modifies the effective inductance of the SQUID as seen from capacitor C_2 and thereby tunes the resonance frequency of the SQUID-resonator. This should establish an opto-mechanical kind of interaction between the electrical resonators, where the flux in the LC-resonator is the analogue for the position of the mechanical oscillator. The SQUID-resonator then is the analogue of the optical cavity.

This idea has first been proposed in Ref. [30] for a setup with transmission line resonators as discussed in the sections 2.2.4 and 3.2.2. In this chapter we analyse a lumped element varient of the circuit analogue of an opto-mechanical system as depicted in Figs. 5.1. We first derive the classical equations of motion from Kirchhoff's laws and then construct the circuit Lagrangian. It is demonstrated how current traversing the SQUID can generate a flux in the SQUID loop, exerting a radiation pressure force on the LC-resonator through the mutual inductance. In order to quantise the system, we Legendre transform the Lagrangian to a Hamiltonian and then apply the canonical quantisation postulate. We will also discuss the implications the intrinsic non-linearity of the SQUID may have. A goal is to map the expressions in terms of circuit parameters to the corresponding parameters in cavity opto-mechanics.

5.1 Lumped element SQUID opto-mechanics curcuit

The full circuit for the lumped element SQUID opto-mechanics setup is drawn in Fig. 5.1b. The circuit consists of three parts:

1. An LC-resonator, whose element are labelled with 1 in the circuit diagram, which fulfils the role analogue to the mechanical resonator in opto-mechanics.

2. A SQUID-resonator, fulfilling the role of the optical cavity in opto-mechanics. The frequency tuneability by the "*mechanical*" resonator will be mediated by the SQUID and a mutual inductance.

3. The SQUID embedded fulfils the double role as inductance in the "*optical*" cavity, and together with the mutual inductance as mediator for the interaction between the two resonators. It is formed by the loop containing two Josephson junctions a and b whose respective capacitances are represented in the circuit diagram by a parallel combination with the capacitances C_a and C_b.

The self inductance L_ℓ of the SQUID loop is equally divided over the two branches of the loop and incorporated in the circuit as

$$L_\mathrm{a} = L_\mathrm{b} = \frac{L_\ell}{2}\,. \tag{5.1}$$

Each of the loop arm inductances L_a and L_b has an equal but opposite mutual inductance with inductor L_1

$$M_\mathrm{a} = -M_\mathrm{b} = \frac{M}{2} \tag{5.2}$$

that is half the net mutual inductance M between the inductor and the SQUID loop inductance.

5.2 Classical equations of motion

Because Josephson junctions are usually made with very high plasma frequency due to the Junction capacitances being very small, we can work in the limit where $C_\mathrm{a} = C_\mathrm{b} \approx 0$ since their dynamics occur at much smaller time scales than the other parts of the circuit. This corresponds to neglecting the SQUID plasma modes. Below we derive the classical equations of motion from the constitutive relations and the constraints imposed by the network topology.

5.2.1 Inductance matrix

Let us first give the expressions for the magnetic fluxes in the linear inductors as a function of branch currents in the absence of an externally applied fields

$$\begin{pmatrix}\phi_{\mathrm{L}_1}\\ \phi_{\mathrm{L}_\mathrm{a}}\\ \phi_{\mathrm{L}_\mathrm{b}}\end{pmatrix}=\begin{pmatrix}L_1 & \frac{M}{2} & -\frac{M}{2}\\ \frac{M}{2} & \frac{L_\ell}{2} & 0\\ -\frac{M}{2} & 0 & \frac{L_\ell}{2}\end{pmatrix}\begin{pmatrix}\mathcal{I}_1\\ \mathcal{I}_\mathrm{a}\\ \mathcal{I}_\mathrm{b}\end{pmatrix} \tag{5.3}$$

expressed as a matrix equation where ϕ_e is an external bias flux. Since the two branches of the SQUID are connected in a loop, we can define

$$\mathcal{I}_\ell \equiv \frac{\mathcal{I}_\mathrm{a}-\mathcal{I}_\mathrm{b}}{2} \quad \text{and} \quad \mathcal{I}_\Sigma \equiv \mathcal{I}_\mathrm{a}+\mathcal{I}_\mathrm{b}\,, \tag{5.4}$$

respectively a loop current and a net current traversing the loop. Transforming to these new variables and defining analogously

$$\phi_\ell \equiv \phi_{\mathrm{L}_\mathrm{a}}-\phi_{\mathrm{L}_\mathrm{b}} \quad \text{and} \quad \phi_{\mathrm{L}_\Sigma} \equiv \frac{\phi_{\mathrm{L}_\mathrm{a}}+\phi_{\mathrm{L}_\mathrm{b}}}{2}\,, \tag{5.5}$$

respectively the loop flux and orthogonal average magnetic loop arm flux, we rewrite Eq. (5.3) as

$$\begin{pmatrix}\phi_{\mathrm{L}_1}\\ \phi_\ell\\ \phi_{\mathrm{L}_\Sigma}\end{pmatrix}=\begin{pmatrix}L_1 & M & 0\\ M & L_\ell & 0\\ 0 & 0 & \frac{L_\ell}{4}\end{pmatrix}\begin{pmatrix}\mathcal{I}_1\\ \mathcal{I}_\ell\\ \mathcal{I}_\Sigma\end{pmatrix}. \tag{5.6}$$

In this form the inductance matrix is easily inverted giving us the branch currents as a function of the flux variables

$$\begin{pmatrix}\mathcal{I}_1\\ \mathcal{I}_\ell\\ \mathcal{I}_\Sigma\end{pmatrix}=\frac{1}{L_1L_\ell-M^2}\begin{pmatrix}L_\ell & -M & 0\\ -M & L_1 & 0\\ 0 & 0 & \frac{4\left(L_1L_\ell-M^2\right)}{L_\ell}\end{pmatrix}\begin{pmatrix}\phi_{\mathrm{L}_1}\\ \phi_\ell\\ \phi_{\mathrm{L}_\Sigma}\end{pmatrix}. \tag{5.7}$$

5.2.2 SQUID inductances and constraints

Referring to Sec. 3.1.4, the current $\mathcal{I}_\Sigma$ traversing over the SQUID as well as the circulating loop current $\mathcal{I}_\ell$ both are a function of the

$$\text{averaged sum} \quad \phi_{\mathrm{J}_\Sigma}=\frac{\phi_\mathrm{a}+\phi_\mathrm{b}}{2} \quad \text{and difference} \quad \Delta\phi_\mathrm{J}=\phi_\mathrm{a}-\phi_\mathrm{b} \tag{5.8}$$

of the generalised fluxes in the individual junctions (note that the average generalised flux is directly related to the average phase as $\phi_{\mathrm{J}_\Sigma}=\frac{\phi_0}{2\pi}\delta_0$). The latter is related to the loop flux and any externally applied flux by Krichhoff's voltage law

$$\phi_\mathrm{a}+\phi_{\mathrm{L}_\mathrm{a}}-\phi_\mathrm{b}-\phi_{\mathrm{L}_\mathrm{b}}=\phi_\mathrm{e} \quad \text{or equivalently} \quad \Delta\phi_\mathrm{J}=\phi_\mathrm{e}-\phi_\ell\,. \tag{5.9}$$

Substitution of this constraint into the constitutive relations for the SQUID yields

$$\mathcal{I}_\Sigma = 2I_\mathrm{c}\cos\left(\frac{\pi}{\phi_0}\left(\phi_\ell-\phi_\mathrm{e}\right)\right)\sin\left(\frac{2\pi}{\phi_0}\phi_{\mathrm{J}_\Sigma}\right), \tag{5.10a}$$

$$\mathcal{I}_\ell = -I_\mathrm{c}\cos\left(\frac{2\pi}{\phi_0}\phi_{\mathrm{J}_\Sigma}\right)\sin\left(\frac{\pi}{\phi_0}\left(\phi_\ell-\phi_\mathrm{e}\right)\right). \tag{5.10b}$$

5.2.3 Capacitive relations

Referring to Sec. 4.2.1, the current to the linear capacitors can be expressed in terms of the time derivative of the net generalised fluxes across the in parallel connected capacitive branches

$$\mathcal{I}_1 = -C_1\ddot{\phi}_1 \quad \text{and} \quad \mathcal{I}_\Sigma = -C_2\ddot{\phi}_2\,, \tag{5.11}$$

where as derived from Kirchhoff's voltage law $\phi_1 = \phi_{\mathrm{L}_1}$ and $\phi_2 = \phi_{\mathrm{J}_\Sigma} + \phi_{\mathrm{L}_\Sigma}$ are the net generalised fluxes over the in parallel connected inductive branches.

5.2.4 Two extra constraints in the limit of zero junction capacitances

Before we construct the equations of motion, there is one observation that we must discuss. We have two expressions for the current $\mathcal{I}_\Sigma$ and for the current $\mathcal{I}_\ell$. This is a consequence of setting the junction capacitances to zero.

Had we not set the junction capacitances to zero, then the circuit would contain two extra degrees of freedom, thus two extra equations of motion. These correspond with the plasma modes in the SQUID. Usually they are of very high frequency and have therefore on the much longer timescales at which the evolution of the other modes occur negligible effects. Setting the junction capacitances to zero however does transform the equations of motion for the plasma modes to constraints we have encountered twice in the form of two distinct expressions for the same variable.

The two constraints, for both the SQUID currents equating the two expressions, are

$$\mathcal{I}_\ell = \frac{-M\phi_1 + L_1\phi_\ell}{L_1L_\ell - M^2} = -I_\mathrm{c}\cos\left(\frac{2\pi}{\phi_0}\phi_{\mathrm{J}_\Sigma}\right)\sin\left(\frac{\pi}{\phi_0}\left(\phi_\ell - \phi_\mathrm{e}\right)\right)\,, \tag{5.12a}$$

$$\mathcal{I}_\Sigma = \frac{4}{L_\ell}\left(\phi_2 - \phi_{\mathrm{J}_\Sigma}\right) = 2I_\mathrm{c}\cos\left(\frac{\pi}{\phi_0}\left(\phi_\ell - \phi_\mathrm{e}\right)\right)\sin\left(\frac{2\pi}{\phi_0}\phi_{\mathrm{J}_\Sigma}\right)\,. \tag{5.12b}$$

These are transcendental expressions that cannot properly be solved analytically. On the other hand, numerical approximations to their solutions can be found, and this will be useful to find the equilibrium positions of the system. Moreover, if the solutions of the system correspond with small oscillations, then we can make a Taylor expansion around the equilibrium positions and then considerably simplify the equations of motion.

5.2.5 Exact equations of motion in the limit of zero junction capacitances

With the circuit elements constitutive relations and the constraints from Kirchhoff' laws and those imposed by the SQUID with zero junction capacitances, we have a closed set of equations. The equations of motion are obtained by equating for each capacitor the current coming from the connecting inductive branches to the current going into the capacitor; this yields two equations of motion

$$C_1\ddot{\phi}_1 + \frac{L_\ell\phi_1 - M\phi_\ell}{L_1L_\ell - M^2} = 0\,, \tag{5.13a}$$

$$C_2\ddot{\phi}_2 + \frac{4}{L_\ell}\left(\phi_2 - \phi_{\mathrm{J}_\Sigma}\right) = 0\,. \tag{5.13b}$$

Then the constraints should be embedded. In order to do that we must first solve the constraints in Eqs. (5.12) in closed form for two different variables

$$\phi_1 = \frac{I_\mathrm{c}}{M}\left(L_1L_\ell - M^2\right)\cos\left(\frac{2\pi}{\phi_0}\phi_{\mathrm{J}_\Sigma}\right)\sin\left(\frac{\pi}{\phi_0}\left(\phi_\ell - \phi_\mathrm{e}\right)\right) + \frac{L_1}{M}\phi_\ell\,, \tag{5.14a}$$

$$\phi_2 = \phi_{\mathrm{J}_\Sigma} + I_\mathrm{c}\frac{L_\ell}{2}\cos\left(\frac{\pi}{\phi_0}\left(\phi_\ell - \phi_\mathrm{e}\right)\right)\sin\left(\frac{2\pi}{\phi_0}\phi_{\mathrm{J}_\Sigma}\right)\,. \tag{5.14b}$$

Note that there are only two variables for which we can bring the constraints to closed form. It constitutes a non-invertible map from the squid phase coordinates to the integrated voltages the capacitors see.

Combing the equations of motion with the constraints gives

$$C_1 \frac{\mathrm{d}^2}{\mathrm{d}t^2}\left(\frac{L_1}{M}\phi_\ell + \frac{L_1 L_\ell - M^2}{M} I_\mathrm{c} \cos\left(\frac{2\pi}{\phi_0}\phi_{\mathrm{J}_\Sigma}\right)\sin\left(\frac{\pi}{\phi_0}\left(\phi_\ell - \phi_\mathrm{e}\right)\right)\right) + \frac{1}{M}\phi_\ell + \frac{L_\ell}{M} I_\mathrm{c}\cos\left(\frac{2\pi}{\phi_0}\phi_{\mathrm{J}_\Sigma}\right)\sin\left(\frac{\pi}{\phi_0}\left(\phi_\ell - \phi_\mathrm{e}\right)\right) = 0 \tag{5.15a}$$

$$C_2 \frac{\mathrm{d}^2}{\mathrm{d}t^2}\left(\phi_{\mathrm{J}_\Sigma} + I_\mathrm{c}\frac{L_\ell}{2}\cos\left(\frac{\pi}{\phi_0}\left(\phi_\ell - \phi_\mathrm{e}\right)\right)\sin\left(\frac{2\pi}{\phi_0}\phi_{\mathrm{J}_\Sigma}\right)\right) + 2I_\mathrm{c}\cos\left(\frac{\pi}{\phi_0}\left(\phi_\ell - \phi_\mathrm{e}\right)\right)\sin\left(\frac{2\pi}{\phi_0}\phi_{\mathrm{J}_\Sigma}\right) = 0 \tag{5.15b}$$

which in the limit of zero junction capacitances are the exact equations of motion for this system. Observe how, if one works out the derivatives, the coordinate transformation has in a way made the capacitors non-linear. Note also that by employing a non-invertible transformation to new coordinates, there may be side effects of a more mathematical nature. I have no idea how to generally solve these equations of motion, but let's see what we can derive from them[1].

5.2.6 Equilibrium positions

The second of the constraints, Eq. (5.12b), corresponds with the current $\mathcal{I}_\Sigma$ traversing the SQUID. Since the current is collected by a capacitor and it would be unphysical to build up infinite charge on the capacitor plates, we can safely assume that in static equilibrium the current is zero. Then because the $\mathcal{I}_\Sigma$ is odd symmetric with respect to the generalised flux ϕ_{J_Σ}, we deduce that in static equilibrium

$$\overline{\phi_{\mathrm{J}_\Sigma}} = 0\,, \tag{5.16}$$

if there is no symmetry breaking synchronisation between ϕ_ℓ and ϕ_{J_Σ}.

The first constraint, the one related to the loop current is in general non-zero at equilibrium. However, the constraint solved for the inductor flux Eq. (5.14a) can be substituted into the equation for the current in inductor L_1, the first of Eqs. (5.7), which yields

$$\mathcal{I}_1 = \frac{L_\ell\phi_1 - M\phi_\ell}{L_1 L_\ell - M^2} = \frac{I_\mathrm{c} L_\ell}{M}\cos\left(\frac{2\pi}{\phi_0}\phi_{\mathrm{J}_\Sigma}\right)\sin\left(\frac{\pi}{\phi_0}\left(\phi_\ell - \phi_\mathrm{e}\right)\right) + \frac{1}{M}\phi_\ell \tag{5.17}$$

Requiring the current $\mathcal{I}_1$ to be zero, as should be the case at static equilibrium together with the already discussed equilibrium position in ϕ_{J_Σ}, gives an expression for the equilibrium position in the loop flux

$$I_\mathrm{c} L_\ell \overline{\cos\left(\frac{2\pi}{\phi_0}\phi_{\mathrm{J}_\Sigma}\right)}\sin\left(\frac{\pi}{\phi_0}\left(\overline{\phi_\ell} - \phi_\mathrm{e}\right)\right) + \overline{\phi_\ell} = 0\,. \tag{5.18}$$

An overline indicates the average of its argument. The odd symmetry in this constraint is broken by the addition of an extra bias flux ϕ_e under the sine function. Therefore in general $\overline{\phi_\ell} \not\approx 0$. Also, because the expression contains the sum of a linear and a trigonometric term that are both a function of ϕ_1, this transcendental equation must be solved self consistently. As a side note, this relation, if we leave out the averaging, is actually the same relation we would have obtained had we neglected the mutual inductance and added the contributions to the loop flux from an external magnetic field and the loop current; this is to be expected as a mutual inductance is just a channel for externally applying a flux into the SQUID loop.

When ϕ_{J_Σ} is not identically zero for all time but some function that is oscillating around zero, then the cosine shifts away from unity as a function of its amplitude. This can be interpreted as a kind of radiation pressure force shifting the displacing the equilibrium point of the loop flux.

[1] It is also very difficult, perhaps impossible, to find a Lagrangian that would generate these equations of motion.

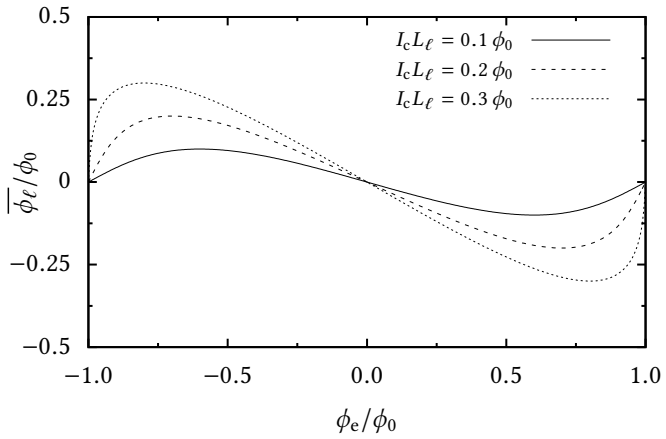

Figure 5.2: Equilibrium position for the loop flux as a function of external flux applied to the SQUID loop at zero radiation pressure, or equivalently solutions to the self consistency relation Eq. (5.18) for different loop inductances or critical currents, under zero radiation pressure, i.e. with $\phi_{J_\Sigma} = 0$ for all time. Note that there is an asymmetry causing the loop flux to be periodic with two flux quanta instead of one with respect to the externally applied flux. However, the boundary conditions for the superconducting condensate in the SQUID are periodic with one flux quantum. This means that, taking the previous two statements together, the solution for the loop flux is bi-stable. Radiation pressure, may decrease the effect. Generally speaking however, the effect only becomes significant for large loop inductances and critical currents.

Further, as can be seen in a plot, Fig. 5.2, of a numerical solution to Eq. (5.18) for the equilibrium loop flux under zero radiation pressure as a function of external flux, there seems to be a doubling in the oscillation period of $\overline{\phi_\ell}$ as a function of ϕ_e from one flux quantum to two flux quanta. This would make the solution for $\overline{\phi_\ell}$ depend on whether the externally applied loop flux ϕ_e is near an even or an odd integer flux quanta. This seems strange, since usually there should be no specific preference for any specific number of flux quanta (i.e. some kind of guage invariance). In fact there can be no such preference since, as we have derived in Sec. 3.1.4, the boundary conditions on the wave-function for the superconducting condensate in a SQUID are invariant to any integer shift in the amount of loop flux-quanta. This means that the system is bi-stable in loop flux; this is similar to what is the case in a flux qubit [56].

There are a couple of other consequences to mention about the external flux induced symmetry breaking. One consequence is that, whenever the slope of the linear term is less steep than that of the trigonometric term with respect to $\overline{\phi_\ell}$,

$$I_c L_\ell \frac{\pi}{\phi_0} > 1\,, \tag{5.19}$$

there may exist even more solutions for the loop flux equilibrium point depending on flux biassing. Figure 5.3 graphically demonstrates above's statement.

5.2.7 A first attempt at an approximate solution

Given that we are interested in oscillatory harmonic like solutions, we note that for such solutions of small amplitudes a Taylor expansion to second order usually gives a reasonably good approximation of the dynamics. What makes the equations of motion complicated is the non-linear nature of the Josephson junctions; not only that, but also the non-linear constraint we need to impose on the system due to the inductances with and in the SQUID loop.

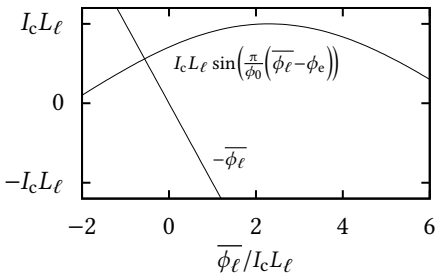

Figure 5.3: Graphical solution for the equilibrium loop flux. Note that when the amplitude of the trigonometric term exceeds unity, more than one solutions may be possible depending on the external flux. For the figure, the flux tuning was set to a quarter flux quantum.

A Taylor expansion up to leading terms of the trigonometric terms brings the constraint to the form

$$\alpha_1\phi_1 + \alpha_\ell\phi_\ell + \alpha_\Sigma{\phi_{J_\Sigma}}^2 - \alpha_0 = 0\,, \tag{5.20a}$$

$$\beta_2\phi_2 - \beta_\Sigma\phi_{J_\Sigma} - \beta_\ell\phi_\ell + \beta_0 = 0\,. \tag{5.20b}$$

While this set of equations can be solved for both the pairs ϕ_1, ϕ_2 and ϕ_ℓ, ϕ_{J_Σ}, there are two solutions for the last pair which correspond with the same ϕ_1 and ϕ_2. This is caused by the squared term[2]in the first equation. Thus the constraints constitute a two-to-one map of the coordinates ϕ_ℓ, ϕ_{J_Σ} to ϕ_1, ϕ_2.

Because the two solutions for ϕ_ℓ with ϕ_{J_Σ} correspond to physically different conditions, this makes one wonder whether it is valid to incorporate such a coordinate transformation in the equations of motion. After some though, I believe this is no problem for the reason that a specific solution to the equations of motion depends on the initial conditions of the system, which actually constitute a choice along which of the two possible paths the system starts[3]. Thus working in the coordinates ϕ_ℓ and ϕ_{J_Σ}, we postpone the choice, while if we choose to work in the coordinates ϕ_1 and ϕ_2 we make the choice explicit.

5.2.8 A complication in Lagrangian mechanics

Since our goal is to find a quantised Hamiltonian description of this system, through a path called canonical quantisation, we need to derive a Lagrangian that would generate the same equations of motion as we have derived, be it in its exact form or a Taylor expanded version. It is here that a complication arises.

A Lagrangian is essentially defined for mechanical systems as the total kinetic energy minus the potential energy in the system

$$\mathcal{L} = \mathcal{E}_{\text{kin}} - \mathcal{E}_{\text{pot}}\,. \tag{5.21}$$

The equations of motion are then generated from the Lagrangian by the Euler-Lagrange equations

$$\frac{\mathrm{d}}{\mathrm{d}t}\frac{\partial\mathcal{L}}{\partial\dot{x_n}} - \frac{\partial\mathcal{L}}{\partial x_n} = 0 \quad \text{for any coordinate } n \text{ in the system}\,. \tag{5.22}$$

Here an over-dot denotes a time derivative. The Euler-Lagrange equations can be derived from Newton's laws or by a variational method (Hamilton's principle), however an explanation is beyond the scope of

[2]We cannot neglect this term since it is of the same order as the radiation pressure force which as we shall see is quadratic in the same variable.

[3]There may be a problem if there are conditions at which the coordinates and velocities are the same for both possible evolution trajectories.

this work; for further reading on that topic consult a book such as Ref. [52]. An important property of the Lagrangian is that under a transformation to new coordinates, the Euler-Lagrange equations remain invariant. The latter is not the case if the transformation to new coordinates is not one-to-one. The book by Goldstein on classical mechanics mentions that it is always assumed that the transformation is invertible [52].

Given that we are dealing with a two-to-one coordinate transformation, the complication mentioned above applies to our system. A way around could be to instead of merging two branches to one, as occurs when transforming to ϕ_ℓ and ϕ_{J_Σ}, specifically choose one branch of the two possible paths for the transformation to the variables ϕ_1 and ϕ_2. One could say that in that case, the transformation is invertible, but I cannot say for sure until I have successfully applied this to our system. In any case, if this works, then the equations of motion and the Lagrangian would be quite a complicated function of its coordinates, since solving Eqs. (5.20) for ϕ_ℓ and ϕ_{J_Σ} is algebraically complicated.

For now, we will try to find a regime in which the non-linear coordinate transformation is avoided.

5.2.9 Small loop inductance approximation

The complications we have encountered are due to non-invertible constraints in the form of self-consistency relations that emerge due to the non-linear Josephson inductances being a function of the flux in the linear inductances in the SQUID loop. In Eqs. (5.14), it is clear that the self-consistency relations vanish when the the self and mutual inductances in the SQUID loop are set to zero. With that we arrive at the goal this section discusses, which is to find an approximation regime where we can accurately describe the system yet avoid the complications arising from the mentioned loop inductances.

Starting with the constraint in Eq. (5.14b), we see that

$$\phi_2 \approx \phi_{J_\Sigma} \quad \text{for} \quad I_c L_\ell \ll \phi_{J_\Sigma}\,, \tag{5.23}$$

that, if the average junction flux is much larger than the average magnetic flux in the arms of the loop, we can regard the net flux in the SQUID cavity as equivalent to the average generalised flux across the tunnel junctions. This removes the bifurcation in the solution of the constraints for ϕ_{J_Σ}. Note that in order for the loop inductance to be small while maintaining a significant mutual inductance, the latter being defined as $M \equiv k\sqrt{L_1 L_\ell}$ with $0 \leq k \leq 1$, one requires the inductance L_1 to be large.

For the other constraint in Eq. (5.14a), we similarly see that

$$\phi_1 \approx \frac{L_1}{M} \quad \text{for} \quad I_c M \ll \frac{L_1}{M}\phi_\ell\,. \tag{5.24}$$

where we have essentially applied the same approximation but for the mutual inductance.

There is a problem however, which we encounter upon substitution of these simplified constraints into the unconstrained equations of motion Eqs. (5.13). We not only decouple the LC-resonator from the SQUID—thereby removing all inter resonator interactions—but we also bring the SQUID-cavity equation of motion into undefined territory by essentially dividing zero by zero. The here proposed simplifications are therefore too strong and a more refined approximation is needed.

5.2.10 First order recursive approximation

The constraints presented in Eqs. (5.14) are what is called self-consistency relations; a relation of that kind equates a variable to a function of the same variable. The solution is the position in the variable for which the values of both are consistent to the relation between them. The main point to be made is that the constraints we are dealing with can be solved implicitly for the variables in question as a

transcendental function of themselves. The constraints in Eqs. (5.14) therefore have a recursive structure as exemplified below for both of them

$$\begin{aligned}\phi_\ell &= \frac{M}{L_1}\phi_1 - \frac{I_c}{L_1}\left(L_1L_\ell - M^2\right)\cos\left(\frac{2\pi}{\phi_0}\phi_{J_\Sigma}\right)\sin\left(\frac{\pi}{\phi_0}\left(\phi_\ell - \phi_e\right)\right)\\ &= \frac{M}{L_1}\phi_1 - \frac{I_c}{L_1}\left(L_1L_\ell - M^2\right)\cos\left(\frac{2\pi}{\phi_0}\phi_{J_\Sigma}\right)\\ &\quad\times\sin\left(\frac{\pi}{\phi_0}\left(\frac{M}{L_1}\phi_1 - \frac{I_c}{L_1}\left(L_1L_\ell - M^2\right)\cos\left(\frac{2\pi}{\phi_0}\phi_{J_\Sigma}\right)\sin\left(\frac{\pi}{\phi_0}\left(\phi_\ell - \phi_e\right)\right) - \phi_e\right)\right),\end{aligned} \tag{5.25a}$$

$$\begin{aligned}\phi_{J_\Sigma} &= \phi_2 - \frac{I_cL_\ell}{2}\cos\left(\frac{\pi}{\phi_0}\left(\phi_\ell - \phi_e\right)\right)\sin\left(\frac{2\pi}{\phi_0}\phi_{J_\Sigma}\right)\\ &= \phi_2 - \frac{I_cL_\ell}{2}\cos\left(\frac{\pi}{\phi_0}\left(\phi_\ell - \phi_e\right)\right)\sin\left(\frac{2\pi}{\phi_0}\left(\phi_2 - \frac{I_cL_\ell}{2}\cos\left(\frac{\pi}{\phi_0}\left(\phi_\ell - \phi_e\right)\right)\sin\left(\frac{2\pi}{\phi_0}\phi_{J_\Sigma}\right)\right)\right)\end{aligned} \tag{5.25b}$$

where we have essentially substituted the solution into itself for both relations. Because the two relation are actually inter-depend on each solutions, the recursion should actually be done in two dimension, one for each self-consistent variable. With that the constraints after a single recursion are written as

$$\begin{aligned}\phi_\ell &= \frac{M}{L_1}\phi_1 - \frac{I_c}{L_1}\left(L_1L_\ell - M^2\right)\cos\left(\frac{2\pi}{\phi_0}\left(\phi_2 - \frac{I_cL_\ell}{2}\cos\left(\frac{\pi}{\phi_0}\left(\phi_\ell - \phi_e\right)\right)\sin\left(\frac{2\pi}{\phi_0}\phi_{J_\Sigma}\right)\right)\right)\\ &\quad\times\sin\left(\frac{\pi}{\phi_0}\left(\frac{M}{L_1}\phi_1 - \frac{I_c}{L_1}\left(L_1L_\ell - M^2\right)\cos\left(\frac{2\pi}{\phi_0}\phi_{J_\Sigma}\right)\sin\left(\frac{\pi}{\phi_0}\left(\phi_\ell - \phi_e\right)\right) - \phi_e\right)\right),\end{aligned} \tag{5.26a}$$

$$\begin{aligned}\phi_{J_\Sigma} &= \phi_2 - \frac{I_cL_\ell}{2}\cos\left(\frac{\pi}{\phi_0}\left(\frac{M}{L_1}\phi_1 - \frac{I_c}{L_1}\left(L_1L_\ell - M^2\right)\cos\left(\frac{2\pi}{\phi_0}\phi_{J_\Sigma}\right)\sin\left(\frac{\pi}{\phi_0}\left(\phi_\ell - \phi_e\right)\right) - \phi_e\right)\right)\\ &\quad\times\sin\left(\frac{2\pi}{\phi_0}\left(\phi_2 - \frac{I_cL_\ell}{2}\cos\left(\frac{\pi}{\phi_0}\left(\phi_\ell - \phi_e\right)\right)\sin\left(\frac{2\pi}{\phi_0}\phi_{J_\Sigma}\right)\right)\right).\end{aligned} \tag{5.26b}$$

In principle one can recur like this indefinitely, but for the sake of simplicity we keep the number of iterations at one. The main point is that this provides a path for a more refined approximation by truncating the recursive structure. That is achieved by setting both the variables ϕ_ℓ and ϕ_{J_Σ} according to a guess for which we choose zero[4]

$$\phi_{J_\Sigma} \approx \phi_2 - \frac{I_cL_\ell}{2}\cos\left(\frac{\pi}{\phi_0}\left(\frac{M}{L_1}\phi_1 - \phi_e\right)\right)\sin\left(\frac{2\pi}{\phi_0}\phi_2\right) \tag{5.27a}$$

$$\phi_\ell \approx \frac{M}{L_1}\phi_1 - \frac{I_c}{L_1}\left(L_1L_\ell - M^2\right)\cos\left(\frac{2\pi}{\phi_0}\phi_2\right)\sin\left(\frac{\pi}{\phi_0}\left(\frac{M}{L_1}\phi_1 - \phi_e\right)\right). \tag{5.27b}$$

This way we avoid the linearisation and uncoupling of the LC-resonator to the SQUID and restore the SQUID-cavity equation of motion. Note that while the error in the loop flux ϕ_ℓ introduced by the truncation may be absorbed into an effect external flux tuning ϕ_e, this cannot be done for the generalised SQUID flux ϕ_{J_Σ} since its dynamics are odd symmetric around zero; we therefore need the loop inductance L_ℓ to be small compared to the SQUID inductance.

One may wonder how accurate this first order recursive approximation is. It is probably a quiet crude description of the actual solution which can be seen as being the result of an infinite recursive chain, so

[4]The equilibrium position for the loop flux $\overline{\phi_\ell}$ would arguably be a better choice for the loop flux variable. The effect to first order, however, is a relatively uninteresting shift in the flux biassing; that is if we are not crossing a critical point from which the recursive approximation would start converging to a different solution when there is more than one possible, see section 5.2.6.

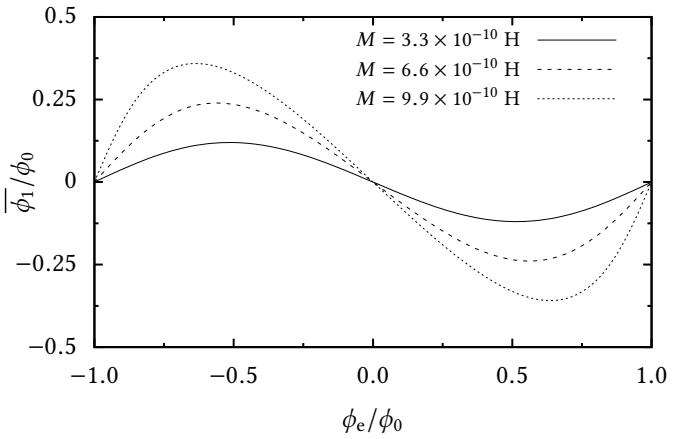

Figure 5.4: Average magnetic flux in inductor L_1 as a function of bias flux ϕ_e in the SQUID loop and zero radiation pressure, or equivalently solutions to the self consistency relation Eq. (5.29a) for different mutual inductances. The critical current for the Josephson junctions is $I_c = 0.75$ μA and the inductor self inductance $L_1 = 2.6$ nH. Note that there is an asymmetry causing the inductor flux to be periodic with two flux quanta instead of one with respect to the externally applied flux ϕ_e. The the strength off the asymmetry is also influenced by the critical current I_c. Radiation pressure, referring may decrease the effect. Generally speaking however, the effect only becomes significant for large mutual inductances. Given a small loop inductance $L_\ell = 10^{-15}$, a more realistic value is $M \propto \sqrt{L_1 L_\ell} \propto 10^{-12}$.

definitely the approximation is different. On the other hand, since figuratively speaking all elements in the recursive chain are identical, and the approximation embeds one such element, its characteristics should be similar, but probably of a strength slightly stronger or weaker than in the real solution.

5.2.11 Approximate equations of motion

Combining the simplified constraints in Eqs. (5.27) together with the unconstrained equations of motion presented in Eqs. (5.13), gives the approximate equations of motion

$$C_1 \frac{\mathrm{d}^2\phi_1}{\mathrm{d}t^2} + \frac{1}{L_1}\phi_1 + \frac{M}{L_1} I_c \cos\left(\frac{2\pi}{\phi_0}\phi_2\right) \sin\left(\frac{\pi}{\phi_0}\left(\frac{M}{L_1}\phi_1 - \phi_e\right)\right) = 0 \tag{5.28a}$$

$$C_2 \frac{\mathrm{d}^2\phi_2}{\mathrm{d}t^2} + 2I_c \cos\left(\frac{\pi}{\phi_0}\left(\frac{M}{L_1}\phi_1 - \phi_e\right)\right) \sin\left(\frac{2\pi}{\phi_0}\phi_2\right) = 0\,. \tag{5.28b}$$

Note that in the approximation we now use flux variables corresponding to what the capacitors see.

5.2.12 Equilibrium position inductor flux

Since the time derivatives in the equations of motion should be zero on average, we have from the approximate equations of motion Eqs. (5.28) two expression for the average currents in the two resonators

as a function of the cavity coordinates rather than the SQUID coordinates

$$\overline{I_1} = \frac{\overline{\phi_1}}{L_1} + \frac{MI_c}{L_1}\overline{\cos\left(\frac{2\pi\phi_2}{\phi_0}\right)}\sin\left(\frac{\pi}{\phi_0}\left(\frac{M}{L_1}\overline{\phi_1} - \phi_e\right)\right) = 0 \tag{5.29a}$$

$$\overline{I_2} = 2I_c\overline{\cos\left(\frac{\pi}{\phi_0}\left(\frac{M}{L_1}\phi_1 - \phi_e\right)\right)}\sin\left(\frac{2\pi\overline{\phi_2}}{\phi_0}\right) = 0 \tag{5.29b}$$

which are both zero since it would be rather unphysical to build up infinite charge on the capacitors. Here we have made use of the odd symmetry in the sine function around zero, and have taken the liberty of approximating the sine function in the first equation with an offset term as being locally linear. We see that

$$\overline{\phi_2} = 0 \quad \text{from symmetry, but also that} \quad \overline{\phi_1} \neq 0 \tag{5.30}$$

due to the odd symmetry around the equilibrium point being broken in Eq. (5.29a) caused by the external tuning flux ϕ_e under the sine function. These are very similar to the one we derived earlier for the SQUID variables ϕ_ℓ and ϕ_{J_Σ}. See Fig. 5.4 for a plot of the average inductor flux as a function of flux biassing under zero radiation pressure.

Observe that modulation of the critical current by oscillations in ϕ_2 cause an on average non-zero shift in the displacement of ϕ_1. Further, the equilibrium positions in ϕ_1 and ϕ_2 determine the point around which ideally a Taylor expansion should be taken, which we will later do to simplify the description of the system we are discussing.

5.3 Circuit Lagrangian

The next task is to find a Lagrangian that generates the same equations of motion as we have derived in the preceding section. In doing so we find expressions for what can be considered the analogue for kinetic and potential energy in classical mechanics. Since it is for reasons already discussed difficult to find a Lagrangian for the exact equations of motion, we in this section derive a Lagrangian corresponding with the approximate equations of motion.

5.3.1 Approximate Lagrangian

Because the time derivatives in the approximate equations of motion (5.28) operate on linear functions, it is easy to verify that they are Euler-Lagrange equations that are generated from the Lagrangian

$$\mathcal{L} = \frac{1}{2}C_1\dot{\phi_1}^2 + \frac{1}{2}C_2\dot{\phi_2}^2 - \frac{1}{2}\frac{1}{L_1}\phi_1^2 + \frac{I_c\phi_0}{\pi}\cos\left(\frac{\pi}{\phi_0}\left(\frac{M}{L_1}\phi_1 - \phi_e\right)\right)\cos\left(\frac{2\pi}{\phi_0}\phi_2\right), \tag{5.31}$$

where we denote a time derivative with a dot above the respective variable as a short hand notation.

Here we recognise as the analogue kinetic energy the energy stored in the capacitors

$$\mathcal{E}_k = \frac{1}{2}\left(C_1\dot{\phi_1}^2 + C_2\dot{\phi_2}^2\right) \tag{5.32a}$$

and as the analogue potential energy the sum of the Josephson energy in the SQUID (neglecting energy in the loop self inductance) and inductive energy in the inductor

$$\mathcal{E}_p = \frac{1}{2L_1}\phi_1^2 - \frac{I_c\phi_0}{\pi}\cos\left(\frac{\pi}{\phi_0}\left(\frac{M}{L_1}\phi_1 - \phi_e\right)\right)\cos\left(\frac{2\pi}{\phi_0}\phi_2\right). \tag{5.32b}$$

A notable absence from the energy expressions is the is the inductive energy stored in the SQUID loop. Evidently, we have in our approximations left out contributions from the loop inductance to the dynamics. The loop inductance must therefore be small compared to the SQUID inductance for the approximation to be valid.

5.4 Quantum mechanical description

This section describes the route we take for deriving a quantum mechanical description for the SQUID opto-mechanics system. First we derive the momenta conjugate to the coordinates used in the Lagrangian. These are needed for the quantum mechanical commutation relations one needs to impose on the system in order to satisfy Heisenberg's uncertainty principle. After the Hamiltonian is derived as a Legendre transform of the Lagrangian, the system is quantised by promoting the canonically conjugate positions and momenta to quantum operators and imposing the canonical commutation relations.

5.4.1 Legendre transform the Lagrangian to a Hamiltonian

Before transforming the circuit Lagrangian into a Hamiltonian, we first find expressions for the conjugate momenta for each of the generalised coordinates. From its definition as a derivative of the Lagrangian over the respective generalised velocity we obtain

$$q_1 = \frac{\partial \mathcal{L}}{\partial \dot{\phi}_1} = C_1 \dot{\phi}_1 \,, \tag{5.33a}$$

$$q_2 = \frac{\partial \mathcal{L}}{\partial \dot{\phi}_2} = C_2 \dot{\phi}_2 \,. \tag{5.33b}$$

The conjugate momenta are seen to correspond respectively with the electrical charges stored on the capacitors.

Since above two relations are easily inverted, we can express the generalised velocities in terms of the conjugate momenta. Therefore, a Hamiltonian, defined as a Legendre transform of the Lagrangian from the generalised velocities $\dot{\phi}_1$ and $\dot{\phi}_2$ to the conjugate momenta q_1 and q_2, is obtained as

$$\mathcal{H} = \frac{{q_1}^2}{2C_1} + \frac{{q_2}^2}{2C_2} + \frac{{\phi_1}^2}{2L_1} - \frac{I_c \phi_0}{\pi} \cos\left(\frac{\pi}{\phi_0}\left(\frac{M}{L_1}\phi_1 - \phi_e\right)\right) \cos\left(\frac{2\pi}{\phi_0}\phi_2\right) , \tag{5.34}$$

the sum of the inductive and capacitive energy stored in the system.

5.4.2 Simplifying the Hamiltonian

Before discussing the quantum mechanical aspects of this Hamiltonian, we first make the harmonic nature of the resonant modes as a first order approximation explicit. Under the assumption that the amplitude of oscillation in both resonators is small, the trigonometric expressions for the Josephson energy are Taylor expanded around the averages of ϕ_1 and ϕ_2, the first of which is non-zero as derived in Sec. 5.2.12 while the latter is zero.

The non-zero average inductor flux would create a static offset term in the Taylor expansion. However, if one transforms to coordinates centred around the static offset, the term drops out and is instead absorbed into ϕ_e as an effective flux tuning of the SQUID. In this understanding we carry out the expansion around zero in both the variables, noting that a slight shift in flux tuning is to be expected. Expanding under the

given assumptions the Hamiltonian to fourth order around zero yields

$$\begin{aligned}\mathcal{H} = &\frac{{q_1}^2}{2C_1} + \frac{{q_2}^2}{2C_2} + \frac{1}{2}\left(\frac{1}{L_1} + \frac{\pi I_c}{\phi_0}\left(\frac{M}{L_1}\right)^2 \cos\left(\frac{\pi\phi_e}{\phi_0}\right)\right){\phi_1}^2 \\ &+ \frac{2\pi I_c}{\phi_0}\cos\left(\frac{\pi\phi_e}{\phi_0}\right){\phi_2}^2 - \frac{2I_c}{3}\left(\frac{\pi}{\phi_0}\right)^3 \cos\left(\frac{\pi\phi_e}{\phi_0}\right){\phi_2}^4 \\ &+ \frac{2I_c M}{L_1}\left(\frac{\pi}{\phi_0}\right)^2 \sin\left(\frac{\pi\phi_e}{\phi_0}\right)\phi_1{\phi_2}^2 - I_c\left(\frac{\pi}{\phi_0}\right)^3\left(\frac{M}{L_1}\right)^2 \cos\left(\frac{\pi\phi_e}{\phi_0}\right){\phi_1}^2{\phi_2}^2\end{aligned} \tag{5.35}$$

where we have left out constant contributions and contributions of order higher than two in the inductor flux ϕ_1, but we keep the Duffing non-linearity in the SQUID-cavity in the Hamiltonian. We further disregard a linear term in ϕ_1 which corresponds with a static displacement in the inductor flux and thus only influences the SQUID flux tuning.

Had we carried out the Taylor expansion further, higher order non-linear terms and especially more interaction terms would have emerged. They will al be of the form

$$k_{nm}\left(\overline{\phi_1}\right){\phi_1}^n{\phi_2}^m \quad \text{with} \quad n \in \{0, 1, 2\ldots\} \quad \text{and} \quad m \in \{0, 2, 4\ldots\}\,. \tag{5.36}$$

A further thing of note being made explicit in the simplified Hamiltonian is that there is a renormalisation of the LC-resonator inductance L_1. This can be interpreted as the SQUID forming a parallel inductance

$$L_{1_\Sigma} = \frac{\phi_0 {L_1}^2}{\pi I_c M^2 \cos\left(\frac{\pi}{\phi_0}\phi_e\right)} \tag{5.37}$$

as a consequence of the mutual inductance with the SQUID loop. The effect is the result of a second order term in ϕ_1 in the Taylor expansion. Because in the here discussed Hamiltonian description the effect is static, we will leave it out from now on.

5.4.3 Canonical quantisation

We then promote the generalised coordinates and momenta to quantum operators and impose canonical commutation relation between the conjugate position and momentum pairs[5]

$$[\phi_1, q_1] = \mathrm{i}\hbar \quad \text{and} \quad [\phi_2, q_2] = \mathrm{i}\hbar\,. \tag{5.38}$$

Transforming the Hamiltonian to new observables defined as

$$Q_1 = \sqrt{C_1}\phi_1\,, \quad P_1 = \frac{q_1}{\sqrt{C_1}} \tag{5.39a}$$

and

$$Q_2 = \sqrt{C_2}\phi_2\,, \quad P_2 = \frac{q_2}{\sqrt{C_2}} \tag{5.39b}$$

[5] Generally speaking, the commutation relations are related to the classical Poisson brackets

$$\{A, B\} = 1 \rightarrow \frac{1}{\mathrm{i}\hbar}[A, B] = 1$$

as shown by Dirac [55].

brings, preserving the commutation relations, the Hamiltonian to a form that corresponds with two mechanical harmonic oscillators of mass one (the form described in Sec. 4.3.2) plus a non-linear correction and an interaction term

$$\mathcal{H} = \frac{1}{2}\left({P_1}^2 + {\omega_1}^2{Q_1}^2\right) + \frac{1}{2}\left({P_2}^2 + {\omega_2}^2{Q_2}^2\right) + \mathcal{H}_{\text{Duffing}} + \mathcal{H}_{\text{interaction}} \tag{5.40}$$

with

$$\omega_1 = \frac{1}{\sqrt{L_1 C_1}} \tag{5.41a}$$

$$\omega_2 = \sqrt{\frac{1}{C_2}\frac{4\pi I_c}{\phi_0}\cos\left(\frac{\pi}{\phi_0}\phi_e\right)} \tag{5.41b}$$

the resonance frequencies for the two resonators in the absence of interactions and anharmonicity.

The next step is to express the Hamiltonian in terms of boson creation and annihilation operators

$$a = \frac{\omega_2 Q_2 + \mathrm{i}P_2}{\sqrt{2\hbar\omega_2}} \quad \text{and} \quad b = \frac{\omega_1 Q_1 + \mathrm{i}P_1}{\sqrt{2\hbar\omega_1}} \tag{5.42}$$

which, as can be derived from the commutators for the flux and charge variables, satisfy the commutation relations

$$[a, a^\dagger] = 1 \quad \text{and} \quad [b, b^\dagger] = 1\,. \tag{5.43}$$

Note that conforming to literature on opto-mechanics we use the b operators for the LC-resonator as the mechanical analogue and the a operators for the SQUID-resonator as the analogue optical cavity. With these definitions we may express the flux and charge observables as

$$\phi_x = \phi_{\text{zpf}_x}\left(a_x + {a_x}^\dagger\right), \quad q_x = -\mathrm{i}q_{\text{zpf}_x}\left(a_x - {a_x}^\dagger\right) \quad \text{with} \quad x \in \{1, 2\} \tag{5.44}$$

and as the flux zero point fluctuations

$$\phi_{\text{zpf}_x} = \sqrt{\frac{\hbar}{2C_x\omega_x}} \quad \text{and} \quad q_{\text{zpf}_x} = \sqrt{\frac{\hbar C_x\omega_x}{2}}\,. \tag{5.45}$$

This results in the following Hamiltonian

$$\mathcal{H} = \hbar\omega_1\left(b^\dagger b + \frac{1}{2}\right) + \hbar\omega_2\left(a^\dagger a + \frac{1}{2}\right) - \hbar\frac{\chi}{6}\left(a + a^\dagger\right)^4 + \hbar\frac{g_0}{2}\left(a + a^\dagger\right)^2\left(b + b^\dagger\right) - \hbar\frac{g_1}{4}\left(a + a^\dagger\right)^2\left(b + b^\dagger\right)^2\,. \tag{5.46}$$

What will be the strength of the Kerr non-linearity is defined as

$$\chi = \frac{\hbar}{{C_2}^2{\omega_2}^2} I_c\left(\frac{\pi}{\phi_0}\right)^3 \cos\left(\frac{\pi}{\phi_0}\phi_e\right) = \frac{\hbar}{4C_2}\left(\frac{\pi}{\phi_0}\right)^2\,. \tag{5.47}$$

The optomechanical single-photon coupling constant is defined as

$$g_0 = \frac{4I_c}{C_2\omega_2}\sqrt{\frac{\hbar}{2C_1\omega_1}}\left(\frac{\pi}{\phi_0}\right)^2\frac{M}{L_1}\sin\left(\frac{\pi}{\phi_0}\phi_e\right)\,. \tag{5.48}$$

One can easily check that the single photon opto-mechanical coupling rate is in fact equivalent to

$$g_0 = -\phi_{\mathrm{zpf}_1} \frac{\mathrm{d}\omega_2}{\mathrm{d}\phi_1}\,, \tag{5.49}$$

in correspondence with the traditional explanation of the opto-mechanical Hamiltonian. Finally, what later may be regarded the strength of the quadratic opto-mechanical or cross-Kerr interaction is defined as

$$g_1 = \frac{\hbar I_\mathrm{c}}{C_1 C_2 \omega_1 \omega_2} \left(\frac{\pi}{\phi_0}\right)^3 \left(\frac{M}{L_1}\right)^2 \cos\left(\frac{\pi\phi_\mathrm{e}}{\phi_0}\right)\,. \tag{5.50}$$

5.4.4 A further approximation

The term relating to the Duffing non-linearity can be simplified by expanding the quartic term, and throwing away terms that do not conserve the number of excitations or energy since we are considering a closed system[6]. Leaving out constant contributions to the Hamiltonian, we approximate

$$\left(a + a^\dagger\right)^4 \approx 6\left(a^\dagger a\right)^2 + 6a^\dagger a\,. \tag{5.51}$$

This result is in agreement with what one would obtain had one treated a harmonic oscillator with perturbation theory using the Duffing non-linearity as perturbation [57].

Similarly we expand the cubic interaction term $\hbar\frac{g_0}{2}\left(a + a^\dagger\right)^2\left(b + b^\dagger\right)$ and simplify by similarly throwing away all terms that do not preserve energy

$$\left(a + a^\dagger\right)^2 = a^2 + 2a^\dagger a + 1 + a^{\dagger 2} \approx 2a^\dagger a + 1\,. \tag{5.52}$$

Since this is done within a product, the constant appearing in above's equation carries physical meaning: It corresponds with a shift in the LC- or analogue mechanical resonator, which, since it is a byproduct of the non-commutative nature of quantum observables, we may interpret as being caused by the zero-point fluctuations in the SQUID-resonator, the analogue optical cavity. When taking into account a reference amplitude, however, the zero-point fluctuation induced displacement cancels out because it is also part of the reference amplitude.

Doing the same with the quartic interaction term $\hbar\frac{g_1}{4}\left(a + a^\dagger\right)^2\left(b + b^\dagger\right)^2$ gives

$$\left(a + a^\dagger\right)^2\left(b + b^\dagger\right)^2 \approx \left(2a^\dagger a + 1\right)\left(2b^\dagger b + 1\right) = 4a^\dagger a b^\dagger b + 2a^\dagger a + 2b^\dagger b + 1\,. \tag{5.53}$$

where again we will neglect the static shifts of the two resonator resonance frequencies and the constant term.

With these approximations and dropping constant terms we may write the Hamiltonian as

$$\mathcal{H} = \hbar\omega_1 b^\dagger b + \hbar\omega_2 a^\dagger a - \hbar\chi\left(a^\dagger a\right)^2 + \hbar g_0 a^\dagger a\left(b + b^\dagger\right) - \hbar g_1 a^\dagger a b^\dagger b\,. \tag{5.54}$$

Besides the presence of both an opto-mechanical and a cross-Kerr interaction, an addition is a photon dependent shift of the cavity due to the Kerr non-linearity.

This is the main result of this work. We have derived the leading interactions occurring between the two resonators in the proposed circuit and we have shown that it includes interactions equivalent to those that are the focus of the cavity opto-mechanics field.

[6] Had we added a drive and transformed the Hamiltonian to a frame rotating with the drive frequency, this would be called the rotating wave approximation. A hand-waving explanation is that in such a rotating frame the neglected terms are rapidly oscillating with respect to the dynamics occurring in the frame of interest and would therefore average out—in addition to being off-resonance with any other part of the system, thus driving no transitions.

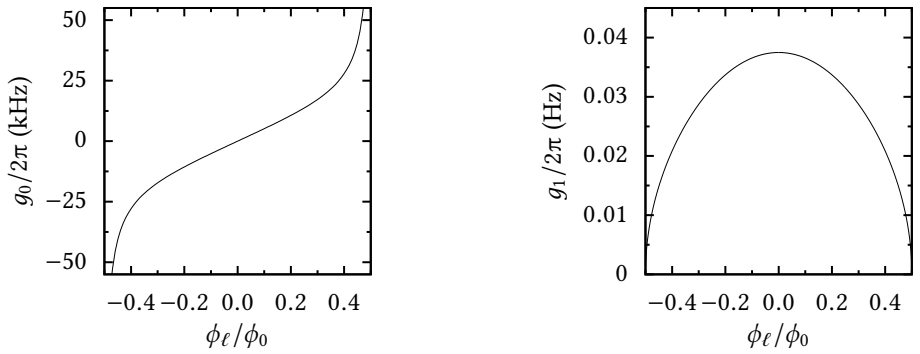

(a) Single photon opto-mechanical coupling rate

(b) Cross-Kerr interaction strength

Figure 5.5: Strengths for **(a)** the single photon opto-mechanical coupling and **(b)** the cross Kerr interaction, both as a function of loop flux. Screening effects due to the mutual inductance and self-inductance are neglected. The parameters for this system are as follows: $C_1 = 1.88$ nF, $C_2 = 9.21$ pF, $L_1 = 2.6$ nH, $I_c = 0.75$ μA, and $M = 1$ pH assuming a loop inductance of $L_\ell = 10^{-3}$ pH; the parameters are however unoptimised.

5.4.5 Characterisation

The opto-mechanical single photon coupling strength is plotted in Fig. 5.5a as a function of loop flux. With the parameters given in that figure, the strength of the Kerr non-linearity is $\frac{\chi}{2\pi} = 1.05$ MHz, much stronger than the opto-mechanical coupling as in the plot. The cross-Kerr interaction is insignificant compared to all the other terms in the Hamiltonian. The question is whether we can increase g_0 while decreasing χ by optimising the parameters.

The self-Kerr non-linearity as expressed by Eq. (5.47) is made smaller by increasing the SQUID-cavity capacitance C_2. In order to keep the resonance frequency ω_2 constant, one must then increase the critical current I_c. The latter has however, as discussed in Sec. 5.2.6, may introduce a bi-stability in the SQUID loop flux.

Referring to Eq. (5.48) and Eqs. (5.41), the single photon opto-mechanical coupling strength is increased by increasing *both* the resonance frequencies ω_1 and ω_2, as well as increasing the mutual inductance M. The latter, however, requires one to increase the SQUID loop inductance, which would complicate the SQUID dynamics; or increase the inductor inductance L_1, which reduces the resonance frequency ω_1. On the other hand decreasing the capacitance C_1 has no such limitations. The increase in resonance frequency ω_2 is limited by the self-Kerr non-linearity χ and one's ability to fabricate large critical current Josephson junctions.

Chapter 6

Conclusion and Outlook

The main result presented in this work is an investigation of an approach to analogue simulation of an opto-mechanical system with a superconducting lumped element circuit.

In contrast to microwave implementations of opto-mechanical systems, where in an LC-resonator one of the capacitor plates constitutes a mechanical drum and hence the capacitance is a function of mechanical position, the implementation considered here employs the variable inductance of a SQUID in the harmonic limit. Since the inductance of a SQUID is a function of flux threading its loop, the analogue of the mechanical position is the flux of an additional LC-resonator whose magnetic flux threads the SQUID loop. The idea is that this makes the frequency of the resonator embedding the SQUID a function of the flux in the other resonator, similar to how in cavity opto-mechanics the relative position of the mirrors in an optical resonator sets the cavity resonance frequency.

6.1 SQUID opto-mechanics with loop inductances

An analysis has been conducted on the interaction between an inductor and a SQUID through a mutual inductance with the inductor and SQUID loop. The results are relations between the currents and voltages across the inductor and the SQUID including its constitutive parts, which are the inductances and junctions in both arms of its loop. Since we are considering any capacitance in the junctions as negligible, we can in principle eliminate two of the four degrees of freedom and express the net voltage across the SQUID and the inductor in terms of the loop flux and the average of the gauge invariant phases across the two tunnel junctions. From the two net voltage relations two expressions for the generalised fluxes across the SQUID and inductor in terms of the phase and loop flux are easily derived—these in essence constitute the constraints by which the number of degrees of freedom in the system is reduced.

Arranging the inductor in parallel with a capacitor and doing the same with the SQUID gives us the setup for the lumped element analogue opto-mechanics simulation. The equations of motion are obtained by equating the current from each capacitor to the current through the corresponding in parallel connected inductive element (Kirchhoff's current law). These equations of motion are expressed in terms of the flux through the SQUID loop and the average phase across the SQUID.

6.1.1 Complications in Lagrangian mechanics

There is a problem however that arises when we try to find a Lagrangian that would generate the same equations of motion: The relations between the resonator generalised fluxes (the constraints) and the loop flux with the average junction phase do not constitute an invertible one-to-one map, but rather a non-linear many-to-one map. This seems to give problems in Lagrangian mechanics because in general

the equations of motion are not invariant for the the specific branch in the transformation along which the system dynamics are evolving. Since a Lagrangian does not encode such information, a Lagrangian circuit description for these kinds of systems may therefore not exist.

It is known that canonical circuit quantisation schemes only work when each pair of conjugate capacitive and inductive branches has only zero or one of the two containing non-linearities. In a sense, the non-invertible transformation to the generalised coordinates has made the linear capacitors in the circuit effectively non-linear. Note however that in our case, this is not a limitation in circuit theory having to do the with the invertibility of either the capacitive or the inductive branch connecting to a circuit node, it is rather a limitation in Lagrangian mechanics.

6.1.2 A way out?

A way around this complication might be to Taylor expand the constraints around a point at one of the possible solutions and truncating before multiple solutions become possible, thus constructing a locally valid one-to-one map for the constraint. This approach is problematic as even quadratic terms may introduce multiple solutions which then prohibits the inclusion of any cubic (as required for opto-mechanics) or higher order interaction terms.

Another approach is to include the junction capacitances[1], thereby eliminating the constraints but increasing the degrees of freedom to four. This approach has not been attempted (however do see the appendix for a start) but should in principle allow us to find an exact Lagrangian description since it does not involve any non-linear transformation and the underlying circuit contains only linear capacitors. Moreover, if successful, we may be able to eliminate two degrees of freedom from the system by taking the limit to zero junction capacitances on the level of the Lagrangian or Hamiltonian, but *after* transforming it to a normal mode basis where the two plasma modes (in the basis of the loop flux and average junction phase such that their linear interaction with each other decouples) hybridise pairwise with the two cavity modes due to a linear interaction mediated by the loop self and mutual inductances; thus avoiding the non-linear constraint by letting the two now *hybridised* plasma mode frequencies approach infinity effectively rendering the corresponding degrees of freedom inaccessible.

6.1.3 Speculations on consequences and possible applications

The above mentioned complications are a consequence of putting tunnel junctions in series with linear inductances. The precise dynamics that emerge from such setups are non-linear and may admit more than one stable solution. The former is intrinsic to Josephson junctions, but the latter follows specifically from the interplay between the linear inductances and the junctions. An interesting application of the bi-stability in loop flux we encountered is in the flux qubit whose state is encoded in the occupation of two stable loop flux states. What makes this interesting is that the phases of the resonant modes coupled to the SQUID depend on the branch taken in the bifurcation of the SQUID state—one could consider this a kind of symmetry breaking; the same should apply to the interaction between the resonant modes.

For example consider flux-biassing the SQUID loop to halve a flux quantum in the opto-mechanics simulation setup; then, due to even symmetry and the existence of two solutions for the net loop flux (akin to a flux qubit), the opto-mechanical interaction for both solutions differ in sign but are otherwise identical. Now doing opto-mechanical driving of the LC-resonator through OMIT there are two possible coherent states into which the system can be driven, differing only by a π phase shift. Something to look into for future experiments would be to use techniques developed for the flux-qubit to bring the SQUID

[1] Incidentally there is a note in the lecture notes by Devoret [51] that mentions that there should be no node connected to only inductances (and that the sub-network of capacitances must be connex) in order for the conjugate momenta to be defined. This would not have been relevant had the elimination of the corresponding degrees of freedom through non-linear constraints not given us problems in the Lagrangian mechanics.

in a superposition without altering the dynamics of interaction between the resonant modes. This could e.g. be used to drive the LC-resonator into a cat state starting from a superposition of the SQUID[2].

Whether this may be possible might depend on the degree of anharmonicity in the resonant modes since the theory of opto-mechanics is formulated assuming harmonic resonances.

6.2 SQUID opto-mechanics in first order recursive approximation with small loop inductances

For this thesis, another path has been followed as, also with a Taylor expansion of the trigonometric terms, the equations of motion are not easy to analyse due to mixed time derivatives, making it difficult to find the normal coordinates. Instead we tried to find a solution in the limit where the SQUID loop inductances can be considered small such that self-reference disappears from the constraints. This approach did not work because it removes the SQUID mediated interaction between the resonators and brings the SQUID cavity equation of motion into undefined territory.

The way out as employed here is to substitute the self-consistency relations into themselves and then make the small loop inductances approximation. This way we truncate the infinitely recursive structure in the self-consistency relations. We will have to accept a deviation in the predicted interaction strengths, but the main characteristics should remain intact because a single instance of the self-consistency relations (which essentially contains all the information) is embedded in the approximation; only the cumulative effects in the infinite structure are left out.

In this approximation, we have inverted self-consistency relations opening the way to express the equations of motion in terms of cavity variables rather then SQUID variables while maintaining the interaction between them but also non-linearities, not only in the interaction but also in the resonant modes. The latter is inherent in circuits incorporating tunnel junctions and can be made weaker by increasing the capacitance of the SQUID cavity[3] (and increasing the critical to compensate for the change in the cavity resonance frequency). Increasing the critical current however has the same strengthening effect on the bi-stability in loop flux as the loop inductance. The opto-mechanical interaction can be made stronger by increasing the frequency of both the resonators as well as the mutual inductance; for the latter one must however take care to keep the loop inductance small compared to the SQUID inductance.

For the approximate equations of motion a classical Lagrangian and Hamiltonian are easily derived without the need for a Taylor expansion of the trigonometric terms. Doing the latter to second order in LC-resonator flux and to fourth order in the SQUID-cavity flux gives quadratic terms for the flux in both resonators corresponding to a harmonic oscillator, a quartic duffing or self-Kerr non-linearity in the SQUID-cavity, a cubic radiation pressure interaction term linear in LC-resonator flux but quadratic in the SQUID-cavity flux, and a quartic interaction term quadratic in both the resonator fluxes which corresponds with a quadratic opto-mechanical or a cross-Kerr interaction. The latter is however much weaker than all the other terms in the Hamiltonian.

Following the canonical quantisation procedure and introducing creation and annihilation operators we obtain a Hamiltonian that can easily be transformed to the standard opto-mechanics Hamiltonian by leaving out terms that do not conserve energy. Effects of losses and external driving can be added through input-output theory (see e.g. an appendix in Ref. [12] or a chapter in Ref. [4] for an introduction),

[2]Speculating a bit further, a similar bifurcation also exists in the generalised flux across the SQUID and one could imagine adding current biassing the SQUID-cavity. Generally speaking the opto-mechanics simulation setup in analogy may be considered twice the combination of resonant modes with a spin (the Hilbert space is the direct product of the resonant modes with the spin states) interacting opto-mechanically. From a theoretical point of view the system has quite a bit of symmetry and it is only flux biassing (or current biassing) that allows the asymmetric opto-mechanical interaction to emerge.

[3]Or by employing an array of SQUIDS which allows one to keep the inductance constant while lowering the non-linearity.

and from this the semi-classical and quantum equations of motion are usually obtained, but that is not anything new with respect to the Hamiltonian of an opto-mechanical system.

6.3 Final remarks

The essence of this work is a rigorous derivation of the Hamiltonian of a circuit consisting of two resonators interacting through a mutual inductance with a SQUID embedded in one of the resonators. We have shown that under

- a loop inductance that is small compared to the SQUID inductance, and
- a recursive approximation, truncated after one iteration, for the self-consistency relations imposed on the circuit as constraint by the SQUID,

such a device is described by an opto-mechanical kind of Hamiltonian.

Therefore the circuit is shown to be indeed an analogue simulation of said systems. In contrast to earlier work, we have fully incorporated the mutual inductance in the model and have from that explicitly derived the interaction. We are thus able to fully explain the physics behind the interaction whereas in earlier work it has been derived on a more phenomenological level emerging as a seeming action at a distance from the dependence of the resonance frequency in one resonator on the flux from the other resonator.

The results can be used for optimising the circuit parameters for the analogue simulation in order to try increasing the coupling strength and to try reaching the single photon strong coupling regime. Note, however, that the effects of loop inductances are incorporated in simplified form and likely result in a different coupling strength in practice; a numerical approximation for the self-consistency relations may allow for a more accurate prediction of the opto-mechanical interaction strengths.

Bibliography

[1] J. Kepler. De cometis libelli tres (typis andreae apergiri). 1619.

[2] M. Aspelmeyer, T. J. Kippenberg, and F. Marquardt. Cavity optomechanics. *Rev. Mod. Phys.*, 86:1391–1452, 2014.

[3] C. K. Law. Interaction between a moving mirror and radiation pressure: A hamiltonian formulation. *Phys. Rev. A*, 51:2537–2541, 1995.

[4] D. F. Walls and G. J. Milburn. *Quantum Optics*. Springer, 2nd edition, 2008.

[5] J. Chan, T. P. M. Alegre, A. H. Safavi-Naeini, J. T. Hill, A. Krause, S. Gröblacher, M. Aspelmeyer, and O. Painter. Laser cooling of a nanomechanical oscillator into its quantum ground state. *Nature*, 478:89–92, 2011.

[6] J. D. Teufel, T. Donner, D. Li, J. W. Harlow, M. S. Allman, K. Cicak, A. J. Sirois, J. D. Whittaker, K. W. Lehnert, and R. W. Simmonds. Sideband cooling of micromechanical motion to the quantum ground state. *Nature*, 475:359–363, 2011.

[7] G. S. Agarwal and S. Huang. Electromagnetically induced transparency in mechanical effects of light. *Phys. Rev. A*, 81:041803–4, 2010.

[8] S. Weis, R. Rivière, D. Rémi, S. G. Deléglise, E. Gavartin, O. Arcizet, A. Schliesser, and T. J. Kippenberg. Optomechanically induced transparency. *Science*, 330:1520–1523, 2010.

[9] F. Massel, T. T. Heikkilä, J.-M.Pirkkalainen, S. U. Cho, H. Saloniemi, P. J. Hakonen, and M. A. Sillanpää. Microwave amplification with nanomechanical resonators. *Nature*, 480:351–354, 2011.

[10] F. Hocke, X. Zhou, A. Schliesser, T. J. Kippenberg, H. Huebl, and R. Gross. Electromechanically induced absorption in a circuit nano-electromechanical system. *New J. Phys.*, 14:123037–15, 2012.

[11] T. P. Purdy, R. W. Peterson, and C. A. Regal. Observation of radiation pressure shot noise on a macroscopic object. *Science*, 339:801–804, 2013.

[12] A. A. Clerk, M. H. Devoret, S. M. Girvin, F. Marquardt, and R. J. Schoelkopf. Introduction to quantum noise, measurement and amplification. *Rev. Mod. Phys.*, 82:1155–1208, 2010.

[13] A. H. Safavi-Naeini, S. Gröblacher, J. Hill, J. T. Chan, M. Aspelmeyer, and O. Painter. Squeezed light from a silicon micromechanical resonator. *Nature*, 500:185–189, 2013.

[14] T. P. Purdy, P.-L. Yu, R. W. Peterson, N. S. Kampel, and C. A. Regal. Strong optomechanical squeezing of light. *Phys. Rev. X*, 3:031012–8, 2013.

[15] E. E. Wollman, C. U. Lei, A. J. Weinstein, J. Suh, A. Kronwald, F. Marquardt, A. A. Clerk, and K. C. Schwab. Quantum squeezing of motion in a mechanical resonator. *Science*, 349:952–955, 2015.

[16] J.-M. Pirkkalainen, E. Damskägg, M. Brandt, F. Massel, and M. A. Sillanpää. Squeezing of quantum noise of motion in a micromechanical resonator. *Phys. Rev. Lett.*, 115:243601–5, 2015.

[17] F. Lecocq, J. B. Clark, R. W. Simmonds, J. Aumentado, and J. D. Teufel. Quantum nondemolition measurement of a nonclassical state of a massive object. *Phys. Rev. X*, 5:041037–8, 2015.

[18] V. Fiore, Y. Yang, M. C. Kuzyk, R. Barbour L. Tian, and H. Wang. Storing optical information as a mechanical excitation in a silica optomechanical resonator. *Phys. Rev. Lett.*, 107:133601–5, 2011.

[19] T. A. Palomaki, J. W. Harlow, J. D. Teufel, R. W. Simmonds, and K. W. Lehnert. Coherent state transfer between itinerant microwave fields and a mechanical oscillator. *Nature*, 495:210–214, 2013.

[20] E. Schrödinger. Die gegenwärtige situation in der quantenmechanik. *Naturwissenschaften*, 23:823–828, 1935.

[21] Z. R. Gong, H. Ian, Yu-xi Liu, C. P. Sun, and Franco Nori. Effective hamiltonian approach to the kerr nonlinearity in an optomechanical system. *Phys. Rev. A*, 80:065801–4, 2009.

[22] E. Knill, R. Laflamme, and G. J. Milburn. A scheme for efficient quantum computation with linear optics. *Nature*, 409:46–52, 2001.

[23] O. Shevchuk, G. A. Steele, and Y. M. Blanter. Ultrastrong optomechanics incorporating the dynamical casimir effect. *Phys. Rev. B*, 96:014508–9, 2017.

[24] P. D. Nation, J. Suh, and M. P. Blencowe. Ultrastrong optomechanics incorporating the dynamical casimir effect. *Phys. Rev. A*, 93:022510–7, 2016.

[25] G. Via, G. Kirchmair, and O. Romero-Isart. Strong single-photon coupling in superconducting quantum magnetomechanics. *Phys. Rev. Lett.*, 114:143602–5, 2015.

[26] A. J. Rimberg, M. P. Blencowe, A. D. Armour, and P. D. Nation. A cavity-cooper pair transistor scheme for investigating quantum optomechanics in the ultra-strong coupling regime. *New J. Phys.*, 16:055008–16, 2014.

[27] T. T. Heikkilä, F. Massel, J. Tuorila, R. Khan, and M. A. Sillanpää. Enhancing optomechanical coupling via the josephson effect. *Phys. Rev. Lett.*, 112:203603–6, 2014.

[28] J.-M. Pirkkalainen, S.U. Cho, F. Massel, J. Tuorila, T.T. Heikkilä, P.J. Hakonen, and M.A. Sillanpää. Cavity optomechanics mediated by a quantum two-level system. *Nat. Commun.*, 6:7981–6, 2015.

[29] J. T. Santos, J. Li, J. Ilves, C. F. Ockeloen-Korppi, and M. Sillanpää. Optomechanical measurement of a millimeter-sized mechanical oscillator approaching the quantum ground state. *New J. Phys.*, 19:103014–11, 2017.

[30] J. R. Johansson, G. Johansson, and F. Nori. Optomechanical-like coupling between superconducting resonators. *Phys. Rev. A*, 90:053833–10, 2014.

[31] C. Eichler and J. R. Petta. Realizing a circuit analog of an optomechanical system with longitudinally coupled superconducting resonators. *Phys. Rev. Lett.*, 120:227702–6, 2018.

[32] D. M. Pozar. *Microwave Engineering*. Wiley, 4th edition, 2012.

[33] B. Peikari. *Fundamentals of Network Analysis and Synthesis*. Jaico, 2008.

[34] R. N. Simons. *Coplanar Waveguide Circuits, Components, and Systems.* Wiley, 2001.

[35] S. Gevorgian, L. J. P. Linnér, and E. L. Kollberg. Cad models for shielded multilayered cpw. *IEEE Trans. Microwave Theory Techn.*, 43:772–779, 1995.

[36] K. Watanabe, K. Yoshida, T. Aoki, and S. Kohjiro. Kinetic inductance of superconducting coplanar waveguides. *Jpn. J. Appl. Phys.*, 33:5708–5712, 1994.

[37] J. R. Clem. Inductances and attenuation constant for a thin-film superconducting coplanar waveguide resonator. *J. Appl. Phys.*, 113:013910–10, 2013.

[38] Y. V. Nazarov and J. Danon. *Advanced Quantum Mechanics.* Cambridge, 2013.

[39] R. P. Feynman, R. B. Leighton, and M. L. Sands. *Feynman lectures on physics.* Addison-Wesley, 1963.

[40] J. Bardeen, L. N. Cooper, and J. R. Schrieffer. Theory of superconductivity. *Phys. Rev.*, 108:1175–1204, 1957.

[41] F. London and H. London. The electromagnetic equations of the supraconductor. *Proc. Roy. Soc. (London) A*, 149:71–88, 1935.

[42] B. D. Josephson. Possible new effects in superconductive tunnelling. *Physics Letters*, 1:251–253, 1962.

[43] J. M. Martinis and K. Osborne. *Superconducting Qubits and the Physics of Josephson Junctions.* Les Houches LXXIX. Elsevier, 2003.

[44] J. Clarke and A. L. Braginski. *The SQUID Handbook*, volume I. Wiley, 2004.

[45] A. H. Nayfeh and D. T. Mook. *Nonlinear Oscillations.* Wiley, 1995.

[46] G. Duffing. *Erzwungene Schwingungen bei Veränderlicher Eigenfrequenz.* F. Vieweg u. Sohn, Braunschweig, 1918.

[47] M. Wallquist, V. S. Shumeiko, and G. Wendin. Selective coupling of superconducting charge qubits mediated by a tunable stripline cavity. *Phys. Rev. B*, 74:224506–10, 2006.

[48] J. R. Johansson, G. Johansson, C. M. Wilson, and F. Nori. Dynamical casimir effect in superconducting microwave circuits. *Phys. Rev. A*, 80:052509–17, 2010.

[49] S. Pogorzalek, K. G. Fedorov, L. Zhong, J. Goetz, F. Wulschner, M. Fischer, P. Eder, E. Xie, K. Inomata, T. Yamamoto, Y. Nakamura, A. Marx, F. Deppe, and R. Gross. Hysteretic flux response and nondegenerate gain of flux-driven josephson parametric amplifiers. *Phys. Rev. Applied*, 8:024012–10, 2017.

[50] M. Abramowitz and I. A. Stegun. *Handbook of Mathematical Functions.* Dover, 10th edition, 1972.

[51] M. Devoret. *Quantum Fluctuations in Electrical Circuits.* Les Houches LXIII. Elsevier, 1995.

[52] H. Goldstein, C. Poole, and J. Safko. *Classical mechanics.* Addison-Wesley, 3rd edition, 2004.

[53] B. Yurke and J. S. Denker. Quantum network theory. *Phys. Rev. A*, 29:1419–1437, 1084.

[54] J. Ulrich and F. Hassler. Dual approach to circuit quantization using loop charges. *Phys. Rev. B*, 94:094505–19, 2016.

[55] P. A. M. Dirac. *The Principles of Quantum Mechanics.* Oxford University Press, 1930.

[56] T. P. Orlando, J. E. Mooij, L. Tian, C. H. van der Wal, S. Lloyd, and J. J. Mazo. Superconducting persistent-current qubit. *Phys. Rev. B*, 60:15398–413, 1999.

[57] J. Koch, T. M. Yu, J. Gambetta, A. A. Houck, D. I. Schuster, J. Majer, A. Blais, M. H. Devoret, S. M. Girvin, and R. J. Schoelkopf. Charge-insensitive qubit design derived from the cooper pair box. *Phys. Rev. A*, 76:042319–19, 2007.

Appendix - full Hamiltonian for the SQUID opto-mechanics circuit

In this appendix we derive the circuit Hamiltonian for the full circuit including plasma modes for the SQUID opto-mechanics circuit. To get a better overview of the degrees of freedom we have rearranged the network as drawn in Fig. 1. Because this circuit is topologically a bit more complicated we will apply the method of nodes for finding the degrees of freedom, as explained in Ref. [51].

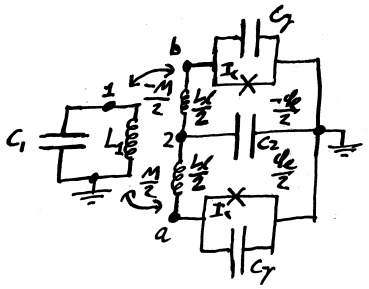

Figure 1: The opto-mechanics simulation circuit rearranged to emphasize the different node flux degrees of freedom. The nodes are labelled 1, 2, a and b and marked as such in drawing. The SQUID loop self inductance is divided with even symmetry over the arms, while the external flux tuning and mutual inductance are divided with odd symmetry over the loop arms.

Method of nodes

The circuit has six nodes, but since there are two disjoint circuits, we have chosen two nodes as corresponding with ground. At the remaining nodes we define so-called node fluxes as

$$\Phi_n = \int_{-\infty}^{t} \mathcal{V}_n \, \mathrm{d}t \tag{1}$$

the time integral of the net voltage at the node relative to ground. A node flux corresponds to the net sum of branch fluxes in any path connecting the node to ground. Note that branch fluxes correspond with the difference between the node fluxes in the connecting nodes. This way the circuit constitutive relations are easily expressed in terms of node fluxes.

The next step is to define a spanning tree connecting each node to ground by a path that does not form any loops. For our purpose it is most convenient to choose the tree such that it contains only inductive branches. Note that all branches not in the spanning tree, the capacitive branches with our choice of spanning tree, are closure branches which when combined with the spanning tree form loops.

The equations of motion, four for our circuit, are then obtained by equating the currents arriving at a node from the inductive branches to the current leaving into the capacitive branches. For this to work in terms of flux variables, the constitutive relations need to be known, and one needs to be able to invert the capacitive ones.

Inductive constitutive relations

The constitutive relations for the Josephson junctions are known

$$\mathcal{I}_\mathrm{a} = I_\mathrm{c} \sin\left(2\pi \frac{\phi_\mathrm{a}}{\phi_0}\right) \tag{2}$$

$$\mathcal{I}_\mathrm{b} = I_\mathrm{c} \sin\left(2\pi \frac{\phi_\mathrm{b}}{\phi_0}\right) \tag{3}$$

but the relations for the linear inductors are more complicated due to the mutual inductances. To find the constitutive relations for the inductors we need to invert the following set of equations

$$\begin{pmatrix} \phi_{\mathrm{L}_1} \\ \phi_{\mathrm{L}_\mathrm{a}} \\ \phi_{\mathrm{L}_\mathrm{b}} \end{pmatrix} = \begin{pmatrix} L_1 & \frac{M}{2} & -\frac{M}{2} \\ \frac{M}{2} & \frac{L_\ell}{2} & 0 \\ -\frac{M}{2} & 0 & \frac{L_\ell}{2} \end{pmatrix} \begin{pmatrix} \mathcal{I}_{\mathrm{L}_1} \\ \mathcal{I}_{\mathrm{L}_\mathrm{a}} \\ \mathcal{I}_{\mathrm{L}_\mathrm{b}} \end{pmatrix} \tag{4}$$

which we have expressed in branch fluxes for now, the conversion to node fluxes we will do when deriving the equations of motion. Inverting the inductance matrix we obtain the constitutive relations for the inductors

$$\begin{pmatrix} \mathcal{I}_{\mathrm{L}_1} \\ \mathcal{I}_{\mathrm{L}_\mathrm{a}} \\ \mathcal{I}_{\mathrm{L}_\mathrm{b}} \end{pmatrix} = \frac{1}{L_1 L_\ell - M^2} \begin{pmatrix} L_\ell & -M & M \\ -M & \frac{2L_1L_\ell - M^2}{L_\ell} & \frac{-M^2}{L_\ell} \\ M & \frac{-M^2}{L_\ell} & \frac{2L_1L_\ell - M^2}{L_\ell} \end{pmatrix} \begin{pmatrix} \phi_{\mathrm{L}_1} \\ \phi_{\mathrm{L}_\mathrm{a}} \\ \phi_{\mathrm{L}_\mathrm{b}} \end{pmatrix}. \tag{5}$$

Constraints

Before we can write the equations of motion, however, we should consider the constraints imposed by Kirchhoff's voltage law, which states that in a loop, all branch fluxes plus any external magnetic flux threading the loop should add up to zero. This must be taken into account when writing the constitutive relations in terms of node fluxes. The constraints are

$$\phi_{\mathrm{L}_1} = \phi_{\mathrm{C}_1} = \Phi_1 \tag{6a}$$

$$\phi_{\mathrm{L}_\mathrm{a}} = \phi_{\mathrm{C}_2} - \phi_\mathrm{a} + \frac{\phi_\mathrm{e}}{2} = \Phi_2 - \Phi_\mathrm{a} + \frac{\phi_\mathrm{e}}{2} \tag{6b}$$

$$\phi_{\mathrm{L}_\mathrm{b}} = \phi_{\mathrm{C}_2} - \phi_\mathrm{b} - \frac{\phi_\mathrm{e}}{2} = \Phi_2 - \Phi_\mathrm{b} - \frac{\phi_\mathrm{e}}{2} \tag{6c}$$

where we have also written the linear inductive branches in terms of the node fluxes.

Equations of motion

The equations of motion are obtained by

$$C_1 \ddot{\phi}_{\mathrm{L}_1} + \mathcal{I}_{\mathrm{L}_1} = 0 \tag{7a}$$

$$C_2 \ddot{\phi}_2 + \mathcal{I}_{\mathrm{L}_\mathrm{a}} + \mathcal{I}_{\mathrm{L}_\mathrm{b}} = 0 \tag{7b}$$

$$C_\mathrm{J} \ddot{\phi}_\mathrm{a} + \mathcal{I}_\mathrm{a} - \mathcal{I}_{\mathrm{L}_\mathrm{a}} = 0 \tag{7c}$$

$$C_\mathrm{J} \ddot{\phi}_\mathrm{b} + \mathcal{I}_\mathrm{b} - \mathcal{I}_{\mathrm{L}_\mathrm{b}} = 0 \tag{7d}$$

for each node equating the currents arriving at the node from the inductive branches (i.e. the spanning tree) to the current going into the capacitive branch from the node. This gives together with the constraints

$$C_1\ddot{\Phi}_1 + \frac{L_\ell\Phi_1 + M\Phi_\mathrm{a} - M\Phi_\mathrm{b} - M\phi_\mathrm{e}}{L_1L_\ell - M^2} = 0 \tag{8a}$$

$$C_2\ddot{\Phi}_2 - \frac{2}{L_\ell}\Phi_\mathrm{a} - \frac{2}{L_\ell}\Phi_\mathrm{b} + \frac{4}{L_\ell}\Phi_2 = 0 \tag{8b}$$

$$C_\mathrm{J}\ddot{\Phi}_\mathrm{a} + I_\mathrm{c}\sin\left(2\pi\frac{\Phi_\mathrm{a}}{\phi_0}\right) - \frac{2}{L_\ell}\Phi_2 + \frac{M\Phi_1 - \frac{M^2}{L_\ell}\Phi_\mathrm{b} + \frac{1}{L_\ell}\left(2L_1L_\ell - M^2\right)\Phi_\mathrm{a} - L_1\phi_\mathrm{e}}{L_1L_\ell - M^2} = 0 \tag{8c}$$

$$C_\mathrm{J}\ddot{\Phi}_\mathrm{b} + I_\mathrm{c}\sin\left(2\pi\frac{\Phi_\mathrm{b}}{\phi_0}\right) - \frac{2}{L_\ell}\Phi_2 + \frac{-M\Phi_1 - \frac{M^2}{L_\ell}\Phi_\mathrm{a} + \frac{1}{L_\ell}\left(2L_1L_\ell - M^2\right)\Phi_\mathrm{b} + L_1\phi_\mathrm{e}}{L_1L_\ell - M^2} = 0\,. \tag{8d}$$

These equations of motion become much compacter if we transform the representation from the junction coordinates to the average junction flux and loop flux relative to the external flux bias

$$\phi_\ell = \phi_{\mathrm{L_a}} - \phi_{\mathrm{L_b}} = \Phi_\mathrm{b} - \Phi_\mathrm{a} + \phi_\mathrm{e} \tag{9a}$$

$$\phi_\Sigma = \frac{\Phi_\mathrm{b} + \Phi_\mathrm{a}}{2} \tag{9b}$$

as coordinates, which yields

$$C_1\ddot{\Phi}_1 + \frac{L_\ell\Phi_1 - M\phi_\ell}{L_1L_\ell - M^2} = 0 \tag{10a}$$

$$C_2\ddot{\Phi}_2 - \frac{4}{L_\ell}\phi_\Sigma + \frac{4}{L_\ell}\Phi_2 = 0 \tag{10b}$$

$$2C_\mathrm{J}\ddot{\phi}_\Sigma + 2I_\mathrm{c}\cos\left(\pi\frac{\phi_\ell - \phi_\mathrm{e}}{\phi_0}\right)\sin\left(2\pi\frac{\phi_\Sigma}{\phi_0}\right) - \frac{4}{L_\ell}\Phi_2 + \frac{4}{L_\ell}\phi_\Sigma = 0 \tag{10c}$$

$$\frac{C_\mathrm{J}}{2}\ddot{\phi}_\ell + I_\mathrm{c}\cos\left(2\pi\frac{\phi_\Sigma}{\phi_0}\right)\sin\left(\pi\frac{\phi_\ell - \phi_\mathrm{e}}{\phi_0}\right) + \frac{-M\Phi_1 + L_1\phi_\ell}{L_1L_\ell - M^2} = 0\,. \tag{10d}$$

Observe that in this basis the linear interaction between the plasma modes decouples. Also note that if we take the limit $C_\mathrm{J} \to 0$ we will obtain the same transcendental constraints we encountered earlier in this work.

Circuit Lagrangian and Hamiltonian

Instead, however, we try to find a Lagrangian that generates above equations of motion, which, after a bit of work, is found as

$$\begin{aligned}\mathcal{L} =& \frac{C_1}{2}\dot{\Phi}_1{}^2 + \frac{C_2}{2}\dot{\Phi}_2{}^2 + C_\mathrm{J}\dot{\phi}_\Sigma{}^2 + \frac{C_\mathrm{J}}{4}\dot{\phi}_\ell{}^2 \\ &- \frac{1}{2}\frac{L_\ell}{L_1L_\ell - M^2}\Phi_1{}^2 - \frac{1}{2}\frac{L_1}{L_1L_\ell - M^2}\phi_\ell{}^2 - \frac{2}{L_\ell}\Phi_2{}^2 - \frac{2}{L_\ell}\phi_\Sigma{}^2 \\ &+ \frac{I_\mathrm{c}\phi_0}{\pi}\cos\left(\pi\frac{\phi_\ell - \phi_\mathrm{e}}{\phi_0}\right)\cos\left(2\pi\frac{\phi_\Sigma}{\phi_0}\right) + \frac{M}{L_1L_\ell - M^2}\Phi_1\phi_\ell + \frac{4}{L_\ell}\Phi_2\phi_\Sigma\,.\end{aligned} \tag{11}$$

If we convert the result to a Hamiltonian and Taylor expand the trigonometric term up to second order and leading interaction terms, we obtain

$$\begin{aligned}\mathcal{H} =& \frac{{q_1}^2}{2C_1} + \frac{{q_2}^2}{2C_2} + \frac{{q_\Sigma}^2}{4C_\mathrm{J}} + \frac{{q_\ell}^2}{C_J} + \frac{1}{2}\frac{L_\ell}{L_1L_\ell - M^2}{\Phi_1}^2 + \frac{2}{L_\ell}{\Phi_2}^2 \\ &+ \frac{1}{2}\left(\frac{L_1}{L_1L_\ell - M^2} + I_\mathrm{c}\frac{\pi}{\phi_0}\cos\left(\pi\frac{\phi_\mathrm{e}}{\phi_0}\right)\right){\phi_\ell}^2 + \frac{1}{2}\left(\frac{4}{L_\ell} + 4I_\mathrm{c}\frac{\pi}{\phi_0}\cos\left(\pi\frac{\phi_\mathrm{e}}{\phi_0}\right)\right){\phi_\Sigma}^2 \\ &+ 2I_\mathrm{c}\left(\frac{\pi}{\phi_0}\right)^2\sin\left(\pi\frac{\phi_\mathrm{e}}{\phi_0}\right)\phi_\ell{\phi_\Sigma}^2 - \frac{M}{L_1L_\ell - M^2}\Phi_1\phi_\ell - \frac{4}{L_\ell}\Phi_2\phi_\Sigma\end{aligned} \tag{12}$$

where we drop a meaningless constant contributions and a static displacements of the loop flux; the first does not contribute to the dynamics while the latter only induces a shift in the effective flux biassing. The conjugate momenta correspond with charge on the respective capacitors, and for the plasma modes respectively with the total charge and the charge difference in both junctions.

This Hamiltonian consists of four Harmonic oscillators labelled 1 and 2 for the two circuit modes, and ℓ and Σ for the two plasma modes. The uncoupled resonance frequencies are seen to be

$$\omega_1 = \sqrt{\frac{L_\ell}{C_1\left(L_1L_\ell - M^2\right)}} \tag{13a}$$

$$\omega_2 = \sqrt{\frac{4}{C_2L_\ell}} \tag{13b}$$

$$\omega_\ell = \sqrt{\frac{2}{C_\mathrm{J}}\left(\frac{L_1}{L_1L_\ell - M^2} + I_\mathrm{c}\frac{\pi}{\phi_0}\cos\left(\pi\frac{\phi_\mathrm{e}}{\phi_0}\right)\right)} \tag{13c}$$

$$\omega_\Sigma = \sqrt{\frac{1}{2C_\mathrm{J}}\left(\frac{4}{L_\ell} + 4I_\mathrm{c}\frac{\pi}{\phi_0}\cos\left(\pi\frac{\phi_\mathrm{e}}{\phi_0}\right)\right)} \tag{13d}$$

but do note that apart from the opto-mechanical interaction there is a linear interaction mediated by the SQUID loop inductances between the resonators 1 and ℓ, and between 2 and Σ. The linear interaction causes the oscillator pairs to hybridise, upon which four new modes with different resonance frequencies emerge.

Quantisation

The next step is to quantise this system in terms of boson creation and annihilation operators. For that we substitute

$$\phi_x = \sqrt{\frac{\hbar}{2C_x\omega_x}}\left(a_x + a_x^\dagger\right) \quad \text{and} \quad q_x = -\mathrm{i}\sqrt{\frac{\hbar C_x\omega_x}{2}}\left(a_x - a_x^\dagger\right) \tag{14}$$

with

$$\left[a_x, a_x^\dagger\right] = 1 \quad \text{and} \quad x \in \{1, 2, \ell, \Sigma\} \tag{15}$$

and where we take $C_\Sigma = 2C_\mathrm{J}$ and $C_\ell = \frac{C_\mathrm{J}}{2}$. The result, leaving out constant contributions, is

$$\begin{aligned}\mathcal{H} =&\hbar\omega_1 a_1^\dagger a_1 + \hbar\omega_2 a_2^\dagger a_2 + \hbar\omega_\ell a_\ell^\dagger a_\ell + \hbar\omega_\Sigma a_\Sigma^\dagger a_\Sigma \\ &+ \frac{\hbar}{2}\frac{I_\mathrm{c}}{C_\mathrm{J}\omega_\Sigma}\sqrt{\frac{\hbar}{C_\mathrm{J}\omega_\ell}}\left(\frac{\pi}{\phi_0}\right)^2 \sin\left(\pi\frac{\phi_\mathrm{e}}{\phi_0}\right)\left(a_\ell + a_\ell^\dagger\right)\left(a_\Sigma + a_\Sigma^\dagger\right)^2 \\ &- \frac{\hbar}{2}\sqrt{\frac{2}{C_\mathrm{J}C_1\omega_\ell\omega_1}}\frac{M}{L_1L_\ell - M^2}\left(a_1 + a_1^\dagger\right)\left(a_\ell + a_\ell^\dagger\right) \\ &- \frac{\hbar}{2}\sqrt{\frac{1}{2C_\mathrm{J}C_2\omega_\Sigma\omega_2}}\frac{4}{L_\ell}\left(a_2 + a_2^\dagger\right)\left(a_\Sigma + a_\Sigma^\dagger\right)\,.\end{aligned} \tag{16}$$

Discussion

The results presented in this appendix in their current form are merely useful for qualitatively discussing the dynamics of the circuit. In the given basis, there are two pairs of linearly interacted modes, each pair coupling a plasma mode and a circuit mode of highly different frequency, while a radiation pressure kind of interaction exists between the two plasma modes. The problem is that the descriptions are presented in the wrong basis. For the case of very small loop inductance and very small junction capacitances, this becomes especially evident, not only in the diverging uncoupled resonance frequencies, but also in divergences in the linear interaction terms.

While it is to be expected that plasma modes become unbounded in the limit of zero junction capacitance, this can not be the case for the remaining two circuit modes. It is therefore important to find the normal modes for the circuit. The latter can be done in the absence of the radiation pressure interaction since it is much weaker than the linear interactions. A transformation to a basis spanned by these modes, corresponds to a block diagonalisation of the Hamiltonian around the radiation pressure interaction. The latter then should become a four mode opto-mechanical interaction, though two would likely be of inaccessibly high frequency.

In a classical picture, finding the normal modes in a system of linearly coupled harmonic oscillators is a solved problem, though a bit tedious. I therefore leave it as an exercise for the reader. In quantum mechanics, there should similarly exist a unitary transformation that decouples linear interactions between harmonic oscillators.